The cellular ligand field stabilisation energy: a new term for modelling open-shell transition metals within molecular mechanics

Kemp, Christopher McGowan

Award date:
1993

Awarding institution:
University of Bath

The Cellular Ligand Field Stabilisation Energy: A New Term For Modelling Open-Shell Transition Metals Within Molecular Mechanics

submitted by Christopher McGowan Kemp

for the degree of PhD

of the University of Bath

1993

ProQuest LLC
789 East Eisenhower Parkway
P.O. Box 1346
Ann Arbor, MI 48106-1346

For

Herbert Sydney, Joe and Finnigan McGowan;

Yesterday, Today and Tomorrow

Abstract

The Cellular Ligand Field Stabilisation Energy, CLFSE, a new term for Molecular Mechanics (MM), provides a metal-centred treatment of Ligand Field Stabilisation Energies and Jahn-Teller effects which are often responsible for severe distortions in coordination complexes, and which cannot be treated in general by traditional MM methods. The theoretical basis of the CLFSE term, the Cellular Ligand Field, CLF, model is described and the computational procedures by which a CLFSE may be generated are outlined. The nature of the CLFSE term is investigated for a variety of coordination numbers, geometries and ligand types in both a qualitative and quantitative fashion.

Relatively simplistic calculations upon three series of six coordinate complexes, $M(NH_3)_6^{2+}$ for M = Mn^{II}, Fe^{II}, Co^{II}, Ni^{II}, Cu^{II} and Zn^{II}, $M(en)_3^{2+}$ (en = ehtylenediamine) for Ni^{II}, Cu^{II} and Zn^{II}, and $[NiX_2[n]ane]$ (X = Cl^- or NCS^-; n = 14,15 or 16 and [n]ane represents an n-membered tetraaza macrocycle) and more complex treatments of the six, four and five coordinate complexes, $M(NH_3)_6^{2+}$ for M = Ni^{II}, Cu^{II} and Zn^{II}, MCl_4^{2+} for M = Mn^{II}, Fe^{II}, Co^{II}, Ni^{II}, Cu^{II} and Zn^{II}, and $[M(Me_6tren)Br]^+$ (Me_6tren = tris((dimethylamino)ethyl)amine) for M = Mn^{II}, Fe^{II}, Co^{II}, Ni^{II}, Cu^{II} and Zn^{II}, give excellent agreement with observed structures and demonstrate the basic utility of the method. The localised nature of the CLF parameterisation scheme in combination with MM provides a useful insight into the chemistry of the $[NiX_2[n]ane]$ and $[M(Me_6tren)Br]^+$ series of complexes.

Cellular Ligand Field analyses are reported for seven tetragonal-octahedral nickel (II) complexes $[NiCl_2(tfeh)_4]$ [tfeh = (tetrafluoroethyl)hydrazine] and $[NiX_2[n]ane]$ (X = Cl^- or NCS^-; n = 14,15 or 16 and [n]ane represents an n-membered tetraaza macrocycle). Consistent sets of parameters emerge which require the spectra of five out of the seven complexes to be reassigned. The resulting parameter values uncover an interesting feature of axial coordination to the macrocyclic systems.

Acknowledgements

It is a very strange feeling, to be sitting here writing this as the last thing I write in this thesis. A thesis is a very difficult thing to finish, and it is most peculiar when you have. I imagine (I'll find out in about 18 years) that it is a similar feeling to that which a parent feels when a child leaves home. I have nurtured, cherished, indeed loved this project, to varying degrees, during the three and a half years of its duration and tomorrow morning it will be gone, at least until the viva rears its ugly head. What on earth will I do with myself ? (actually I am in absolutely no doubt what I am going to do, I only wish I could have started doing it months ago).

Anyway, after a very long time in Bath, it is only right that I should thank a few people who have contributed to my life, both academically and otherwise. On the academic and social front I must extend my warmest thanks to Dr. Rob Deeth, my supervisor, for talking me out of going to Oxford, for maintaining his enthusiasm for the CLFSE model when things were at their bleakest (that sounds a bit melodramatic - if the truth be known things never got even close to what you might describe as bleak, frantic - yes, bleak - no), and for generally being a jolly good supervisor, or at least I presume so, as neither he nor I have done this sort of thing before. The other member of the group, Phil Gilbert provided company in the office, and was responsible for the initial stages of programming the CFLSE routine and inserting it into the VFFN program of Dr.D.J.Osguthorpe, to whom thanks are also due. On the topic programs I must also thamk Dr.Malcolm Gerloch for the copy of CAMMAG1, which was employed for the ligand field calculations of chapter 3. Dr. Brian Brisdon also deserves a thank-you for steering me towards computational chemistry during my undergraduate final year project. It was an opportunity that I was only too glad to grasp in view of my practical ineptitude. Going further back in time I must also thank Dr. John (I think his name was John) Williams, admissions tutor back in 1985, who let me into Bath University despite the fact that I got a C in my A level chemistry when I was asked for a B. He assumed

that I had a bad day when I sat my exams, as all my other results were rather better, ...little did he know !

On a non-academic front I must thank Joe, and more recently Finn, for all their love, support, tolerance and friendship, it would have been a pretty empty few years without them. I must also thank my friends who, with the exception of Fay, Neil, John, Olga and Andy, may be grouped together under the notorious title of Captain Bob's Circus. What marvellous distractions they provide, although often the distraction proved detrimental to both work and health. I can't wait to be on the road with them.

My family deserve a special mention, in what have been difficult times for the Kemp clan, but they have all remained as supportive of me as ever, never once questioning if I was doing the right thing, regardless of what I have managed to come up with. I must try harder in future.

Finally, I must thank my A level chemistry teacher, Mrs Smith (now Mrs Lee - I always new there was something going on there), who didn't know what she was starting when she refused to tell me what was special about a d^3 configuration in terms of heats of hydration, orbital diagrams being beyond the scope of A levels at the time. Anyway Mrs Smith, after seven years of further chemistry I reckon that I now know what is special about a d^3 configuration, but wouldn't it have been easier all round if you'd just told me ?

Contents

Abbreviations

AOM	Angular overlap model
CFT	Crystal field theory
CLF	Cellular ligand field
CLFSE	Cellular ligand field stabilisation energy
EFF	Empirical force field
en	Ethylenediamine
FF	Force field
LFSE	Ligand field stabilisation energy
LFT	Ligand field theory
Me_6tren	tris(2-dimethylaminoethyl)amine
MM	Molecular mechanics
MO	Molecular orbital
[n]ane	n-membered tetraaza macrocycle
TFEH	Tetrafluoroethylhydrazine
TM	Transition metal
v.d.W.	van der Waals
VSEPR	Valence shell electron pair repulsion

Chapter 1

Molecular Mechanics

1.1: Introduction

Computer-aided molecular design requires the implementation of computational procedures for the prediction of molecular structures and energetics. A variety of computational techniques, ranging from ab initio to semiempirical to completely empirical techniques, can be employed in the estimation of molecular energetics[1]. Because of their computational efficiency and accuracy, empirical force field (EFF) techniques are frequently the methods of choice, particularly for large molecules in their ground states. One such EFF method, Molecular Mechanics (MM), has emerged as a popular and powerful method for modelling molecular structure and conformational energies[2] with well-parameterised force fields available for treating many "organic" problems in chemistry and biochemistry[3-7].

The Molecular Mechanics method considers a molecule as a collection of atoms held together by elastic or harmonic forces. These forces can be described by potential energy functions of the structural features such as bond lengths, bond angles, nonbonded interactions and so on. The combination of these potential energy functions makes up the force field. The energy, E, of the molecule in the force field arises from deviations from "ideal" structural features, and can be approximated by the sum of the energy contributions of the force field, equation 1.1.

$$E = E_s + E_b + E_\omega + E_{nb} + ... \qquad \text{Eqn. 1.1}$$

The total energy E is referred to as the steric or strain energy, and is the difference in energy between the real molecule and a hypothetical molecule where all the structural values such as bond lengths and bond angles are exactly at their ideal or "natural" values. The individual terms in the force field refer to the energy of a bond being

stretched or compressed from its natural bond length, E_s, the energy of bending bond angles from their natural values, E_b, the torsional energy due to twisting about bonds, E_ω , and the energy of nonbonded interactions, E_{nb}. If there are other intramolecular mechanisms affecting the energy, such as electrostatic (Coulombic) interactions or hydrogen bonding, then these too may be added to the force field along with more complex functions describing, for example, out-of-plane deformations and non-diagonal cross terms such as angle-torsion terms. In general, there are no strict rules concerning how many or what types of potential energy functions should be used, and indeed the terms that are required are dependant upon the molecule under investigation. This has lead to the development of many different molecular mechanics force fields (see, for example, 1-6)[8].

It is important to recognise that the energy, E, computed by a set of force field terms is only a measure of intramolecular strain relative to a hypothetical situation, and by itself E has no physical meaning. It is, however, the differences in E for a given set of calculations that are important, and hence it is these energy differences that are appropriate for comparison with experimentally observable physical properties such as the rotational barriers or conformer populations of a given molecule.

Once the force field has been constructed using appropriate potential functions, as will be described in the next section, and suitable parameters, such as natural bond lengths, natural bond angles etc. have been chosen, a trial geometry is specified in terms of atomic coordinates and an initial strain energy is calculated. Thereafter the geometry is optimised, using one of the many gradient search or analytical methods of minimisation, to render the inherent strain energy as small as possible.

Molecular mechanics is then an attempt to formulate as reliable a recipe as possible for reproducing the potential energy surface for the movement of atoms within a molecule. The basic philosophy of molecular mechanics rests on the fact that the force field is a computational model for describing the potential surface for all internal degrees of

freedom in a molecule. Strictly speaking, each molecule has its own unique force field, but fortunately experience has shown that the interpolation or extrapolation of existing data is usually adequate. Force fields have been parameterised to give excellent geometries, relative conformational energies, heats of formation, crystal packing arrangements and even transition state structures and reactivities for an increasingly wide range of species[2].

1.2: Potential Functions of Force Fields

In the molecular mechanics model the atoms of a molecule may be thought of as being joined together by mutually independent springs, restoring "natural" values of bond lengths and angles. Most force fields employ a harmonic potential with Hooke's law functions for both bond stretching and angle bending, V_r and V_θ respectively, as shown in equations 1.2 and 1.3.

$$V_r = 1/2\ k_r\ (r - r_o)^2 \qquad \text{Eqn. 1.2}$$

$$V_\theta = 1/2\ k_\theta\ (\theta - \theta_o)^2 \qquad \text{Eqn. 1.3}$$

where k_r and k_θ are the force constants for each term, r and θ represent the actual bond length and angle, and r_o and θ_o represent the ideal values of the bond length and angle. At very large deformations from the ideal bond length one would expect deviations from the harmonic potential, however, and a Morse function would be the more general potential. The Morse potential is of the form show by equation 1.4, where D_b is the depth of the potential well, α is the force constant, b is the actual bond length and b_o is the ideal bond length.

$$V_r = D_b[1-e^{-\alpha(b-b_o)}]^2 - D_b \qquad \text{Eqn. 1.4}$$

Morse potentials are not generally employed in molecular mechanics force fields because they require excessive amounts of computer time. Simpler approximations have been designed which give equivalent results provided that the deviation from the equilibrium bond length is not too large. The most generally used approximation is to include a cubic term into equation 1.2, as shown by equation 1.5, at the cost of additional parameterisation.

$$V_r = 1/2\ k_r\ (r - r_o)^2 + k'\ (r - r_o)^3 \qquad \text{Eqn. 1.5}$$

A potential function including a cubic term shows the desired properties in a certain range, as shown by figure 1.1, and is adequate for large distortions. The disadvantage of cubic terms, however, is that the function inverts at very large distortions, again shown by figure 1.1. It is apparent then, for systems that are likely to show very large deviations from the ideal bond length, that a Morse function must be used to describe the bond stretch potential.

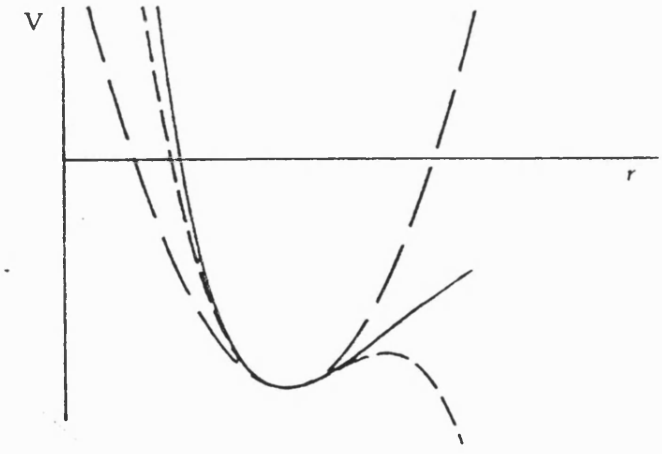

Figure 1.1: Harmonic and anharmonic stretching and bending functions, solid curve - Morse type potential, long dashes - harmonic potential, short dashes - harmonic potential with cubic term added.

The harmonic angle bending term does not seem to suffer from the same problem for large angle deformations. For organic species, angles that are opened to unusually large values show a deformation from normal of only about 15^{o}. There is no compelling evidence that the quadratic function is inadequate for deformations of this size. More severe angle deformations only occur in the opposite sense, especially for three and four membered rings. For such cases the angle bend term must either employ a different value for the force constant, or some form of nonbonding between atoms bound to a common atom must be introduced, usually in the form of a Urey-Bradley term. The Urey-Bradley term assigns a natural distance between two atoms bonded to a common atom, and hence geminal interactions contribute to the strain energy via the nonbonded term. An alternative solution to this problem is to employ a "cross term" such as the stretch-bend potential shown in equation 1.6. in which k_{ij}^{sb} is the force constant, l_i and l_j are the actual bond lengths of bonds i and j respectively, l_i^{o} and l_j^{o} are the natural bond lengths, θ_{ij} is the actual angle formed by bonds i and j, and θ_{ij}^{o} is the ideal value for that angle.

$$E_{sb} = \Sigma\, k_{ij}^{sb}/2\ (l_i - l_i^{o} + l_j - l_j^{o})\ (\theta_{ij} - \theta_{ij}^{o}) \qquad \text{Eqn 1.6}$$

This is in recognition of the fact that as an angle is compressed by movement of the common atom, the two associated bond lengths become longer. Other cross terms are not ordinarily needed for geometry and energy predictions, although an analogous coupling of bending and torsional deformations is helpful in describing such effects as the puckering of cyclobutane[2].

Many attempts have been made to design molecular mechanics force fields on the basis of only stretching, bending and van der Waals interactions by varying parameters and potential functions. It has proved impossible, however, to obtain even an approximately correct energy difference between staggered and eclipsed conformations in species such

as ethane when van der Waals parameters obtained from molecular beam scattering or from crystal packing studies were applied[9]. If the van der Waals parameters were chosen to reproduce the torsional barrier, they were found to be unreasonable for the calculation of most other properties[2].

Completely different approaches have been devised in which extensive use is made of electrostatic nonbonded interactions[10], but in a molecular mechanics scheme based on van der Waals interactions, an additional term, the torsional energy, is essential. Internal rotation about bonds is most commonly expressed in terms of a torsional angle, also referred to as the dihedral or twist angle, defined according to figure 1.2.

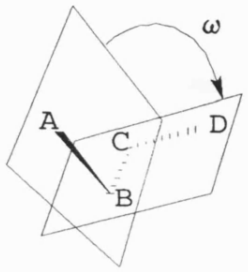

Figure 1.2: Definition of torsional angle, ABCD.

This torsional energy term has usually been thought of as resulting from a repulsion between bonds not covered by van der Waals interactions. Modern molecular mechanics force fields describe the change in energy of the molecule as the torsion angle, ω, changes in terms of the Fourier series shown in equation 1.7.

$$V_{tor} = \sum_{j} (1/2)\, V_j\, (1 - \cos(j\omega)) \qquad \text{Eqn. 1.7}$$

For molecules with C_3 symmetry, such as ethane, all terms with other than 3n-fold periodicity must disappear for symmetry reasons, although even for ethane the data are

barely sufficient for the determination of the sixth term, and hence the torsional potential for ethane has usually been described with j=3 only, for equation 1.7. It has been recognised, however, that a better level of accuracy can be achieved with molecular mechanics force fields when the first two terms of equation 1.7 are also used[11]. By assigning small values to the force constants V_1 and V_2 a conspicuous improvement in the force field results. One physical picture of these torsional terms is that the onefold term is a dipole-dipole interaction, the twofold term is from hyperconjugation in alkanes (or conjugation in unsaturated systems) and the threefold term is steric[12]. For systems involving double bonds the rotation about the double bond involves bond breaking and making and hence is a high energy process. For such systems the twofold term describes the difficult rotation about the bond and hence a large value of V_2 is required.

The fourth term in equation 1.1 is the potential energy term relating to the pairwise nonbonded interaction of atoms as a function of distance between nuclei. As two atoms approach one another, there is the usual attraction due to London dispersion forces and finally a van der Waals repulsion as the atoms become too close. Two of the more common potential energy functions that describe this behaviour are the Lennard-Jones potential, equation 1.8, and the Buckingham potential, equation 1.9;

$$V_{LJ} = A/r^{12} - B/r^{n} \qquad \text{Eqn. 1.8}$$

$$V_{Buck} = A' \exp(B'/r) - C/r^{6} \qquad \text{Eqn. 1.9}$$

where n is usually either 6 or 10 for the Lennard-Jones potential.

Both of these functions describe the attractive part of the curve as r^{-6} dependant (or r^{-10} for the other Lennard-Jones parameterisation) but treat the repulsive part differently. The Lennard-Jones potential assumes an inverse 12th power dependence,

whereas the Buckingham potential assumes an exponential dependence. The curve is characterised mainly by the minimum energy distance, r_o, (related to the van der Waals radii), the depth of the potential well (related to the polarisabilities), and the steepness of the repulsive part (the hardness), as in figure 1.3.

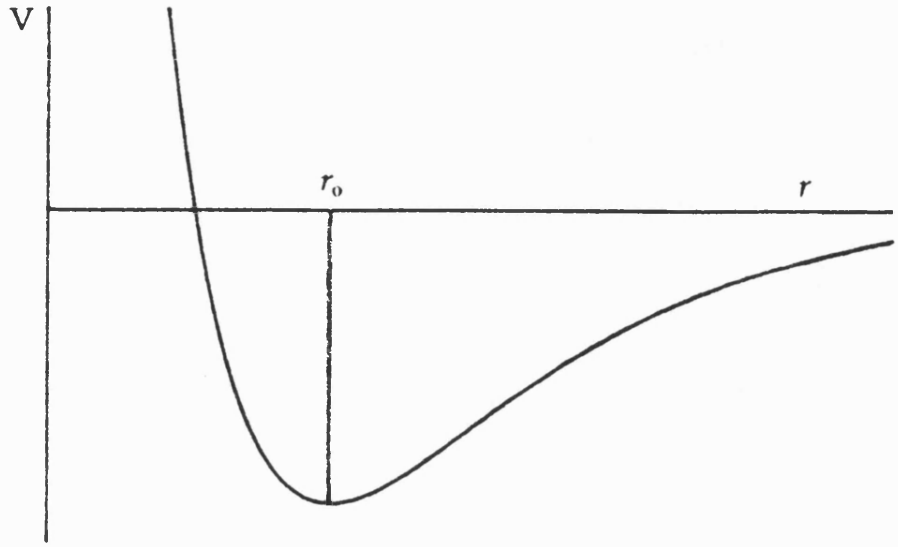

Figure 1.3: Van der Waals energy function.

In practice the exact form of the potential function is not too critical provided the parameterisation is specific to the particular term in use. Typically the nonbonded interaction curves are obtained by measuring nonbonded contact distances between atoms in crystalline hydrocarbons, and by using van der Waals contact data for rare gas atoms. The parameters for the other atoms of the periodic table can then be gained by interpolation or extrapolation using known trends and by comparison of the molecular mechanics results with experiment. This technique assumes that the potentials derived

from intermolecular interactions can reproduce intramolecular interactions, and that these interactions are pairwise additive, that is the nonbonded potential function describing the interaction of two atoms is the same regardless of what other atoms are in the vicinity of the two atoms. Although these appear to be rather radical assumptions, the large number of adjustable parameters allows the method to calculate appropriate interactions.

In addition to the van der Waals nonbonded term, molecular mechanics force fields may also include terms to account for charge/charge, charge/dipole and dipole/dipole interactions. In noncharged polar molecules the dipole/dipole interaction is the dominant term, whereas for interactions between ions the dominant term is the charge/charge interaction, as described by the Coulomb potential, shown in equation 1.10.

$$V_{charge} = q_i q_j / r_{ij} \qquad \text{Eqn. 1.10}$$

The Coulombic term is, however, rarely used in molecular mechanics treatments of organic molecules.

By use of the force field potentials described above, molecular mechanics models are able to provide accurate predictions of both structure and energetics of a wide range of organic species, and have become a popular and powerful tool in organic chemistry. There are three principle reasons for the popularity of the molecular mechanics method. Firstly the method is considerably faster than other theoretical approaches such as quantum mechanical treatments, thus allowing a full energy minimisation of relatively large molecules (> 100 atoms) in a reasonable computational time. Secondly, molecular mechanics is conceptually easier to understand than quantum mechanical methods. Since the total energy is broken down into terms such as compression, bending, nonbonded energies etc., these terms are more comprehensible than, for

example, Fock matrix elements, eigenvalues and eigenvectors, and consequently the bench chemist is more apt to use the molecular mechanics method due to its inherent simplicity. Finally, if and when a molecular orbital treatment is necessary, the molecular mechanics optimised geometry can provide excellent input for a molecular orbital calculation, an approach that is becoming increasingly popular among theoretical chemists[13].

As with all computational models, the molecular mechanics method is not without some shortfalls. The first of these problems applies not only to molecular mechanics but to all molecular geometry optimisation procedures, whether empirical or quantum mechanical. The energy minimisation schemes are designed to vary the available degrees of freedom in such a way that the total energy of the molecule reaches a minimum value. Thus, if the starting geometry is near the lip of some potential well, the molecule will, in effect, slide down the potential energy surface until the bottom is reached. The problem with this is that there may well be other potential wells on the energy surface, some of which may be deeper. In general, automated procedures will not find these other potential wells.

The second drawback of molecular mechanics is that many molecules of interest to chemists are outside the range of molecules for which the molecular mechanics programs are currently parameterised. It is, of course, possible to estimate the appropriate parameter values with some degree of confidence from existing parameterisation schemes, but any new applications should be tested on related molecules whose structures are known, if at all possible. Molecular mechanics is also not suitable for studying properties where electronic effects, such as orbital interactions or bond breaking and making, are predominant.

1.3: Molecular Mechanics Calculations of Coordination Compounds

Molecular mechanics calculations are now well established in the area of coordination chemistry[14,15] where they have most commonly been used for the computation of structures (analysis of disordered structures[16] and prediction of unknown structures[17]), isomer and conformer ratios[18], and metal ion selectivities[19]. The majority of these studies have dealt with cobalt(III) hexamines where a well established force field is available[20]. Force fields have also been reported for several other transition metal complexes including Co(II)[21], Ni(II) (both S=1[22] and S=0[23]), Cu(II)[24] and Pt(II)[25], although the variety of ligands considered in some of these studies tended to be rather limited. Bernhardt and Comba have recently reported[26] force field parameters for complexes of Cr(III), Fe(III) (S=1/2), Co(III), Ni(II) (S=1), Cu(II), Zn(II) and Rh(III) with predominantly "hard" donor atoms such as N and O. Although these applications provide firm evidence for the feasibility of applying molecular mechanics methods to transition-metal complexes, traditional force field formulations are not generalized readily to the variety of molecular shapes exhibited by many inorganic (both main group and transition metal) complexes.

The application of simple valence force field computations to coordination compounds, although possible, is problematic. The first type of problem is revealed by the large variation of ligand-metal-ligand (L-M-L) bond angles observed at transition metal centres. For example, four coordinate metal complexes having a d^8 configuration, such as Rh(I), Ir(I), Pd(II) and Pt(II) complexes, show a strong preference for square-planar geometries. On the basis of an idealised square-planar geometry, L-M-L angle of 90^o (cis ligands) and 180^o (trans ligands) are expected, and indeed many experimental structures conforming to this idealised geometry have been found. However, when four bulky ligands such as trimethylphosphine are coordinated to a single rhodium(I) centre[27], large distortions towards a tetrahedron are observed, resulting in transoid angles of 150^o. Such large distortions suggest a soft angular deformation potential,

which is not well reproduced at such large amplitude motions by the harmonic angular deformation potentials employed by conventional molecular mechanics force fields.

A related problem involving the use of a harmonic angular deformation potential concerns the behaviour of the function at the angular limit, for example $\theta_{L\text{-}M\text{-}L} = 180^{o}$ for a bent triatomic such as water. At this limit, harmonic functions have cusps whereas the slope of $E(\theta)$ should be zero. This behaviour illustrates the intrinsic anharmonicity of the angular deformation potential, particularly in the range of the large deformations that are frequently observed for transition metal species.

An additional problem that is encountered in the application of molecular mechanics to transition metal species is the definition of unique angles and corresponding equilibrium values, referred to as the "unique labelling problem". For example, *cis*-diaminodichloroplatinum(II) requires two N-Pt-Cl equilibrium angle values (90^{o} and 180^{o}). The unique labelling problem arises for any molecular geometry with the possibility of cis and trans orientations, which includes T-shaped, square-planar, trigonal-bipyramidal, square-pyramidal and octahedral idealised geometries. On this basis, description of the frequently observed trigonal-bipyramidal and square-pyramidal geometries requires cumbersome treatment due to the existence of three different L-M-L equilibrium angle values. Since cis and trans orientations are not possible for tetrahedral, trigonal-planar and linear geometries the unique labelling problem is not generally an issue for organic structures.

Molecular mechanics force fields have overcome the unique labelling problem by the incorporation of multiple equilibrium positions and redundant atom labelling schemes at the cost of tedious over-definition of the molecular topology. A more common strategy, however, to circumvent both the unique labelling problem and the problems encountered due to the use of harmonic angular potential functions, is to set the angle bend force constants for the L-M-L angles to zero, and to allow ligand-ligand 1-3 nonbonded interactions, usually in the form of Lennard-Jones or Buckingham

potentials, to determine the angular geometry of the complex. This approach is, of course, analogous to simple VSEPR theory[28] or the more sophisticated but still empirical method of Kepert[29], which have shown that, in the absence of extra electronic effects, ligand-ligand interactions are sufficient to determine the overall angular geometry.

Empirical force field simulations of the geometries of transition metal complexes may be complicated, however, if extra electronic effects are present. These effects include variable coordination numbers and formal oxidation states, the trans effect and the influence of the Ligand Field Stabilisation Energy (LFSE). It is therefore clear that, in order to treat transition metals in a general fashion within a molecular mechanics framework, a separate term is required to treat the metal centre, that does not share the limitations of conventional molecular mechanics treatments. Two such terms have been published to date, reported by Vedani and Huhta[30], and Allured *et al*[31].

Vedani and Huhta have proposed a metal centre term that is designed to form a compromise between a "pure bonded" approach, that is defining the metal ligand bond as a covalent bond and using appropriate parameters for stretching and angle bending, and a "pure nonbonded" approach which does not define a covalent bond between metal and ligand but treats the interaction by means of electrostatic and van der Waals forces. By using a "pure bonded" approach, such as that described for molecular mechanics force fields, most structures can be reproduced from a geometrical point of view, but the approach suffers all the disadvantages already discussed. Most critically the metal can hardly change its coordination type but certainly cannot change its coordination number, since covalent bonds cannot be formed or cleaved during molecular mechanics simulations. Vedani and Huhta are primarily concerned with modelling metalloproteins, and so the fact that the preferred coordination of the metal ion cannot be determined in an unbiased fashion represents a severe restriction of model. However, "pure nonbonded" models generally encounter difficulties on account

of the chosen electrostatic model[32-34]. Calculations based on inappropriate atomic charges or using an unreal dielectric parameter will lead to atomic arrangements around metal centres that lack any resemblance to the more frequently observed types found in small-molecule crystal structures. Vedani and Huhta have therefore sought to achieve a compromise between these two approaches by developing a function that includes two major terms, one describing the radial behaviour of the metal-ligand interactions, the other analysing the first coordination sphere at the metal.

Apart from the metal-ion and ligand-atom type, the radial term of this function depends solely on the metal-ligand distance, equation 1.11. The summation extends over all potential metal-ligand pairs, the term "ligand" currently referring to any O, N or S atom with at least one lone pair available for bonding to the metal.

$$V_{ML} = \sum_{ML\ pairs} (A/r_{ML}^{12} - C/r_{ML}^{10}) \qquad \text{Eqn. 1.11}$$

The coefficients A and C depend upon the equilibrium distance and the well depth of the particular metal-ligand bond. This "semi-bonded" approach allows for mobility of all ligands between various shells, and hence the metal can change both number and arrangement of its proximal ligands during a refinement.

The directional term analyses the first ligand shell at the metal, and computes an energy depending upon the symmetry of the metal centre, the directionality of the metal-ligand bonds and, for transition metals, the ligand field stabilisation energy. It is important however, to stress the fact that the LFSE for this energy term is estimated by hand from tabulations of 10Dq for various metal-ligand interactions and is <u>not</u> added into the energy term as the result of any computational estimate of the LFSE on the basis of metal-ligand bond lengths, d^n configuration or any other "ligand field" property, nor does this term play any role in the minimisation procedure.

This term has been successfully applied to Zn(II) and Co(II) complexes but, although the subject of variable coordination numbers is addressed, it is still not capable of modelling either trans influences or the effect of LSFEs in a general sense, and hence represents little improvement over conventional molecular modelling techniques for transition metal species.

Allured *et al* have approached the problem in a rather different fashion. They report a new force field, SHAPES, that differs from conventional force fields in that the angular potential used to describe the L-M-L bond angles is not of a harmonic form, but takes the form of a Fourier term, similar to that conventionally used to describe torsional energies. A single Fourier term is used, equation 1.12, in which n is the periodicity of the cosine function, ψ is the phase shift which determines the position of the minima, and k^f is the "force constant" which determines the steepness of the function about the minima.

$$E_{angle} = k^f [\, 1 + \cos (n\theta + \psi)] \qquad \text{Eqn. 1.12}$$

Allured *et al* suggest that the Fourier term is a superior representation of the distortion potentials at large bond angles, and does not show the inappropriate behaviour of harmonic potentials that were discussed earlier. In addition to this, it is suggested that Fourier terms (and the related cosine expansions) are better behaved functions for angular distortion potentials because they are capable of simulating the effect of changes in orbital angular overlaps. To allow the use of Fourier potentials and to overcome the unique labelling problem, the positions of the metal and ligands are described by internal coordinates based upon a spherical coordinate system. Definition of a molecular coordinate system based on spherical internal coordinates requires a reference axis. In the SHAPES formulation this axis always contains the metal atom which is the origin of the local coordinate system. For trigonal-planar, trigonal-

bipyramidal and square-planar geometries the reference axis is defined as the line normal to the plane of the ligands and passing through the central atom, as illustrated for ammonia in figure 1.4.

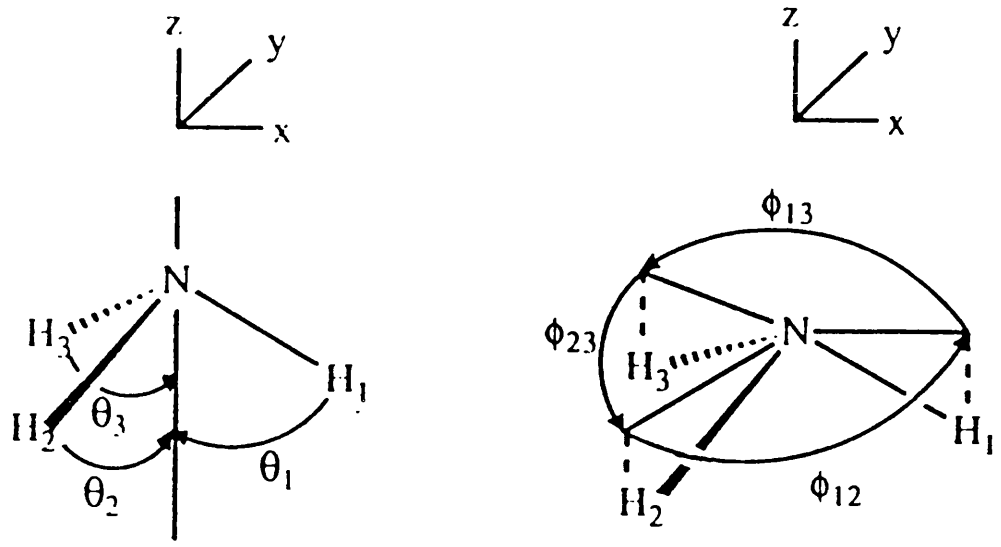

Figure 1.4: Coordinates used to describe angular deformations in the ammonia molecule within the SHAPES force field.

For molecular geometries that have an axial ligand the reference axis is defined as colinear with the line connecting the metal atom to a single ligand identified by the user as being axial. Having defined the reference axis two angles (θ and ϕ) and a bond length (radial vector) uniquely define all nuclear positions. The θ angles are defined by the angle made by the metal atom-to-ligand vectors with the reference axis. The ϕ angles are the angles made by the projections of the metal atom-to-ligand vectors into the plane normal to the reference axis containing the metal atom. The periodicities of the Fourier terms in θ and ϕ, shown in equation 1.13, are determined by the symmetries of the idealised geometries.

$$E = \sum_{\theta} k_{\theta} [1+\cos(n\theta+\psi_{\theta})] + \sum_{\phi} wtk_{\phi} [1+\cos(n'\phi+\psi_{\phi})] \quad \text{Eqn. 1.13}$$

where

$$wt = (r_{ML}r_{ML'}/R_{ML}R_{ML'})^2$$

and R_{ML} is the M-L bond length and r_{ML} is the length of the M-L vector projected into the plane normal to the reference axis containing the metal atom.

The SHAPES force field has been used to accurately reproduce the structures of a variety of square planar rhodium (I) complexes, but has not, as yet, been applied to a sufficient variety of molecular geometries and metal and ligand types to fully evaluate the utility of the method. The formulation of the force field does, however, appear to be a significant improvement upon conventional molecular mechanics force fields, as complex molecular geometries may be described in relatively flexible and convenient fashion, and the connection between angular potentials and angular overlap considerations is intuitively appealing. The SHAPES force field is restricted, however, in that prior assumptions must be made concerning the molecular geometry, and, once again, the force field is unable to account for the effects of LFSEs in a general fashion.

1.4: Conclusion

It is apparent that molecular mechanics force fields have yet to develop a general method for treating the additional effects arising from electronic terms. For instance, the electronic effects of an open d shell can lead to the severe geometrical distortions that are well known in coordination chemistry[35]. Of particular note are the distorted non-cubic geometries displayed by the vast majority of d^9 Cu(II) complexes. For example, $[CuCl_4]^{2-}$ is not tetrahedral but adopts a severely flattened or sometimes even a square planar geometry[36]. Six-coordinate Cu(II) complexes almost invariably display

elongated octahedral geometries[37]. Current molecular mechanics formalisms are unable to reproduce such effects easily. For example, in order to reproduce the geometry of a CuL_6 species it is necessary to define different parameter sets for the axial and equatorial ligands in order to give different axial and equatorial metal-ligand bond lengths, even though L is identical in both cases[26]. The structure of CuL_4 may only be reproduced by defining an idealised square planar geometry, by use of appropriate angular potentials, and employing ligand-ligand nonbonded interactions to yield distortions from that idealised geometry[31]. It is clear that a radically new approach is required to address these issues.

Distortions of coordination complexes can be rationalised in terms of the Jahn-Teller effect or, equivalently, in terms of the ligand field stabilisation energy[37]. The LFSE is a more general concept and its influence extends beyond formally orbitally degenerate systems such as octahedral Cu(II) complexes. For example, the familiar "double hump" behaviour of the heats of hydration of $metal^{II}$ hexaquo complexes can be traced to the LFSE, as can the tendency for four coordinate d^8 metals to be associated with square planar coordination[35]. It appears crucial, therefore, that any general modelling of open-shell transition metal systems needs to explicitly include some kind of ligand field stabilisation energy term in the strain energy expression.

In order that it may be easily incorporated in a molecular mechanics scheme, this LFSE term must be reasonably simple so as not to excessively increase the speed of energy minimisation of a transition metal species, it must be independent of assumptions concerning the coordination number and geometry, so that low symmetry coordination compounds including the active sites of many metalloproteins may be modelled appropriately, and the term should incorporate the chemistry of the metal-ligand bond so as to provide a chemically transparent insight into the local chemistry of the metal centre. These requirements are fulfilled by the Cellular Ligand Field (CLF) model of Gerloch and Woolley[38].

Chapter 2

The CLF Model and the CLFSE

2.1: The CLF Model

The CLF model, described by Gerloch and Woolley[38,39,40,41], was developed from the semi-empirical Molecular Orbital Angular Overlap Model (AOM)[42,43] of Schaffer and Jorgensen. Although both models share superficial similarities, they are fundamentally distinct, the main difference being that the CLF model is defined totally within Ligand Field Theory (LFT), whereas the AOM is based upon the Wolfsberg-Helmholtz semi-empirical Molecular Orbital (MO) scheme. Gerloch and Woolley and Deeth have exposed several inconsistencies inherent to the AOM both theoretically[44,45,46,47] and empirically[47], which are absent from the CLF scheme. Ligand Field Theory is a parametric approach applicable to transition-metal (TM) and lanthanide complexes, with the exception of organometalic complexes and complexes with central metal atoms with a formally zero oxidation state. The CLF model, as with all ligand field models, makes use of the Hamiltonian, H_{LF}, equation 2.1 below, which acts upon a basis within a given d^n (or f^n) configuration.

$$H_{LF} = \Sigma V(i,j) + \zeta \Sigma l_i.s_i + \Sigma V_{LF(i)} \qquad \text{Eqn. 2.1}$$

The terms above describe the effective operators for interelectron repulsion, spin-orbit coupling and the ligand field potential respectively. CLF analyses involve the diagonalisation of an appropriate basis for the n electrons of the system under H_{LF}, with a minimal basis set comprising free ion terms of maximum spin multiplicity. The model requires parameters referring to each part of equation 2.1. Interelectron repulsion is dealt with using the Condon-Shortly[48] or Racah[49] parameters of atomic theory, while an effective spin-orbit coupling constant serves for the second term. The

parameters appropriate for the third term are determined by the particular way in which the ligand field potential, V_{LF}, is expressed.

The most useful information to be obtained from ligand field studies is extracted from the one-electron operator, V_{LF}, acting on a basis of pure d-orbitals. In a complex, the central metal experiences a potential arising from the electron density around it. This potential includes that associated with bond formation and can be divided into two parts: one part is spherically symmetric with respect to the metal, the other is non-spherical. It is the larger, spherical part of the total potential which is notionally used to construct the d-orbital basis. The non-spherical part is then the ligand field potential, V_{LF}, which is parameterised within, for example, the CLF formalism. The important consequence of this construction is that the basis d-orbitals refer to the system as it is[40] and in this sense are optimally defined for each system.

Of principle interest in ligand field studies is the examination of the nature of the metal-ligand bond, and the electron distribution in transition-metal complexes. This aim concentrates upon a localised view of metal-ligand interactions, and so it is evident that the parameterisation scheme must be based upon a corresponding localised approach. In the CLF model, the space around the metal is divided into spatially discrete regions or cells, nominally each cell being associated with a single metal-ligand bond. Within each cell the local ligand field is assumed to be diagonal. Thus, the local d-orbitals divide into σ, π and δ bonding modes, the local z-axis being defined along the metal-ligand axis. The energies, E, of the local d-orbitals in cell *l* are given by the energy parameters e_λ^l, where $\lambda = \sigma, \pi x, \pi y, \delta xy$ and $\delta x^2\text{-}y^2$. Thus:

$$
\begin{aligned}
E(d_{z^2}) &= e_\sigma^l \\
E(d_{xz}) &= e_{\pi x}^l \\
E(d_{yz}) &= e_{\pi y}^l \\
E(d_{x^2-y^2}) &= e_{\delta x^2-y^2}^l \\
E(d_{xy}) &= e_{\delta xy}^l
\end{aligned}
$$

The last two e_δ parameters may be assumed to be zero[50], and so each metal-ligand bond is therefore described by at most three CLF parameters: e_σ, $e_{\pi x}$ and $e_{\pi y}$. Several assumptions may be employed to reduce the degree of parameterisation, however. For so-called linear ligators, such as Cl^- or CN^-, where the local π-bond is cylindrically symmetric, $e_{\pi x} = e_{\pi y}$ and hence only two independent parameters are required. For other ligands such as pyridine or imidazole, the π interaction parallel to the ligand plane is zero ($e_\pi || = 0$), again leaving only two independent non-zero parameters e_σ and $e_{\pi\perp}$. Certain saturated ligands, such as ammonia, have no π-bonding capability at all, hence $e_{\pi x} = e_{\pi y} = 0$ and only a single e_σ parameter is required. The number of parameters may also be reduced by assigning identical parameters to different ligands. This may be reasonably effected provided that the ligands in question are of the same ligand type, have closely similar metal-ligand bond lengths and occupy equivalent coordination environments. In general the sign of a given parameter indicates its donor (positive) or acceptor (negative) role towards the metal.

Having chosen the local parameter values and their local directions, it is then assumed that the total perturbation of the d-orbital basis is given by transforming the local perturbation into some global frame and then summing over all the contributions to yield the total, global ligand-field potential. The global ligand field is now expressed in terms of matrix elements which depend on the molecular geometry and the values of the local e_λ parameters only, as per equation 2.2,

$$V_{ij} = \langle d_i | V_{LF} | d_j \rangle = \sum_l^{\text{cells}} \sum_k^{\text{modes}} T_{ik}^l T_{kj}^l e_k^l \qquad \text{Eqn 2.2}$$

where V_{LF} is the ligand field potential between d-orbitals i and j and the T_{ik} are unitary matrices defining the relationships between local and global axis frames.

In the CLF formalism, the potential in a given cell is assumed to arise exclusively from the electron density contained in that cell, and it is these regions of electron density that

perturb the basis d-orbitals. The dominant contribution to the CLF e_λ parameters is given by equation 2.3.

$$e_\lambda = \frac{|\langle d_\lambda | V | \chi_\lambda \rangle|^2}{E_d - E_{\chi\lambda}} \qquad \text{Eqn 2.3}$$

where d_λ is the local d-orbital of λ symmetry at energy E_d, V is the local ligand field potential, and χ_λ is an orbital of λ symmetry constructed from all possible functions but excluding the basis d-orbital set. It is this formalism that allows interpretation of CLF parameter values to provide a clear and consistent picture of metal-ligand bonding, and its associated effects.

It is conceivable, however, that a cell may contain some electron density which is not accounted for simply by the presence of a ligand. The most obvious example is in square planar complexes where the electron density above and below the plane would contribute to the equatorial perturbations if only four cells (one for each ligand) were considered. For the internal consistency of the model, this "extra" electron density must be enclosed within its own cell. This gives rise to a ligand field effect from a coordination void[44], which is effectively treated as a ligand, but is characterised by significant and negative e_σ parameter values. The negative value for the e_σ parameter associated with a void cell requires a dominant interaction between the d-orbital of σ symmetry in the local, "empty" cell and an orbital χ_σ with a mean energy $E_{\chi\sigma}$ which is more positive than E_d, so that $(E_d - E_{\chi\sigma}) < 0$ determines the sign of e_σ. Were the cell not coordinationally void, then there would exist "bonding" orbitals with mean energies more negative than E_d, and these orbitals would interact more strongly with the d-orbitals than corresponding "antibonding" orbitals because of better overlap. However, being empty, the only localised orbitals which can be associated with these cells, and which have similar energy to the pure metal d-orbitals, are the metal s and p orbitals.

For cationic metals, that are most commonly the subject of ligand field analyses, these orbitals invariably have energies above the d-orbital energy and so make $E_d - E_{\chi\sigma}$ negative as required. Further, the dominant contribution here is likely to derive from the metal s rather than the metal p orbital. So, taking the local and global z-axis to be perpendicular to the coordination plane, coupling between the d_z2 and s orbitals of the metal ion results in a negative e_σ parameter for the void cell, and this negative sign is responsible for the depression of the d_z2 orbital as is experimentally observed for such systems. This yields a self consistent method of rationalising d-s mixing which is absent from other ligand field models.

If the local metal-ligand symmetry is lower than C_{2v}, the local perturbation need no longer be diagonal. The oxygen donors of an acetylacetonate ligand are one example, figure 2.1a). The presence of the oxygen lone pair introduces an off diagonal element, $e_{\pi\sigma}$, into the local energy matrix. This element reflects the fact that the lone pair may interact with both the local σ and πx orbitals. A similar off diagonal element may also be required if "bent bonding" is present, resulting from steric factors preventing the donor orbital of a ligand being oriented along the local z-axis as shown in figure 2.1b).

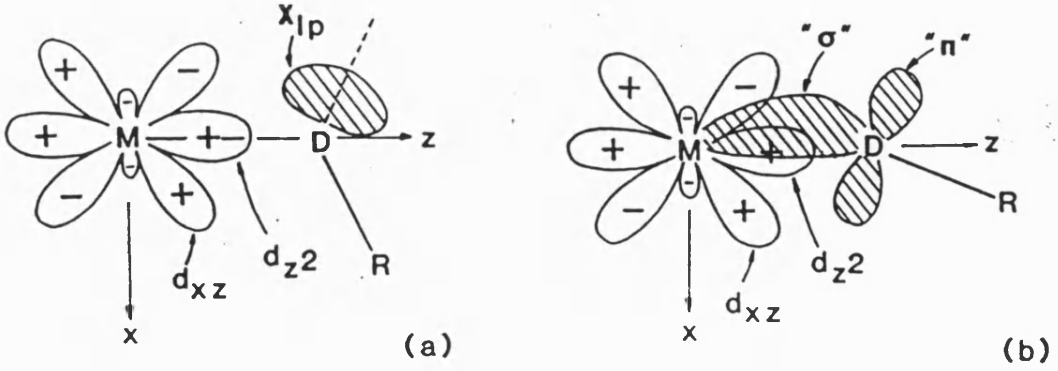

Figure 2.1:a)Illustration of how the presence of a nonbonding, lone-pair orbital, χ_{lp}, on the ligand requires a local ligand-field matrix element connecting d_σ and d_π orbitals.

b) Same interaction arising from the bent σ and π bonds between metal and ligand.

Additional and often frustrating circumstances that may also prevent the clear evaluation of ligand field parameters can arise from the molecular geometry due to the constraints of holohedral symmetry. Due to the purity of the parity of the d-orbitaal basis set occurring within ligand field problems, centrosymmetrically related ligands give rise to potentials that have equal effect upon the metal basis functions. Furthermore, since all radial parts of M-L interactions in ligand field models are included implicitly within the parameters the phenomenon has even greater generality. One cannot, for example, distinguish the ligand field perturbations of ligands on diametrically opposite sides of the metal. The perturbation due to the arrangement in figure 2.2 a) is therefore identical to that in figure 2.2 b).

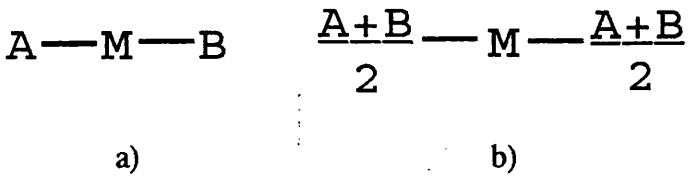

Figure 2.2: Illustration of holohedral symmetry.

It is clear then that the CLF model has a sound theoretical basis, and that the model is, in principle, capable of providing a commentary upon the metal-ligand bonding in a localised sense. However, if this formalism is to be used in conjunction with a empirical scheme such as Molecular Mechanics then the model must also show equivalent practical success. This success must not only be in terms of reproducing the observed ligand field properties for a given complex, as this may achieved by any parametric model given enough variables, but also in the chemical relevance and

transparency of the parameters derived from ligand field analyses and the consistency of the information derived from such results.

Gerloch and co-workers have reported over 120 ligand field analyses carried out within the CLF formalism since 1975, and all studies show reproduction of the ligand field properties that is as good and frequently better than any other ligand field scheme. This ligand field data is generally in the form of d-d spectra, but recourse is also often made to the useful, additional information that can be gained from magnetic susceptibilities and esr g-values. It is, however, in the analysis of the resultant parameter values that the CLF model finds its true worth. The CLF has been found to consistently provide a chemically reasonable commentary upon the nature of the metal-ligand bonding in transition metal complexes both in terms of the magnitude and sign of the CLF parameters, and the variation of these parameters within a series of related compounds. Several CLF studies have highlighted the qualitative and quantitative role of both metal and ligand set within such series. For example, the analyses carried out upon the series $[M(Me_6tren)Br]Br$[51] where M=Fe,Co,Ni and Cu and Me_6tren represents tris(2-dimethylaminoethyl)amine, a "tripod" ligand that provides saturated nitrogen donors for one axial and three equatorial sites of a trigonal bipyramidal structure, illustrate the effect of the metal ion upon the ligand charge donation due to the stereochemical activity of the incomplete d-shell. The effect of modifying the ligand set for a given metal has been shown by analyses such those reported for $[Ni(PPH_3)_2Br_2]$[52] and $[Ni(PPh_3)Br_3]^-$ [53] which illustrate how replacement of one ligand with another effects the CLF parameters of the remainder of the ligands in accordance with general chemical rationale, while the effect of imposing steric constraints upon the coordinating atoms is illustrated by the CLF analyses reported in this work.

Pauling's electroneutrality principle, along with the concept of the functional group, forms much of the basis for the qualitative discussion of chemical bonding. In this vein, one of the most useful results of CLF studies has been the empirical observation and

subsequent exploitation of the "sum-rule", based on the trace, Σ, of the ligand field matrix, V_{LF}[46,54], in simple terms the sum of all the diagonal e_λ of a complex. If individual e_λ represent the donation of electron density from ligand to metal (for positive e_λ), then the trace will monitor the total donation of charge from the overall ligand set to the metal.

The observed invariance of Σ is illustrated by the data shown in table 2.1 below. Average Σ values, standard deviations (σ) and highest and lowest values for Σ are shown for a number of copper systems[47] for which a reasonably reliable estimate of these quantities can be made. The entries are grouped according to the dominant donor set.

Dominant Donor	No. of Complexes	av. Σ	σ	Highest Σ	Lowest Σ
Amine	13	20861	583	21800	19750
Chloride	7	22840	1243	25100	20930
Acetylacetonate	4	21450	252	21800	21200
Imine	3	27800	721	28400	27000

Table 2.1

For the amine systems and, to a lesser extent, the chloro complexes the value of Σ remains remarkably constant irrespective of coordination number or stereochemistry. Amongst the amine complexes are examples of compounds showing nearly square planar, restricted tetragonally elongated, square pyramidal, trigonal bipyramidal and distorted tetrahedral geometries. In contrast the CLF sum may vary significantly as a function of the ligand set, with much larger values of Σ being associated with imine

donors relative to amines, chlorides or acetylacetonates. If the sum is taken to monitor the overall donation of charge from the ligands to the metal, then the magnitude of the sum might be expected to depend upon both entities. At a simplistic level one might expect the combination of ligands of low electronegativity with metals of high electronegativity to be associated with larger values of Σ. However, from the data that are currently available, it appears that the CLF sum is largely insensitive to the nature of the metal, provided that the formal oxidation state remains the same. For example, analyses of the Cr(II) to Cu(II)[51] complexes of tris(dimethylaminoethyl)amine suggest fairly similar values of Σ, as do the sums calculated from the reported values of 10Dq for $Ni(NH_3)_6^{2+}$ [55] and $[Co(en)_3](NO_3)_2$ [56]. In contrast, the $e_\sigma(N)$ reported for the trivalent chromium complex $Cr(NH_3)_6^{3+}$ [57] gives a value of 42000 cm^{-1}, almost twice the value of Σ reported for divalent first-row transition metal hexamines.

The wealth of empirical evidence illustrating the consistency of the observed ligand field trace, Σ, along with a theoretical justification of the CLF sum rule[58], constitutes a defensible basis for the use of the sum rule as both a criterion for parameter transferability and as a measure of the credibility of the results of ligand field analyses within the CLF formalism.

It is apparent then that the Cellular Ligand Field model is an appropriate scheme by which to compute a Ligand Field Stabilisation Energy (LFSE) for a given species. The model has consistently demonstrated an obvious, chemically transparent connection between the CLF parameter values and the nature of the metal-ligand bond[44,45,46], an important factor in both interpreting the results of CLF analyses and in assigning parameters for calculation of a Cellular Ligand Field Stabilisation Energy (CLFSE).

2.2: The Cellular Ligand Field Stabilisation Energy (CLFSE)

In order to generate a CLFSE one must calculate a set of one-electron d-orbital energies. In order to achieve this the computational routine requires the coordinates of the metal and the ligands and, where appropriate, a definition of local axis frames in terms of the coordinates of atoms adjacent to the coordinated atoms, along with the CLF e_λ parameters for each ligand in order to generate the ligand-field matrix. The interelectron repulsion term of equation 2.1 is, of course, unimportant for a one-electron calculation, whilst the spin-orbit coupling term is of little importance for the calculation of orbital energies. The orbital energies that result from the diagonalisation of the ligand field matrix are "automatically" bari-centred, that is the sum of the orbital energies is zero, and this is necessary so as to yield a zero CLFSE for d^{10} and high-spin d^5 species. The CLFSE for a d^n system can then be defined according to equation 2.4,

$$\text{CLFSE} = \sum^{n} p(d_i)\, E\,(d_i) \qquad \text{Eqn. 2.4}$$

where $p(d_i)$ is the occupation number and $E(d_i)$ is the energy of orbital d_i. Within the computational scheme the relevant coordinates are supplied by the energy minimisation routine, while the d-orbital configuration may be pre-defined according to the metal in question. The CLF e_λ parameters, however, must be assigned to each ligand on some parametric basis.

The AOM attempted to solve the problem of assignment of ligand-field parameters by assuming that the perturbation of the d-orbitals[42] arises from the overlap of the metal d-orbitals with appropriate ligand orbitals. The e_λ parameters are then proportional to the squares of the appropriate overlap integrals, equation 2.5,

$$E_\lambda = K_\lambda S_\lambda^{\,2} \qquad \text{Eqn. 2.5}$$

where S_λ is the overlap integral in question and K_λ is a constant.

The constant K_λ is assumed to apply to a given metal and ligand combination, and once determined empirically for a given bond length, can be used to estimate the e_λ for different bond lengths in other complexes by evaluating the overlap integral appropriate to the new separation. This basis for a parameter transferability criterion has often been exploited in applications of the AOM[57]. A second use of this system has been to fix the ratios between e_λ parameters by recourse to overlap integral ratios. These tactics have, however, been shown to be both theoretically and empirically ill-founded[47].

Although within the CLF formalism there is no theoretical justification for a dependence of e_λ upon metal-ligand bond length, the chemical transparency of the CLF parameters in other respects suggests that one might reasonably expect a relationship to develop empirically. Since the e_λ provide a measure of charge donation from ligand to metal, then it would seem reasonable to assume that a larger charge donation, ie a larger e_λ, would correspond to a shorter bond length. The exact nature of the relationship can only be established empirically and the parameters may well, of course, be dependant in part upon factors other than bond length, such as the other ligands in the complex and the coordination site that the ligand in question occupies, but it is feasible that such an empirical relationship will at least provide a reasonable "first guess" at the value of e_λ for a given metal-ligand interaction at a given bond length.

In order to investigate the possibility of such a relationship, and to assist in the formulation of a parametric dependence of e_λ with respect to bond length, a survey of all ligand field calculations reported by Gerloch and co-workers within the CLF formalism has been carried out. These analyses show a range of divalent metals including Cr(II), Mn(II), Fe(II), Co(II), Ni(II) and Cu(II) with a variety of ligands including halides, amines, imines and oxygen donors featuring as the prominent ligand

groups. Limited information is also provided for the trivalent metals Ti(III), V(III) and Cr(III) and for ligands with phosphorous and sulphur coordinating atoms. The data shown here is that collected for the more commonly studied metals of Co(II), Ni(II) and Cu(II), and the following graphs show the variation of e_λ with bond length for the dominant ligand groups of halides and saturated and unsaturated nitrogen donors for these three metals. The additional benefit of such a survey is to highlight those metals and ligand types that would benefit from further CLF study, and to identify those regions of metal-ligand bond length that are poorly defined.

2.3: CLF Database

2.3.1: Cobalt (II) Complexes

Ligand	Bond Length	Donor Set	e_σ cm^{-1}	e_π cm^{-1}	Σ cm^{-1}	Structure	Ref.
Chloride	2.27	Cl_2P_2	3500	2000	19000	Tetrahedral	52
Phosphine	2.28		4000	-1000			
Bromide	2.27	Br_2P_2	3500	1500	16000	Tetrahedral	52
Phosphine	2.28		3500	-1000			
Pyridine	2.19		4500	200,0			
Imine	2.19		3500	1000,0			
Oxygen	2.18	N_3O_2Cl	2500	2000, 400	34700	Pentagonal	59
Chloride/ water	2.31	(H_2O)	4000	800		Bipyramidal	
Bromide	2.38	Br_3N	3000	450	14700	Tetrahedral	60
Quinoline	2.03		3500	-500			
Dabco(N)	2.13	Br_3N	4000	0	20500	Tetrahedral	61
Bromide	2.38		3500	1000			
Dabco	2.09	Cl_3N	4250	0	21350	Tetrahedral	61
Chloride	2.26		3500	1100			
Pyridine	2.115		5000	1000,0			
Imine	2.24	N_5O_2	3000	0	33000	Pentagonal	62
Pyridine	2.095		4000	0		Bipyramidal	
Water	2.18		3500	1000			

Imine/ Phenol	1.85/ 1.86	N_2O_2	7100	-420,300	17320	Square Planar	63
Void	180°		-5000	---			
Imine/ Amine	1.84	N_4	7500	-550,0	20300	Square Planar	63
Void	180°		-3750	---			
Arsine oxide	2.01	O_5	3500	980,875	21970	Square Pyramidal	64
Nitrate	2.12		100	-200,650			
Amine/ Thio-cyanate	2.01	N_5	5600	2000	26400	Trigonal Bipyramidal	65
Amine	2.10		4400	0			
Amine/ Bromide	2.36	NS_3Br	4200	1500	15900	Trigonal Bipyramidal	65
Thiol	2.37		3000	-500			
Chloride		Cl_4	3600	1000	22400	Tetrahedral	65
Thiourea	2.33	S_2O_2	2600	-400	20000	Tetrahedral	65
Acetate	1.96		5800	2000			
Amine/ Bromide	2.29	N_4Br	4250	2000	23250	Trigonal Bipyramidal	65
Amine	2.08		4250	0			
Picoline	1.99	O_5	4550	400,1450	28700	Trigonal	66
oxide	2.08		4150	75,550		Bipyramidal	
Phosphine oxide	1.98	Cl_2O_2	3500	900,600	19900	Tetrahedral	66

Chloride	2.20		3350	800			
Amine	2.06	N_2S_2	3900	0	19400	Tetrahedral	67
Thiol	2.27		5800	0			
Amine/ Thio- cyanate	2.10	N_5	4650	1000	22400	Trigonal Bipyramidal	68
Amine	2.13		3700	0			
Imadazole		N_6	3800	275	24450	Octahedral	47

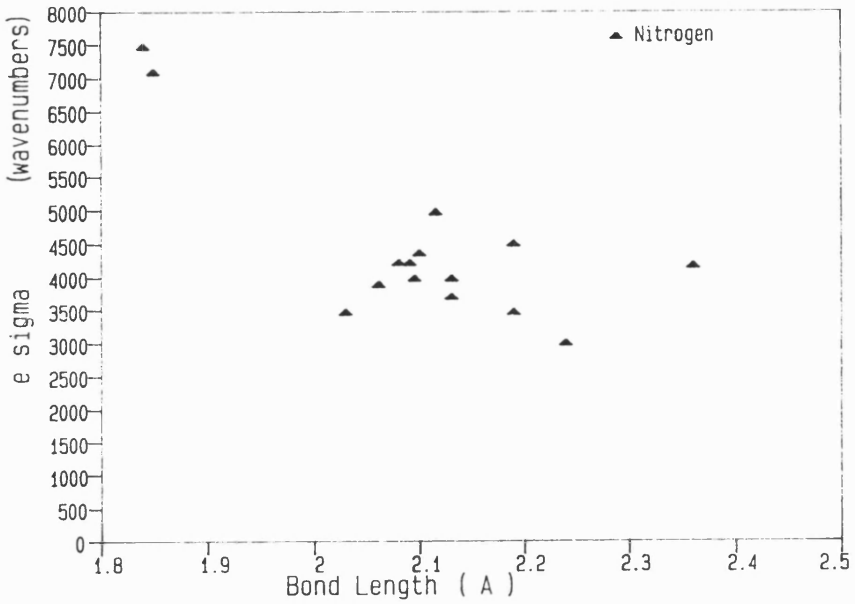

Figure 2.3: Graph of e_σ (cm^{-1}) vs bond length (Å) for saturated and unsaturated nitrogen ligands for cobalt (II) species.

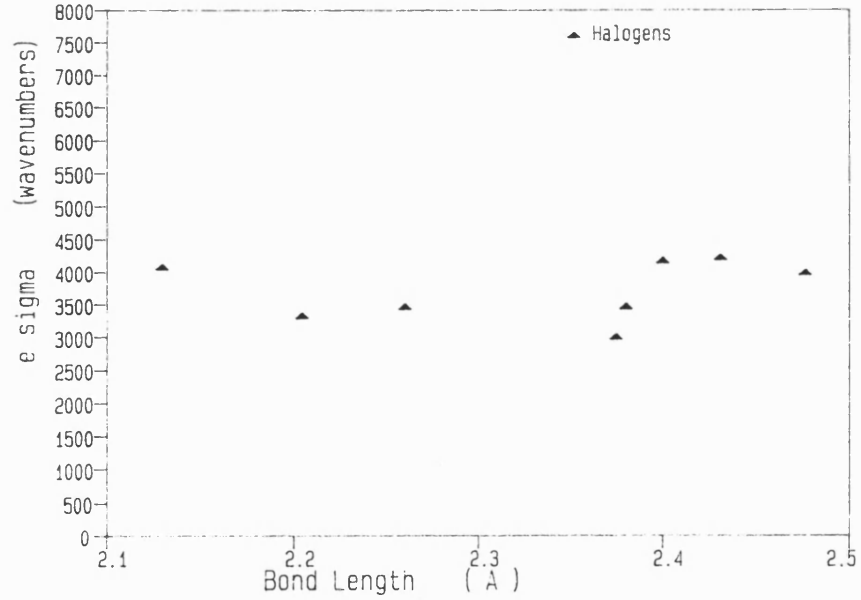

Figure 2.4: Graph of e_σ (cm^{-1}) vs bond length (Å) for halogen ligands for cobalt (II) species.

2.3.2: Nickel (II) Complexes

Ligand	Bond Length	Donor Set	e_σ cm^{-1}	e_π cm^{-1}	Σ cm^{-1}	Structure	Ref.
Amine	1.97	N_2O_2	3800	930	21180	Tetrahedral	69
Phenol	1.90		4200	660,1000			
Amine	2.20		2100	0		Square	
Imine	1.98	N_3O_2	3600	900	23900	Pyramidal	70
Phenol	1.94		4200	1300,900			
Phosphine	2.28	Cl_2P_2	4500	-2500	16000	Tetrahedral	52
Chloride	2.27		4500	2000			
Phosphine	2.28	Br_2P_2	4000	-1500	16000	Tetrahedral	52
Bromide	2.27		4000	1500			
Pyridine	2.06		4800	0,200			
Imine	2.165	N_3O_4	4200	0,1000	32000	Pentagonal	71
Oxygen	2.35		2000	0,100		Bipyramidal	
Water	2.07		5200	500			
Bromide	2.38	Br_3N	4500	1100	23600	Tetrahedral	60
Quinoline	2.03		4000	-500,0			
Phosphine	2.32	Br_3P	5000	-1500	15200	Tetrahedral	53
Bromide	2.38		3000	700			
Phosphine	2.28	I_3P	6000	-1500	12600	Tetrahedral	53
Iodide	2.28		2000	600			
Dabco(N)	2.04	Br_3N	5900	0	20000	Tetrahedral	61
Bromide	2.38		3000	850			

Dabco	2.04	Cl_3N	6100	0	21850	Tetrahedral	61
Chloride	2.24		3250	1000			
Imine	1.97	Br_2N_2	5200	-250,0	20100	Tetrahedral	72
Bromide	2.359		3500	800			
Imine	1.96	N_4	4000	200,0	16800	Tetrahedral	72
Quinoline	1.99	Br_2N_2	4200	-1000,0	16800	Tetrahedral	72
Bromide	2.34		3500	850			
Phosphine	2.32	Cl_2P_2	5000	-1500	17200	Tetrahedral	72
Chloride	2.22		3600	1500			
Phosphine	2.24	I_2P_2	6000	-1500	13000	Tetrahedral	72
Iodide	2.50		2500	500			
Pyridine	2.09	N_5O_2	6000	1500	37100	Pentagonal Bipyramidal	62
Imine	2.30		2500	0			
Pyridine	2.12		3500	0			
Water	2.09		3800	1500			
Amine/ Bromide	2.28	N_4Br	5100	2000	25700	Trigonal Bipyramidal	51
Amine	2.13		4500	0			
Ammonia	2.15	N_6	3667	0	22000	Octahedral	55
Amine	2.14	N_6	3700	0	22200	Octahedral	55
Amine	2.12	N_6	4070	0	24420	Octahedral	55
Amine	2.25	N_6	3100	0	26200	Octahedral	55
Thio-cyanate	1.99		4800	1050			

Amine	2.30, 2.08	N_6	4500, 2800	0	25200	Octahedral	55
Thio-cyanate	2.08		4300	500			
Ammonia	2.15	N_6	3666	0	25664	Octahedral	55
Thio-cyanate	2.07		4300	600			
Amine	2.10	N_6	4140	0	24160	Octahedral	55
Thio-cyanate	2.15		2800	500			
Arsine oxide	2.01	O_5	3550	950,675	22850	Square Pyramidal	64
Nitrate	2.12		1700	100,350			
Amine/ Thio-cyanate	2.01	N_5	6000	2000	26000	Trigonal Bipyramidal	65
Amine	2.10		4000	0			
Chloride		Cl_4	3800	900	22400	Tetrahedral	65
Imine	2.01	N_3O_2	5100	0	23750	Trigonal Bipyramidal	73
Phenol	1.95		4000	1100,25			
Amine	2.09	N_3O_2	3300	0	26350	Trigonal Bipyramidal	73
Imine	2.025		5100	0			
Phenol	1.99		4600	1700,25			
Amine	2.06		3500	0			

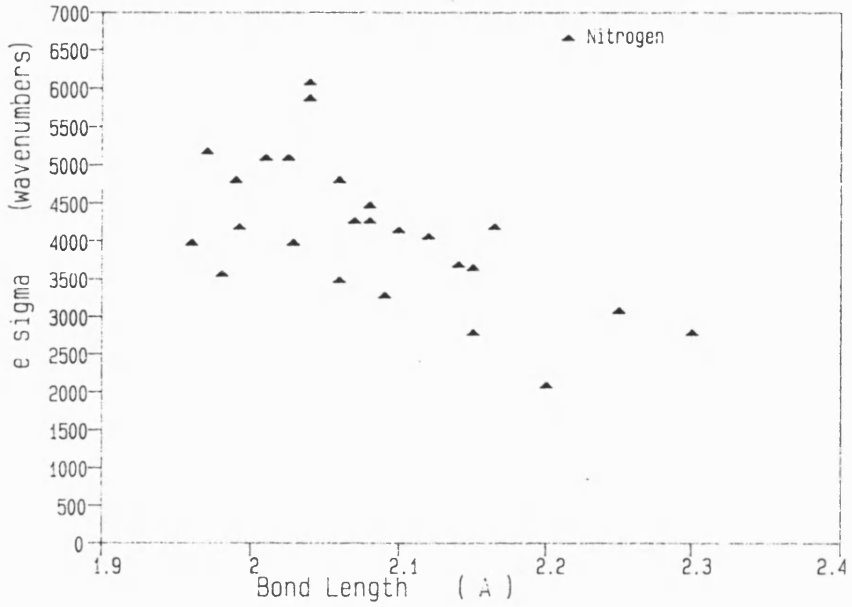

Figure 2.5: Graph of e_σ (cm^{-1}) vs bond length (Å) for saturated and unsaturated nitrogen ligands for nickel (II) species.

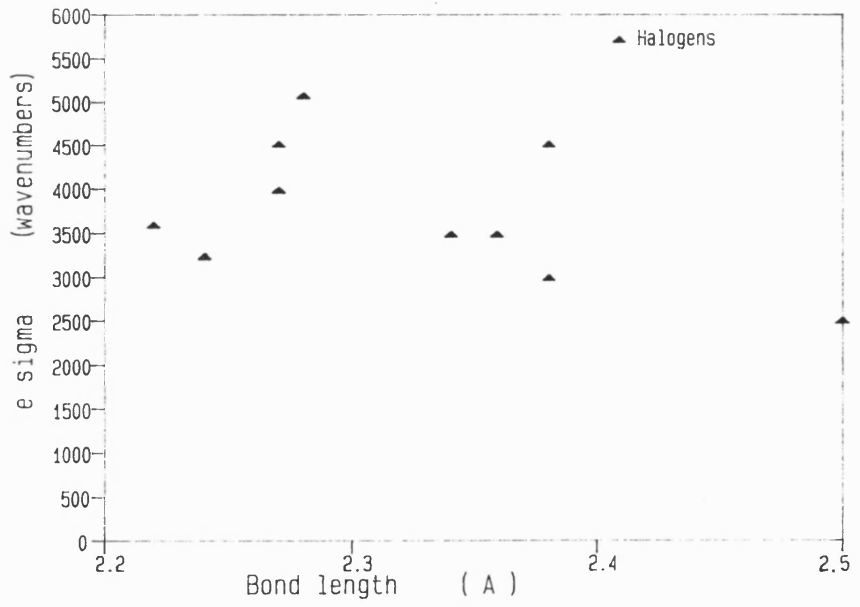

Figure 2.6: Graph of e_σ (cm^{-1}) vs bond length (Å) for halogen ligands for nickel (II) species.

2.3.3: Copper (II) Complexes

Ligand	Bond Length	Donor Set	e_σ cm^{-1}	e_π cm^{-1}	Σ cm^{-1}	Structure	Ref.
Chloride	2.248	Cl_4	5300	900	22400	Square	44
Void	180°		-3000	---		Planar	
Ammonia (eq)	2.03	N_5	5400	0	20850	Square Pyramidal	44
(ax)	2.19		-750	0			
Ammonia	2.08	N_4S_2	5833	0	20698	Octahedral	44
Thio-cyanate	3.00		-1317	0			
Ammonia	1.99	N_6	5700	0	20800	Octahedral	44
Nitrate	2.65		-1000	0			
Ammonia (eq)	2.01	N_6	5800	0	21200	Octahedral	44
(ax)	2.90		-1000	0			
Amine	2.03	N_4F_2	6500	0	20500	Octahedral	44
Fluoride	2.56		-2750	0			
Amine (eq)	2.07	N_6	5100	0	21800	Octahedral	44
(ax)	2.353		700	0			
Chloride (eq)	2.31	Cl_6	4500	1100	23150	Octahedral	46
(ax)	2.78		375	0			

Chloride (eq)	2.30	Cl_6	4800	550	22400	Octahedral	46
(ax)	2.90		-600	0			
Chloride (eq)	2.29	Cl_6	4737	455	20930	Octahedral	46
(ax)	2.98		-828	0			
Chloride (eq)	2.29	Cl_6	4900	600	22900	Octahedral	46
(ax)	3.04		-750	0			
Chloride (eq)	2.29	Cl_6	5100	1100	25100	Octahedral	46
(ax)	3.26		-2050	0			
Amine	2.08	N_5	3300	0	22700	Trigonal	55
Amine	2.03		6400	0		Bipyramidal	
Acetyl-acetonate	1.91	O_4	6000	100,1200	21200	Square Planar	74
Void	180°		-3600	0			
Acetyl-acetonate	1.92	O_4	5700	100,1300	21400	Square Planar	74
Void	180°		-3100	0			
Acetyl-acetonate	1.91	O_4	6000	100,1200	21800	Square Planar	74
Void	180°		-3300	0			
Acetyl-acetonate	1.95	O_4N	5800	400,200	25500	Square Pyramidal	74

Void/ Quinoline	2.36		-100	0			
Amine	2.00	N_4S_2	6500	0	21000	Octahedral	47
Thio-cyanate	3.27		-2500	0			
Amine	2.03	N_4O_2	6375	0	21000	Octahedral	47
Nitrate	2.59		-2250	0			
Amine	2.00	N_4ClO	6125	0	21000	Octahedral	47
Chloride/ Water	2.81/ 2.62		-1750	0			
Ammonia	2.03	N_4O	6000	0	19750	Square Pyramidal	47
Water/ Void	2.34		-4250	0			
Chloride	2.27	Cl_4	5200		23000	Flattened Tetrahedral	47
Void	166.5°		-2500	0			
Amine	2.03	N_4	6350	0	20800	Flattened Tetrahedral	47
Void	152.0°		-2300	0			
Imadazole (eq)	2.03	N_6	5500	1900,0	28000	Octahedral	47
(ax)	2.59		-800	0			
Imadazole	2.01	N_4O_6	6250	1600,0	28400	Octahedral	47
Nitrate	2.57		-1500	0			
Succin-imide	2.00	N_4	6600	1000,0	25200	Square Planar	47
Void	180°		-2600	0			

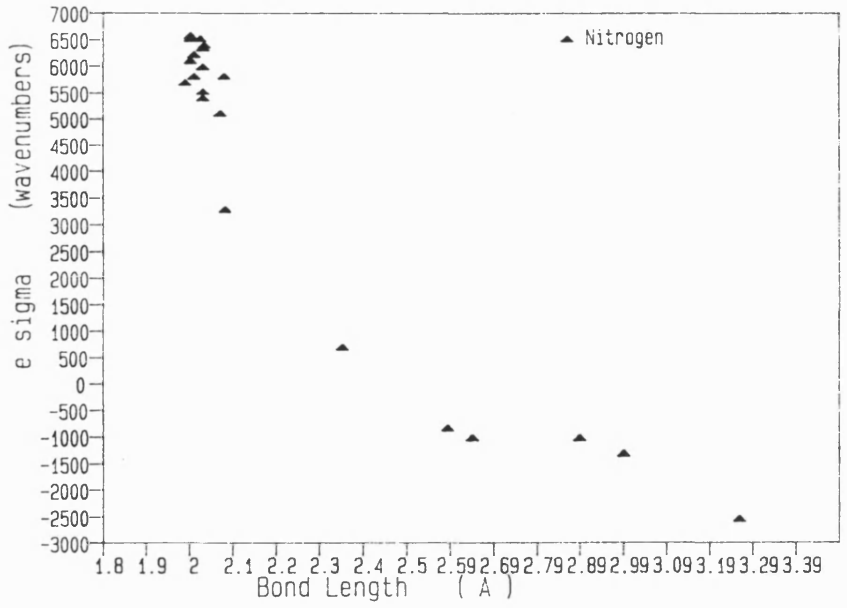

Figure 2.7: Graph of e_σ (cm^{-1}) vs bond length (Å) for saturated and unsaturated nitrogen ligands for copper (II) species.

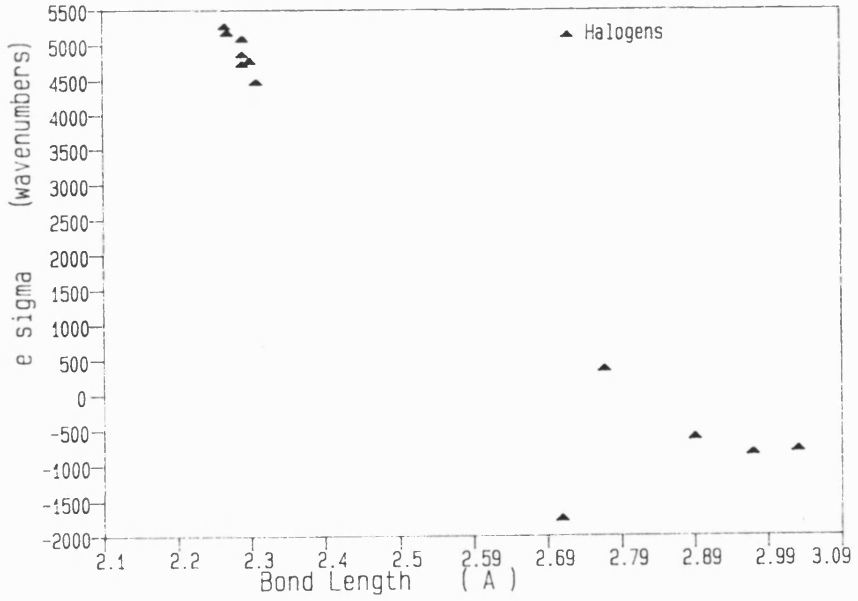

Figure 2.8: Graph of e_σ (cm^{-1}) vs bond length (Å) for halogen ligands for copper (II) species.

The graphs displayed in figures 2.1 and 2.2 for the cobalt(II) complexes with nitrogen and halogen ligands respectively and figures 2.3 and 2.4 for the nickel(II) complexes with the same ligand types display an essentially linear dependence of e_λ upon bond length for the ranges of bond length shown, and this is in accordance with previous studies. For example, many authors have analysed the spectra of tetragonal Ni(II) species[55,75,76,77], and although descriptions of the axial ligands have, in the light of more sophisticated CLF treatments, required revision[55], one general conclusion that has emerged from all the studies is the essentially linear correlation between $e_\sigma(N)$ and the equatorial Ni-N bond length over the range 2.0 to 2.3 Å[76,77,78].

The graphs shown in figures 2.5 and 2.6 for copper(II) species show quite different behaviour, however. Due to the strong Jahn-Teller activity of the Cu(II) d^9 configuration, and the consequent propensity of six coordinate species that show this configuration to undergo tetragonal elongation, a much larger range of metal-ligand bond lengths is shown by the complexes, and this allows a better estimation of the functional form of the e_λ versus bond length relationship. One suggestion for the form of this functional relationship that has emerged from CFT and the AOM is an r^{-5} dependence of e_λ versus bond length. Although such a function reproduces the observed data well for relatively short bond lengths, such as those shown for the Co(II) and Ni(II) complexes, and is approximately linear in these ranges, it is not able to reproduce the negative values for e_λ that are shown at long bond lengths, as are observed for the Cu(II) complexes. In order to accommodate these negative values of e_λ it is necessary to introduce an additional term into the e_λ versus bond length expression. The functional dependence of e_λ versus bond length that is employed for this work is shown below, equation 2.6,

$$e_\lambda = A / (r - \delta)^5 - B (r - \delta) \qquad \text{Eqn. 2.6}$$

where A and B are variable parameters that determine the slope of the curve, and δ is a variable that allows translation of the curve, the utility of which is shown in chapter 5. This function is able to give excellent agreement with the empirical data collected to date.

2.4: Conclusion

It is clear that the CLF model is capable of reproducing the ligand field properties of an open-shell transition metal complex as well, if not better, than any ligand field scheme. The CLF model has, however, proved itself to be superior to other ligand field models in the consistency with which it has provided a chemically reasonable commentary upon the nature of the metal-ligand bonding in a wide variety of complexes, as a result of treating each bond within a complex as an individual region of electron density. It is as a consequence of this localised approach, and by exploitation of the CLF "sum rule", that it has been possible to evaluate the reasonableness or otherwise of a given set of parameters, thereby reducing the problems of underdeterminancy, and leading to a high degree of confidence in the derived final parameter set. The wealth of reliable analyses provided by applications of the CLF model have allowed a relationship between e_λ and metal-ligand bond length to be established, so as to provide at least a "first guess" of the e_λ parameter value as a function of bond length. These values of e_λ, along with the metal configuration and the atomic coordinates, allow the CLFSE to be calculated for a given species. The CLF model therefore provides an excellent basis for the calculation of CLFSEs and CLFSE energy gradients for inclusion into molecular mechanics routines.

Chapter 3

CLF Analyses of Tetragonal Ni(II) Complexes

3.1: Introduction

Modern ligand field analysis relies increasingly on the d-d spectra of transition metal complexes.[44,45,46,65,66,67,73] The absorption spectrum can provide sufficient data to fix unique values for the ligand field parameters, especially when the spectrum is correctly assigned. A correctly assigned spectrum provides considerably more information than transition energies alone often reducing ambiguity in the fitting process such that a unique set of ligand field parameters can be derived. Ideally, assignments should be based on single crystal measurements using polarised light. Single crystal measurements are quite difficult however, and relatively few such studies are reported.[79] Molecules are often unfavourably aligned and group theoretical selection rules may be ambiguous. This is especially so for centrosymmetric complexes where vibronic interactions and selection rules must be considered.[80]

Recourse is therefore usually made to unpolarised measurements often on a series of related complexes where empirical variations in the band energies can be correlated with changing donor sets. Such studies are normally guided by some form of crystal or ligand field theory. In the case of the tetragonal Ni(II) complexes, which are the subject of this study, the reproduction of the d-d band energies is relatively straightforward. By assuming D_{4h} symmetry, such species have been treated by the 'traditional' crystal field model employing the three global parameters Dq, Ds and Dt.[75] However, while the transition energies can be reproduced, there is no guarantee of a reasonable description of the bonding since the global parameterisation cannot, in general, comment on the local nature of the metal-ligand interaction.[41]

Since the M-L bond describes a localised interaction, some form of local parameterisation is more appropriate. The Cellular Ligand Field (CLF) model of Gerloch et al[38], described in the previous chapter, uses parameters which directly

monitor the local σ and π interactions. The magnitudes and variations of the CLF e_λ ($\lambda=\sigma$, πx, πy) parameters correlate with the structures and bonding in metal complexes and provide a more consistent way of comparing a series of species to determine whether the parameter values are reasonable. The CLF model provides not only an accurate method for reproducing experimental data but also a more detailed description of the nature of the M-L bond. The CLF scheme is therefore a more reliable approach for interpreting d-d spectra.

The advantages of the local CLF scheme over the global Dq/Ds/Dt approach are illustrated in this chapter by examining the spectra of seven tetragonal NiN_4X_2 complexes. The complexes $NiCl_2(TFEH)_4$ (TFEH=tetrafluoroethylhydrazine) and NiX_2[n]ane, where $X=Cl^-$ or NCS^-, n=14,15 or 16 and [n]ane represents a fully saturated n-membered tetraaza macrocycle, figure 3.1, are all characterised by four equatorial amine donors and two axial linear ligators.

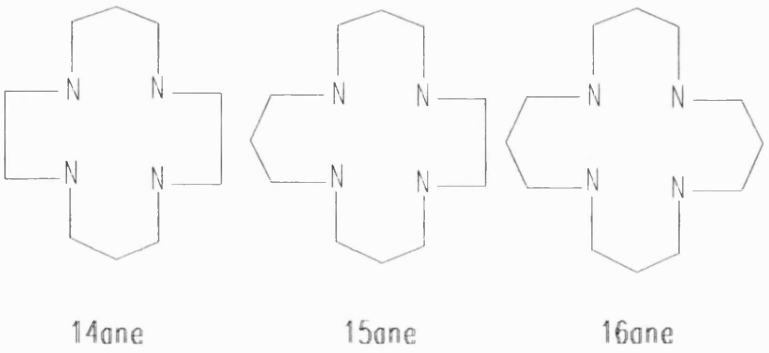

Figure 3.1:Schematic representation of [14]ane, [15]ane and [16]ane macrocycles.

This leads to three CLF parameters, $e_\sigma(N)$, $e_\sigma(X)$ and $e_\pi(X)$ and hence, assuming D_{4h} symmetry for illustrative purposes, to a direct mapping between the CLF and global schemes (3.1):[76]

$$\begin{aligned} e_\sigma(N) &= 10/3\ Dq \\ e_\sigma(X) &= 10/3\ Dq - 2\ Ds - 5/2\ Dt \\ e_\pi(X) &= -3/2\ Ds + 10/4\ Dt \end{aligned} \qquad (3.1)$$

These simple expressions illustrate the potential problems of deriving local bonding information from a global scheme. While there is a direct relationship between the equatorial M-L interaction and Dq, the axial bonding is more complex and has contributions from all three global parameters. Thus, the relationships derived from variations in Ds and Dt with the nature of X may not correspond with the actual variation in σ and π bonding.

For example, the spectra of the macrocyclic complexes described above have been reproduced within the global scheme.[75] Converting the published values of Dq, Ds and Dt into the appropriate CLF values (see later) indicates π-donor roles for Cl and NCS in the [14]ane species but π-acceptor roles for the [15]ane and [16]ane molecules. Moreover, the published assignment for $NiCl_2(TFEH)_4$[81] yields a large negative value for $e_\pi(Cl)$ of -1750 cm^{-1} against an $e_\sigma(Cl)$ of only 550 cm^{-1}. A π-acceptor role for Cl^- is highly unlikely and, based on previous analyses of $Ni(NH_3)_4(NCS)_2$, and related molecules[55] it appears that NCS^- is also not a π-acceptor ligand, at least towards Ni(II). The reason for these anomalies lies in the use of a global scheme which fails to make contact with the chemistry in these complexes. Consequently, the global approach also leads to incorrect spectral assignments as will be seen.

These systems are therefore re-analysed within the CLF model. In contrast to the previous studies, the CLF model requires no artificial symmetry restrictions and D_{4h}

symmetry is not assumed. The actual reported structures derived from X-ray structural studies are employed. Spin-forbidden transitions are also included in the fitting process where appropriate, and use is made of published magnetic moments of $NiCl_2$[15]ane.[75] Consistent sets of parameters emerge which require the spectra of five of the seven complexes to be reassigned. The resulting parameter values uncover an interesting feature of the nature of axial coordination to these macrocyclic systems in that an increase in donor strength need not be accompanied by a decrease in bond length.

3.2: Ligand Field Analyses

As the CLF model is not restricted to any idealised symmetry the present analyses use the reported structures derived from X-ray crystallography.[78,81] All calculations employ the three CLF parameters, $e_\sigma(N)$, $e_\sigma(X)$ and $e_\pi(X)$, (X=Cl or NCS) representing the equatorial σ, axial σ and axial π interactions respectively. The Ni-NCS angles are 165.1°, 153.8° and 160.0° for the [14]ane, [15]ane and [16]ane respectively.[78] Although a Ni-NCS angle of 140° in $Ni(en)_2(NCS)_2$ was associated with a degree of misdirected valence,[55] the results of the present analysis indicate that such interactions are not resolvable here (*vide infra*) and the NCS ligand is treated as a linear ligator. All calculations save those for the [14]ane complexes employ the full d^8 basis comprising ^3F, ^3P, ^1S, ^1D and ^1G terms. The [14]ane species do not exhibit any spin forbidden transitions and therefore only require a ^3F, ^3P basis set, In addition, the calculations employ the Condon-Shortley interelectron repulsion parameters F_2 and F_4 for the full basis set calculations or just the Racah B parameters for the spin-triplet calculations. A nominal value of 500 cm^{-1} is taken for the spin-orbit coupling constant, ζ, except for $NiCl_2$[15]ane where the value is optimised against the observed magnetic moment.

All the complexes have approximately D_{4h} symmetry and the energy levels are labelled accordingly as in figure 3.2. The ground state is of $^3B_{1g}$ symmetry with excited triplet states of ^3E_g and $^3B_{2g}$, derived from the parent octahedral $^3T_{2g}$ term, and two sets of $^3A_{2g}$ and ^3E_g levels derived from the parent octahedral $^3T_{1g}(F)$ and $^3T_{1g}(P)$ terms. The only singlet levels of relevance here are the $^1A_{1g}$ and $^1B_{1g}$ levels derived from the octahedral ^1E_g term. The transition $^3B_{1g} \rightarrow {}^3B_{2g}$ depends solely on $e_\sigma(N)$, note however that this energy is only rigourously equal to $3e_\sigma(N)$ when the inplane bond angles are exactly 90^o.

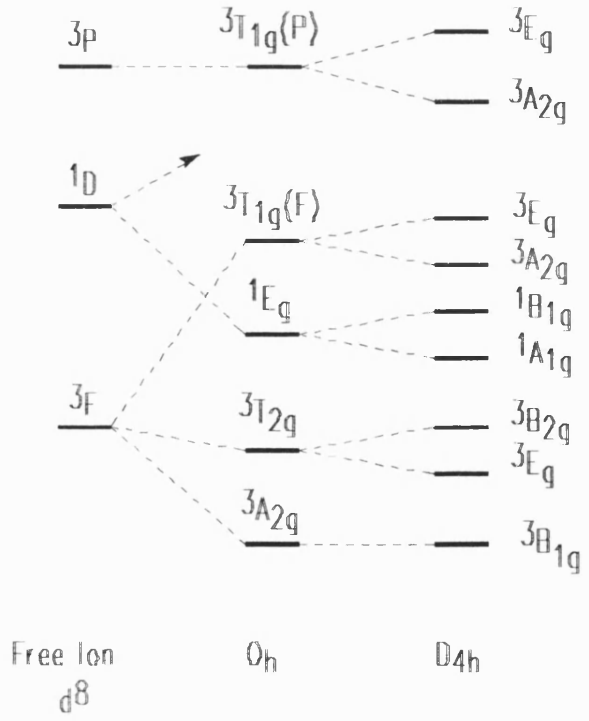

Figure 3.2: Qualitative partial energy level scheme for tetragonal Ni(II) complexes. See text for detailed assignments for individual complexes.

3.2.1: $NiCl_2(TFEH)_4$

The structure and solid state reflectance spectrum for $NiCl_2(TFEH)_4$ have been reported by Rahman et al.[81] Energies for the d-d band maxima are given as 8700, 10600, 12900, 17400 and 27400 cm^{-1} assigned as transitions to ^3E_g, $^3B_{2g}$, $^3A_{2g}$, ^3E_g and the unsplit components of the (octahedral) $^3T_{1g}(P)$ term respectively from the $^3B_{1g}$ ground term. Reproduction of these energies as assigned above to within a few hundred wave numbers yields the following unique CLF parameter values:

$$e_\sigma(N) = 3533\ cm^{-1}$$

$$e_\sigma(Cl) = 550\ cm^{-1}$$

$$e_\pi(Cl) = -1750\ cm^{-1}$$

Clearly such a large negative $e_\pi(Cl)$ value suggests a chemically unacceptable π-acceptor role for Cl^- and suggests that the published assignment needs revision. Given that the 27400 cm^{-1} band corresponds to unsplit $^3A_{2g}$ and ^3E_g levels derived from the parent octahedral $^3T_{1g}(P)$ term, it follows that the $^3T_{1g}(F)$ term should also remain essentially unsplit.[80] If the transition to the $^3A_{2g}$ level, originally placed at 12900 cm^{-1}, is reassigned to lie under the 17400 cm^{-1} band, then one of the first three bands must correspond to a spin-forbidden process while the other two correspond to the transitions to ^3E_g and $^3B_{2g}$. The latter is determined by $e_\sigma(N)$ which would take values of 2900, 3533 and 4300 cm^{-1} respectively.

Previous studies[76,77] indicate a good correlation between bond length and e_σ for saturated equatorial nitrogens in tetragonal Ni systems. The Ni-N bond length in $NiCl_2(TFEH)_4$ of 2.106 Å suggests a value for $e_\sigma(N)$ of 4300 cm^{-1} is most likely and therefore the 12900 cm^{-1} band is reassigned as the $^3B_{1g} \rightarrow {}^3B_{2g}$ transition. The most likely assignment of the spin forbidden process is to the 10600 cm^{-1} band which then yields the best fit CLF parameter values given below. The observed and calculated transition energies are compared in table 3.2.

$$e_\sigma(N) = 4300\ cm^{-1}$$

$$e_\sigma(Cl) = 2480\ cm^{-1}$$

$$e_\pi(Cl) = 400\ cm^{-1}$$

This choice of assignment is further supported by the satisfactory reproduction of the experimental spectrum by CLF parameter values which are more consistent with previous studies and this work (*vide infra*).

3.2.2: $NiCl_2$[14]ane

Martin et al[75] report six absorption maxima for $NiCl_2$[14]ane at 8600, 14750, 15200, 19400, 27250 and 29152 cm^{-1} which are assigned to spin allowed transitions as per figure 3.2. Reproduction of these band energies as assigned gives the essentially unique CLF parameter values displayed below.

$$e_\sigma(N) = 4976\ cm^{-1}$$

$$e_\sigma(Cl) = 1580\ cm^{-1}$$

$$e_\pi(Cl) = 240\ cm^{-1}$$

The agreement with experiment (table 3.2) is again satisfactory while the CLF parameter values appear unexceptional. There is no case for the spectrum to be reassigned on the basis of this ligand field analysis.

3.2.3: $NiCl_2$[15]ane

Six bands are also reported[75] for $NiCl_2$[15]ane, again assigned as per figure 3.2. The CLF analysis based on this assignment leads to the following parameter set:

$$e_\sigma(N) = 4152\ cm^{-1}$$

$$e_\sigma(Cl) = 1680\ cm^{-1}$$

$$e_\pi(Cl) = -180\ cm^{-1}$$

As found for $NiCl_2(TFEH)_4$, the Cl ligand is predicted to be a π-acceptor and again indicates a questionable assignment. Further complications arise in that the spectrum

actually displays three bands in the 12000-13000 cm^{-1} region, only one of which was assigned to a spin-allowed transition while the other, presumably spin-forbidden bands, were ignored. The present CLF analysis therefore seeks not only to derive a more consistent set of parameter values but also to account for the spin-forbidden features. The original paper does not report all the band maxima in this region, hence approximate values of 11900, 12750 and 13100 cm^{-1} were derived graphically from figure 6 of reference 77.

Three assignments were examined in which the $^3B_{2g}$ level is associated with the 13100, 12750 and 11900 cm^{-1} bands respectively. Fixing the $^3B_{2g}$ energy immediately determines the value of $e_\sigma(N)$ while the $^1B_{1g}$ to $^1A_{1g}$ splitting depends on $e_\sigma(Cl)$ and ζ. A lower limit on ζ can be evaluated by computing the effective magnetic moment assuming that Steven's orbital reduction parameter, k, must be less than or equal to unity. The upper limit on ζ is presumably the free-ion value of 650 cm^{-1}.[82] For k=1, a ζ value of 600 cm^{-1} gives a calculated μ_{eff} of 3.220 BM versus the experimental value of 3.22 BM, while for ζ=650 cm^{-1}, k is required to be about 0.94 in order to reproduce μ_{eff}. Best fit CLF parameter values for each assignment are as follows:

1. $^3B_{2g}$ at 13100 cm^{-1}

$e_\sigma(N) = 4390\ cm^{-1}$

$e_\sigma(Cl) = 2250\ cm^{-1}$

$e_\pi(Cl) = 575\ cm^{-1}$

For $\zeta = 600\ cm^{-1}$

2. $^3B_{2g}$ at 12700 cm^{-1}

$e_\sigma(N) = 4265\ cm^{-1}$

$e_\sigma(Cl) = 2850\ cm^{-1}$

$e_\pi(Cl) = 950\ cm^{-1}$

For $\zeta = 580\ cm^{-1}$

3. $^3B_{2g}$ at 11900 cm^{-1}

$e_\sigma(N) = 3985\ cm^{-1}$

$e_\sigma(Cl) = 3200\ cm^{-1}$

$e_\pi(Cl) = 1100\ cm^{-1}$

For $\zeta = 650\ cm^{-1}$

For assignment 3 the free ion value of ζ is employed, which produces a minimum value parameter set for Cl. If ζ is reduced, then $e_\sigma(Cl)$ must be increased to reproduce the splitting between the $^1B_{1g}$ and $^1A_{1g}$ levels and consequently $e_\pi(Cl)$ must be increased to reproduce the other features of the spectrum. Assignment 2 shows the converse relationship between ζ and $e_\sigma(Cl)$. For this assignment the minimum value of ζ required to reproduce μ_{eff} with k=1 yields the minimum parameter set for Cl.
The biggest difference between these fits is that assignments 2 and 3 predict much larger parameter values for Cl than those of assignment 1, especially as assignments 2 and 3 report the minimum parameter values for this ligand. Given the values for $e_\sigma(Cl)$ and $e_\pi(Cl)$ of 2680 and 400 cm^{-1} for $NiCl_2(TFEH)_4$, it is tempting to conclude that the values for assignments 2 and 3 for the [15]ane species are in fact too large. The values for assignment 1 appear to be most reasonable and these data are reported in table 3.1 with the computed transition energies in table 3.2. Further justification for this choice of CLF parameter values is given below.

3.2.4: $NiCl_2$[16]ane

Only five bands are reported[75] for $NiCl_2$[16]ane, the splitting of the levels derived from the ^3P term being apparently unresolved. Again, fitting this assignment within the

CLF scheme leads to the unacceptable parameter set shown below, with e_π(Cl) again taking a negative value.

$$e_\sigma(N) = 3779\ cm^{-1}$$
$$e_\sigma(Cl) = 1560\ cm^{-1}$$
$$e_\pi(Cl) = -200\ cm^{-1}$$

The observation that the parent ^3P term does not split parallels the $NiCl_2$(TFEH) case, however. Reassigning the spectrum of $NiCl_2$[16]ane in like fashion leads to two bands being placed under 15758 cm^{-1} absorption while the 13455 cm^{-1} peak is treated as a spin forbidden transition. This yields the best fit CLF parameter values below with the calculated spectrum given in table 3.2.

$$e_\sigma(N) = 3779\ cm^{-1}$$
$$e_\sigma(Cl) = 3100\ cm^{-1}$$
$$e_\pi(Cl) = 900\ cm^{-1}$$

3.2.5: $Ni(NCS)_2$[14]ane

Four d-d peak energies are reported[75] for $Ni(NCS)_2$[14]ane. Evidently transitions to levels derived from the ^3P free ion term are not observed so only nominal values for the interelectron repulsion parameter can be used. The spectrum is assigned as per figure 3.2. Reproduction of these transitions yields the parameter values below.

$$e_\sigma(N) = 4780\ cm^{-1}$$
$$e_\sigma(NCS) = 3000\ cm^{-1}$$
$$e_\pi(NCS) = 100\ cm^{-1}$$

As found for the chloro complex, a reassignment of the spectrum is not warranted nor are any spin forbidden transitions observed.

3.2.6: $Ni(NCS)_2$[15]ane

Five band maxima are given[75] for $Ni(NCS)_2$[15]ane although the features at 12029 and 15834 cm^{-1} were derived by Gaussian analysis. As for the analogous chloro species, reproduction of the reported assignment within the CLF scheme indicates a π-acceptor role for NCS, as shown below:

$$e_\sigma(N) = 4072\ cm^{-1}$$
$$e_\sigma(NCS) = 2250\ cm^{-1}$$
$$e_\pi(NCS) = -600\ cm^{-1}$$

The isothiocyanate values are inconsistent with those derived for $Ni(NCS)_2$[14]ane. The Ni-NCS bond length decreases in $Ni(NCS)_2$[15]ane from 2.130 Å to 2.079 Å yet the e_π(NCS) value decreases. Moreover, NCS is a π-donor in the [14]ane species but apparently a π-acceptor in the [15]ane complex. Both observations suggest that the spectrum should be reassigned.

Closer inspection of the experimental spectral plot[75] indicates that the broad absorption between 12000 and 13000 cm^{-1} may contain more than the $^3B_{1g} \rightarrow {}^3B_{2g}$ transition reported to be at 12029 cm^{-1}. Indeed, weak absorption around 12900 cm^{-1} is suggested and is assigned here to spin forbidden processes. Moreover, given the general uncertainty inherent in the Gaussian analysis procedure, the exact energy of the $^3B_{1g} \rightarrow {}^3A_{2g}$ band, reported at 15834 cm^{-1}, is uncertain. Accordingly, both components of the transition to the nominal octahedral $^3T_{1g}$(F) term are placed under the 18367 cm^{-1} absorption. This reassignment correlates with the observation of only a single band for the transitions to the $^3T_{1g}$(P) levels and with the proposed reassignments for $NiCl_2(TFEH)_4$ and $Ni(NCS)_2$[16]ane. Reproduction of the reassigned spectrum yields the parameter values listed below and transition energies reported in table 3.2.

$$e_\sigma(N) = 4072\ cm^{-1}$$
$$e_\sigma(NCS) = 3600\ cm^{-1}$$
$$e_\pi(NCS) = 500\ cm^{-1}$$

3.2.7: $Ni(NCS)_2$[16]ane

The CLF analysis of $Ni(NCS)_2$[16]ane is qualitatively the same as for the [15]ane analogue with the exception that the low energy spin forbidden band is better resolved. The reported assignment leads to the parameter set:

$$e_\sigma(N) = 3632\ cm^{-1}$$

$$e_\sigma(NCS) = 2600\ cm^{-1}$$

$$e_\pi(NCS) = -300\ cm^{-1}$$

Reassignment analogous to that for $Ni(NCS)_2$[15]ane gives the more reasonable parameter values shown below with acceptable reproduction of the experimental band energies (table 3.2).

$$e_\sigma(N) = 3632\ cm^{-1}$$

$$e_\sigma(NCS) = 4100\ cm^{-1}$$

$$e_\pi(NCS) = 750\ cm^{-1}$$

3.3: Discussion

The CLF analyses suggest that for the tetragonal Ni(II) complexes studied here, five d-d spectra out of seven require reassignment. The basis for these decisions is the reasonableness or otherwise of the CLF parameter values which in turn rests on the connection between the CLF parameters and the nature of the metal ligand bonding. Although the quantitative differences between the parameter values gained from the global parameterisation scheme and those gained from reanalysis of the spectrum within the CLF formalism are relatively small, they are estimated to be larger than the anticipated uncertainties in the derived values of e_λ. The principle sources of these uncertainties are the inherent approximations of the CLF formalism and the accuracy with which a d-d spectral peak energy can be assigned.

There is no doubt that the CLF scheme reproduces the experimental data as well or better than any other ligand field approach[40] but it is the detailed commentary provided by the e_λ parameters on the local electron distributions and bonding that makes the

CLF model such a powerful and useful tool. This assertion has been illustrated on many occasions.[44,45,46,65,66,67,73] The CLF model provides a consistent description of the electronic structures and metal-ligand interactions for a wide variety of transition-metal complexes. Some of this work is especially relevant here since it supports the choice of e_λ values given in table 3.1.

Complex	$e_\sigma(N)$	Ni-N	$e_\sigma(X)$	Ni-X	$e_\pi(X)$	B/F_2[a]	F_4	Σ
$NiCl_2(TFEH)_4$	4300	2.106	2480	2.444	400	1196	68	23760
$NiCl_2$[14]ane	4976	2.067	1580	2.510	240	790[b]	-	24024
$NiCl_2$[15]ane	4390	2.144	2250	2.497	575	1328	106	24360
$NiCl_2$[16]ane	3779	2.171	3100	2.482	900	1356	106	24916
$Ni(NCS)_2$[14]ane	4780	2.067	3000	2.130	100	790[b]	-	25720
$Ni(NCS)_2$[15]ane	4072	2.131	3600	2.079	500	1300	93	25488
$Ni(NCS)_2$[16]ane	3632	2.179	4100	2.077	750	1278	87	25728

[a] F_2 if value for F_4 given, otherwise B. [b] estimated value.

Table 3.1: Best-fit CLF and interelectron repulsion parameter values (cm^{-1}), metal-ligand bond lengths (Å) and CLF sum values (cm^{-1}) for tetragonal NiN_4X_2 complexes.

Many authors have analysed the spectra of tetragonal Ni(II) species.[55,75,76,77] As was mentioned in the previous chapter, a general conclusion to emerge from all the studies is the essentially linear correlation between $e_\sigma(N)$ and the equatorial Ni-N bond length over the range 2.0 to 2.3 Å.[76,77,78] The value of $e_\sigma(N)$ is determined by the $^3B_{1g} \rightarrow {}^3B_{2g}$ energy which was apparently correctly assigned for all the macrocyclic species. This is not surprising since for D_{4h} Ni(II), the $^3B_{1g} \rightarrow {}^3B_{2g}$ splitting is equal to 10 Dq so that even in the global Dq/Ds/Dt scheme, the increase in the Ni-N bond length with increasing ring size is expected to correlate with a decreasing value for

Complex	$^3B_{1g}\rightarrow$	$^3B_{2g}$	^3E_g	$^1A_{1g}$, $^1B_{1g}$	$^3A_{2g}(F)$, $^3E_g(F)$	$^3A_{2g}(P)$, $^3E_g(P)$
$NiCl_2(TFEH)_4$	obs[+]	12900	8700	8700	17400	27400
	calc	12935	8936, 9299	10146, 11209	15890,17609,17816	26967, 28077,28188
$NiCl_2$[14]ane	obs	14750*	8600	-	15200* 19400	27100,29300
	calc	14748	8457,8885	-	15156 18488,19864	26808,28005,29253
$NiCl_2$[15]ane	obs[+]	13100*	8664	11900*,12750*	14421 17602	26100,27299
	calc	13120	8736,8283	11895, 12756	15186 16963,17745	25522,26814,27534
$NiCl_2$[16]ane	obs[+]	11157	7782	13455	15758	25621
	calc	11154	8079,8510	13422	14217,15054,15604	24792,25490,25688
$Ni(NCS)_2$[14]ane	obs	14150*	11080	-	17800 20225	-
	calc	14156	11083,11427	-	17772 19301,20541	29396,29690,30814
$Ni(NCS)_2$[15]ane	obs[+]	12029*	10326	12900	15834* 18367	28514
	calc	12007	10281,10535	12825, 13000	17057 17588,17867	27736,28081,28384
$Ni(NCS)_2$[16]ane	obs[+]	10724*	9606*	12500*	16500	27063
	calc	10784	9950, 10090	12445, 12480	16049,16491,16940	27031,27135,27290

* Estimated peak energy (usually by Gaussian analysis)

[+] Spectrum reassigned

Table 2: Observed and calculated d-d transition energies for tetragonal NiN_4X_2 species. Calculated spectra use best-fit parameter values from Table 1.

10 Dq. Hence, for saturated equatorial nitrogen donors, an obvious trend is expected even for the global parameterisation scheme.

Where the global scheme breaks down is in the treatment of the axial donors. Such an approach fails to show that for the [15]ane and [16]ane complexes the apparently most obvious assignment of the d-d spectra leads to chemically unreasonable bonding parameters. In the CLF model, however, more is demanded than simply reproducing the band energies. The parameter values must also make chemical sense. The theoretical justification of the chemical relevance of e_λ parameters has been described in detail before[38], suffice to say here that, all other things being equal, chloride is not expected to behave as a π-acceptor under any circumstances. Moreover, previous CLF analyses of $Ni(NH_3)_4(NCS)_2$, $Ni(en)_2(NCS)_2$, (en = ethylenediamine), and $Ni(Tmen)_2(NCS)_2$, (Tmen = tetramethylethylenediamine) also suggest[55] that linearly coordinated isothiocyanate is not a π-acceptor towards Ni(II) either. The e_π parameters for the present systems should always be positive.

An interesting feature of the data in table 3.1 is the inverse correlation between equatorial and axial parameter values. As $e_\sigma(N)$ decreases, $e_\sigma(X)$ and $e_\pi(X)$ increase. This is an obvious example of Pauling's Electroneutrality Principle - as donation from the equatorial ligands decreases, the axial ligands donate more strongly to compensate. Similar behaviour has been observed in other tetragonal Ni(II) amine systems.[55]

Within the CLF model, Pauling's Electroneutrality Principle seems to have another important consequence. In a series of related complexes, the sum of the diagonal CLF parameter values, Σ, is approximately constant. This result has been observed empirically[44] and rationalised theoretically.[58] The so-called CLF sum rule has since been applied successfully to probe the nature of the bonding in chlorocuprates(II)[45] and represents a powerful method for reducing the degree of ambiguity in ligand field analysis. The Σ values for the present complexes are also listed in table 3.1. For the chloro species, $\Sigma = 24300 \pm 600\ cm^{-1}$ while for the isothiocyanate complexes

$\Sigma = 25600 \pm 130\ cm^{-1}$. The latter compares well with values from previous studies[55] on other Ni-NCS complexes.

The present analyses also highlight the essential difference between the CLF model and the earlier MO-based Angular Overlap Model (AOM).[83] In the AOM, the value of e_λ is proportional to the square of the appropriate diatomic overlap integral, equation 3.2,

$$e_\lambda = K_\lambda S_\lambda^2 \qquad \text{Eqn. 3.2}$$

where K is a constant and S is the appropriate overlap integral. However, the relationship has been shown to be empirically unreliable while it is theoretically invalid within the CLF formalism.[44] In the present case, for example, the AOM would predict essentially identical chloride parameter values for all three macrocyclic complexes since the Ni-Cl distances are essentially the same. The CLF model does not suffer from this restriction and predicts that the axial Cl ligands donate more strongly without shortening the bond length significantly. Similar behaviour is well known in Cu(II) complexes. For example, trigonal bipyramidal species like Cu(2,2'-bipyridyl)$_2$X, X=I,NH_3 have bipyridyl ligands spanning both axial and equatorial sites with very similar Cu-N bond lengths, yet the axial e_σ parameter is about twice as large as the equatorial value.[46] This result was correlated with the stereochemical activity of the incomplete d-shell.[51]

In the macrocyclic Ni complexes, steric interactions presumably prevent the closer approach of Cl. Figure 3.3 displays space-filling representations for $NiCl_2$[14]ane which indicate that the H atoms, especially those connected to the ring nitrogens, come into fairly close contact with the axial ligands, the average separation being 2.69 Å in the [14]ane complex. However, the demands of electroneutrality still oblige the chloride to donate more strongly as the equatorial donation weakens. In contrast, the smaller NCS ligand is able to approach more closely if required. Hence, for

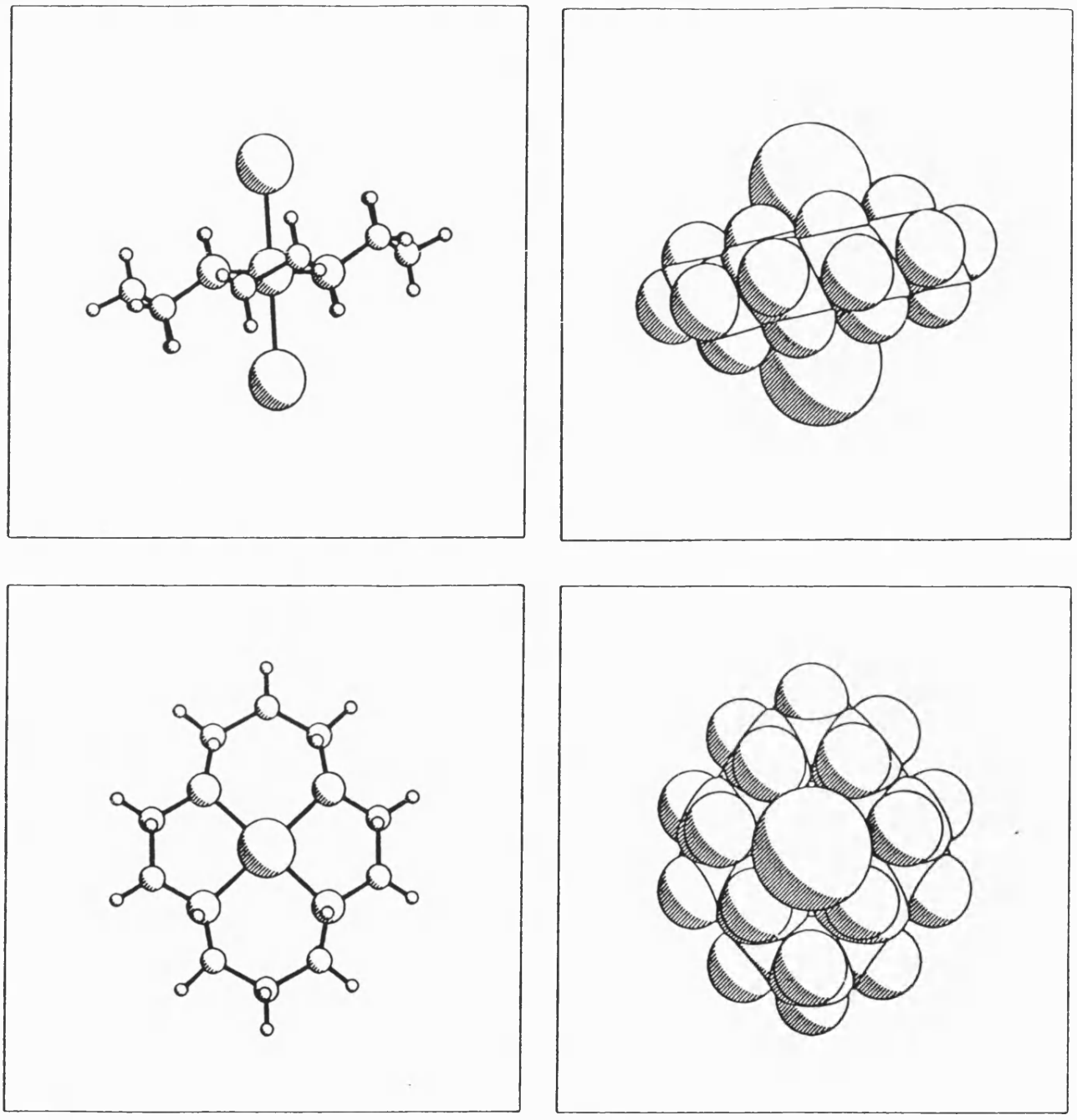

Figure 3.3: Molecular and space-filling representations of $NiCl_2$[14]ane derived from x-ray structural data (Ref. 78).

$Ni(NCS)_2$[14]ane, where the equatorial Ni-N interaction is strong and the bond length the shortest, the axial NCS donation is relatively weak and the Ni-NCS bond length is 2.130 Å. For the [15]ane complex, the equatorial donation weakens significantly and the axial bonding strengthens to compensate. Here the enhanced axial binding is accompanied by a shortening of the Ni-NCS bond from 2.130 to 2.079 Å. Thereafter, in the [16]ane complex, the steric interaction between the macrocyclic and the NCS ligands presumably prevents any further contraction of the Ni-NCS contact, which remains essentially unchanged at 2.077 Å. However, electroneutrality requires the NCS ligands in $Ni(NCS)_2$[16]ane to donate more strongly as monitored by an increase in the NCS CLF parameter values.

3.4: Conclusions

The CLF model applied to seven tetragonal Ni(II) complexes has demonstrated that the assignments of several of the d-d spectra lead to chemically unreasonable CLF parameter values. These spectra were originally analysed using a global parameterisation of the ligand field. The work reported in this chapter indicates that such schemes can give erroneous results and are therefore of limited value for interpreting the spectra of low symmetry species.

The spectra were therefore reanalysed within the CLF formalism. A self-consistent and chemically valuable description of the metal-ligand bonding in these systems emerges. In particular, the demands of the Electroneutrality Principle are evident in that as the strength of the equatorial bonding decreases, the axial ligands donate more strongly. Thus, as the equatorial CLF parameter value falls, the axial parameters increase. This interplay is monitored by the CLF sum, Σ, which, for a given set of donor atoms (i.e. N_4Cl_2 or $N_4N'_2$) remains essentially constant.

Interestingly, the significant increase in axial interaction in the series [14]ane,[15]ane to [16]ane is not accompanied by a similarly dramatic decrease in the axial bond length.

In the macrocyclic complexes, it would appear that steric interactions hold the relatively large Cl^- ligands at about the same distance for all three ring sizes. In contrast, the smaller nitrogen donor atom of NCS^- ligand initially allows for a shortening of the axial bond length from the [14]ane to the [15]ane species. Thereafter, the NCS^- too is held at the same distance for the [16]ane complex, even though the ring size has increased.

Chapter 4

The Nature of the CLFSE

4.1: Introduction

Having described in chapter 2 the method by which the CLFSE is calculated for a given species, it is now important to study the nature of this term under a variety of geometries, coordination numbers and d-configurations. The success, or otherwise, of this approach to modelling transition metals is dependant upon the ability of the additional force field term to accurately reproduce the CLFSE for a given system and, more importantly, to give appropriate CLFSE gradients as a function of ligand displacement. It is only through achieving the correct balance between CLFSE gradients and the energy gradients generated from a traditional Molecular Mechanics force field that one can hope to model transition metals effectively within a Molecular Mechanics framework by this means.

This chapter reports series of CLFSE calculations for four, five and six coordinate geometries, with and without ligand π bonding capability, for anticipated distortions from the parent geometry. As the first row transition metals are of primary importance at present, and these complexes usually display high-spin configurations, the following calculations consider d^1, d^2, d^3 and d^4 high spin configurations only. The CLFSEs calculated are therefore the same as those for d^6, d^7, d^8 and d^9 configurations respectively. Having calculated one electron orbital energies for a given species it is, of course, as trivial to calculate a CLFSE for a low-spin configuration as for a high-spin configuration and so the confines of the work reported here do not represent a limitation of the model in general. Molecular Modelling of low-spin complexes, although beyond the scope of this work, will doubtless form a significant feature of future studies.

4.2: 6-coordination

The most obvious and relevant 6-coordinate geometry to consider is, or course, octahedral. This geometry is also the most straight forward in terms of calculating the CLFSE for a given d-configuration. For O_h and D_{4h} systems the one electron orbital energies and hence CLFSE for each configuration may be derived by hand as a function of the e_λ of the coordinating ligands, as below for D_{4h}.symmetry.

Orbital energies:-

$$E(d_{Z}2) = 2e_\sigma(ax) + e_\sigma(eq)$$

$$E(d_{X}2\text{-}_{y}2) = 3e_\sigma(eq)$$

$$E(d_{xz}) = 2e_\pi(ax) + 2e_\pi(eq)$$

$$E(d_{yz}) = 2e_\pi(ax) + 2e_\pi(eq)$$

$$E(d_{xy}) = 4e_\pi(eq)$$

In order to calculate CLFSEs, the energies of these orbitals must be expressed relative to the bari-centre (B.C.), thus ensuring that the CLFSE for high-spin d^5 and d^{10} configurations is zero.

$$\text{Bari Centre} = 1/5(2e_\sigma(ax)+4e_\sigma(eq)+4e_\pi(ax)+8e_\pi(eq))$$

CLFSEs:-

for an orbital energy ordering appropriate for an axial elongation, and positive e_π parameters,

$$d^1 = E(d_{xz,yz}) - B.C.$$

$$= 6/5e_\pi(ax) + 2/5e_\pi(eq) - 2/5e_\sigma(ax) - 4/5e_\sigma(eq)$$

$$d^2 = 2\{E(d_{xz,yz}) - B.C.\}$$

$$= 12/5e_\pi(ax) + 4/5e_\pi(eq) - 4/5e_\sigma(ax) - 8/5e_\sigma(eq)$$

$$
\begin{aligned}
d^3 &= 2\{E(d_{xz,yz}) - B.C.\} + \{E(d_{xy}) - B.C.\} \\
&= 8/5e_{\pi}(ax) + 16/5e_{\pi}(eq) - 6/5e_{\sigma}(ax) - 12/5e_{\sigma}(eq) \\
d^4 &= 2\{E(d_{xz,yz}) - B.C.\} + \{E(d_{xy}) - B.C.\} + \{E(d_{z2}) - B.C.\} \\
&= 4/5e_{\pi}(ax) + 8/5e_{\pi}(eq) + 2/5e_{\sigma}(ax) - 11/5e_{\sigma}(eq)
\end{aligned}
$$

Due to the local parameterisation and the subtraction of the bari-centre from the orbital energies, these relationships appear complex and of little obvious relevance to traditional crystal field schemes. Familiar relationships emerge, however, if the parameters are expressed in a global sense. For example, if the system is defined as a regular octahedron of six identical ligands, i.e. $e_{\lambda}(ax) = e_{\lambda}(eq)$, then the CLFSEs may be expressed as fractions of Δ_{oct} , where Δ_{oct} is the octahedral ligand field splitting.

$$\Delta_{oct} = 3e_{\sigma} - 4e_{\pi}$$

Substitution of this expression into the above equations yields the following relationships,

$$
\begin{aligned}
d^1 &= -2/5\ \Delta_{oct} \\
d^2 &= -4/5\ \Delta_{oct} \\
d^3 &= -6/5\ \Delta_{oct} \\
d^4 &= -3/5\ \Delta_{oct}
\end{aligned}
$$

as expected from crystal field theory. What is note-worthy here from a Molecular Mechanics point of view, is the dependence of the CLFSEs as a function of metal ligand bond length. As the M-L bond lengths decrease there will be a corresponding increase in e_{λ}, with e_{σ} increasing more rapidly than e_{π}, typically $0.2 < e_{\pi}/e_{\sigma} < 0.25$. As a consequence Δ_{oct} will increase and hence the CLFSE for all d-configurations will

also increase in magnitude as bond lengths shorten. The rate of increase of CLFSE will, of course, be dependant upon the functional form of e_λ versus bond length and the d-configuration.

Of greater interest is the behaviour of the CLFSE as a function of octahedral distortion, the most common distortion being axial elongation or compression. This distortion is now considered for all d-configurations for a variety of ligand types.

4.2.1: No π-bonding

In the absence of π bonding the only orbitals of interest are the e_g set, d_z2 and $d_x2\text{-}y2$. The t_{2g} set remains unperturbed by the axial ligands, the energy of this orbital set being equal to the negative of the bari-centre. The CLFSE for the d^1, d^2 and d^3 configurations is therefore simply equal to one, two and three times the negative of the bari-centre respectively. For a d^4 configuration the CLFSE is equal to the negative of the energy of the highest energy orbital relative to the bari-centre, a useful conceptual relationship that can be shown to be true for all geometries and coordination numbers. For a given set of five bari-centred orbitals, of energy E_1, E_2, E_3, E_4 and E_5, the d^4 CLFSE is given by

$$\begin{aligned} d^4 \text{ CLFSE} &= E_1 + E_2 + E_3 + E_4 \\ &= E_1 + E_2 + E_3 + E_4 + E_5 - E_5 \end{aligned}$$

as the orbitals are bari-centred, $E_1 + E_2 + E_3 + E_4 + E_5 = 0$

thus

$$d^4 \text{ CLFSE} = - E_5$$

This relationship to the highest energy orbital is most important in terms of the Jahn-Teller effect. If, as a function of axial elongation, only the e_σ(ax) parameter changes as a consequence of the lengthening of the axial bond length, the d^4 CLFSE will change

only as a result of the lowering of the bari-centre energy for the system due to the decreasing value of e_σ(ax). This situation would yield an orbital energy change as shown below, figure 4.1.

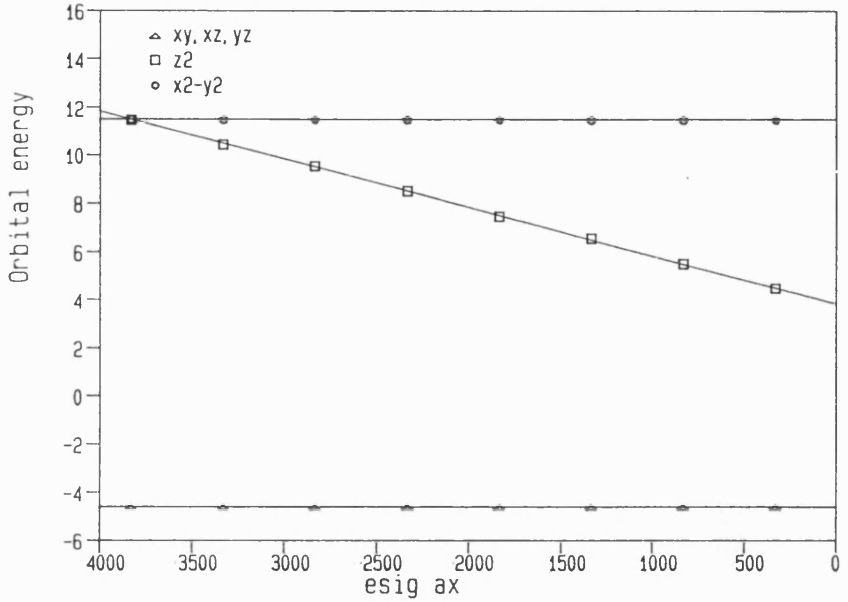

Figure 4.1: Orbital energies as a function of e_σ(ax), for an octahedral species, without π bonding, without a constant CLF Σ value. Orbital energy scale in units of 1000 cm^{-1}, e_σ(ax) in units of cm^{-1}.

This is obviously an unsatisfactory situation, in contravention of the Jahn-Teller theorem, which states that the bari-centre for the e_g orbitals should remain constant. This results in an underestimation of the CLFSE for a d^4 configuration. In addition, the CLFSE for d^1, d^2 and d^3 configurations would increase in magnitude as a function of axial compression, as this would increase the energy of the 'global' bari-centre. This distortion can be reproduced appropriately, however, if the CLF sum remains constant thereby maintaining the 'global' bari centre. If a linear relationship between e_σ(L) and the bond length is assumed, and hence the change in e_σ(L) directly reflects the notional change in bond length, it is possible to reproduce a first order type Jahn-Teller effect. As e_σ(ax) decreases (or increases for an axial compression), e_σ(eq) increases (or

decreases for a compression) to maintain the CLF sum, and this models a concerted distortion along the Jahn-Teller active vibration mode. This gives the orbital energies and CLFSEs shown in figures 4.2 and 4.3, as a function of $e_\sigma(ax)$ for an elongation. The displayed behaviour is as anticipated for a first-order type Jahn-Teller distortion, the d^4 CLFSE showing no preference for either elongation or compression. The same is not true, however, if either the sum is not kept constant or if the d^4 CLFSE is plotted as a function of axial bond length, using the functional form of e_λ versus bond length described in chapter 2. If the sum is not maintained then the following expressions describe the change of d^4 CLFSE as a function of the change in $e_\sigma(ax)$, δ, from the octahedral value.

Octahedral: d^4 CLFSE = $-(3e_\sigma - 6/5e_\sigma)$

Elongation: d^4 CLFSE = $-(3e_\sigma - 6/5e_\sigma + 2/5\delta)$

Compression: d^4 CLFSE = $-(3e_\sigma - 6/5e_\sigma + 8/5\delta)$

Axial compression is therefore favoured over elongation if the sum is not maintained. The same behaviour results if the distortion is considered as a function of axial bond length, even if the sum is kept constant. In this case, the r^{-5} dependence of $e_\sigma(L)$ versus bond length causes a larger $d_{Z^2} - d_{X^2-Y^2}$ splitting for a compression than for an elongation for the same magnitude of axial bond length change from the parent octahedral geometry, and hence a larger magnitude of d^4 CLFSE results. Again, the relationship may be expressed analytically as a function of the change in $e_\sigma(ax)$, δ.

$$d^4 \text{ CLFSE} = -(3e_\sigma - 6/5e_\sigma + 3/2\delta)$$

delta being larger for a compression than for an elongation for the same magnitude of bond length change.

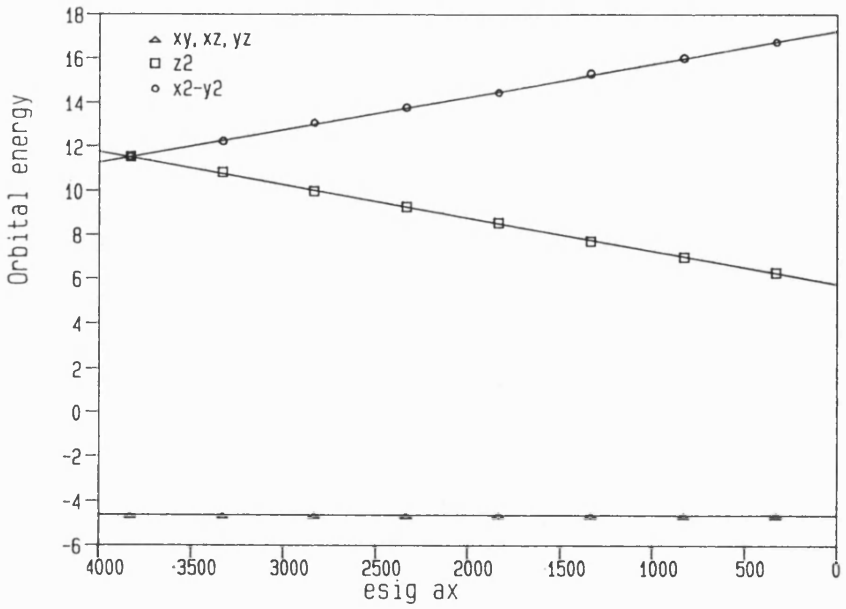

Figure 4.2: Orbital energies as a function of $e_\sigma(ax)$, for an octahedral species, without π bonding, with a constant CLF Σ value. Orbital energy scale in units of 1000 cm^{-1}, $e_\sigma(ax)$ in units of cm^{-1}.

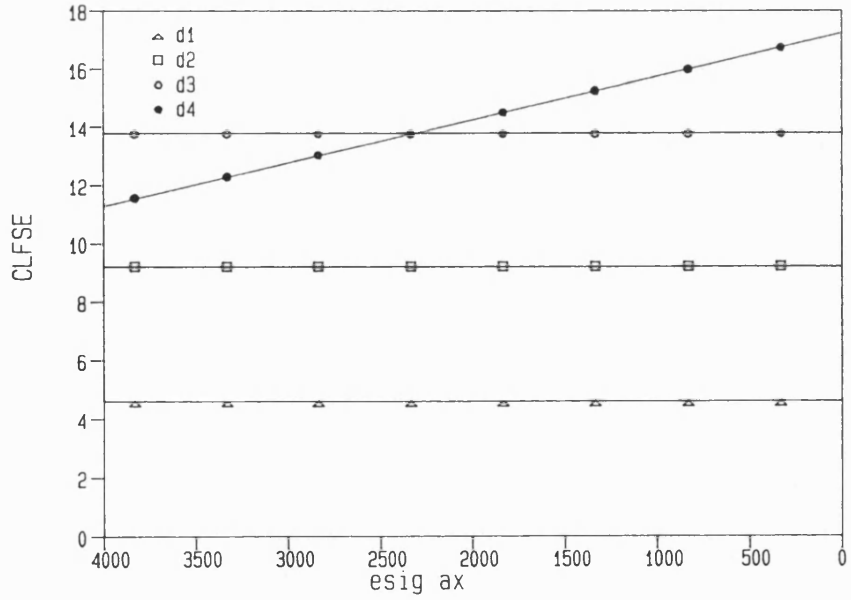

Figure 4.3: Magnitude of the CLFSE as a function of $e_\sigma(ax)$, for an octahedral species, without π bonding, with a constant CLF Σ value. CLFSE scale in units of 1000 cm^{-1}, $e_\sigma(ax)$ in units of cm^{-1}.

4.2.2: Equatorial or axial π bonding

If a π bonding capability is included for either the axial or equatorial ligands, the degeneracy of the t_{2g} orbital set is raised. The behaviour of the component orbitals of this set is, of course, dependent upon whether π bonding has been introduced to the axial or equatorial ligands.

If axial π bonding is introduced, with the sum remaining constant, the d_{xy} orbital remains unperturbed by the ligand field and hence remains at an energy equal to the negative of the bari-centre. The d_{xz} and d_{yz} orbitals increase in energy for π donors relative to the d_{xy} orbital and the e_g pair are reduced in energy in order to keep the sum and hence the 'global' bari-centre constant. As a consequence, the d^1 CLFSE does not change as a result of the introduction of axial π bonding, but the d^2, d^3 and d^4 CLFSEs are reduced in magnitude. If equatorial π bonding is introduced, all three orbitals of the former t_{2g} orbital set increase in energy, with the d_{xy} orbital increasing in energy twice as quickly as the d_{xz} and d_{yz} orbitals as a function of $e_{\pi}(eq)$. Again the e_g pair of orbitals are reduced in energy. The CLFSE for all d-configurations is reduced as the proportion of equatorial pi bonding is increased.

The effect of inclusion of axial or equatorial π bonding upon the CLFSE as a function of axial elongation is now considered.

If axial π bonding is included at a fixed ratio to the axial σ parameter, and the sum is kept constant as $e_{\sigma}(ax)$ decreases, the $d_{Z}2$ and d_{xz} and d_{vz} orbitals decrease in energy. The $d_{X}2_{-y}2$ orbital increases in energy in order to satisfy the requirement of maintaining the sum and hence increases in energy at the same rate as the total decrease in energy of the $d_{z}2$, d_{xz} and d_{yz} orbitals. The result of this decrease in energy of the d_{xz} and d_{yz} orbitals is to increase the magnitude of the CLFSE for the d^2 and d^3 configurations. The d^1 CLFSE remains constant, as the lowest energy orbital, d_{xy}, is unaffected by either the change in axial field or by the increase in $e_{\sigma}(eq)$ to maintain the sum. The d^4 CLFSE again increases in magnitude as a function of axial elongation,

but the rate of increase as a function of $e_\sigma(ax)$ is greater than in the absence of axial π bonding. This is due to maintaining a constant sum. As $e_\sigma(ax)$ decreases, $e_\pi(ax)$ also decreases and hence $e_\sigma(eq)$ must increase to compensate for the fall in both axial parameters. Hence, for a decrease of δ in $e_\sigma(ax)$ and assuming $e_\pi(ax) = 1/5\ e_\sigma(ax)$, a decrease of $1/5\delta$ occurs in $e_\pi(ax)$ and an increase of $7/10\delta$ results in $e_\sigma(eq)$, as opposed to an increase of $1/2\delta$ in the absence of π bonding. This leads to an increase in the d^4 CLFSE of $21/10\delta$ as opposed to $3/2\delta$.

If equatorial π bonding is included at a fixed ratio to $e_\sigma(eq)$, as $e_\sigma(ax)$ decreases the sum is now maintained by both $e_\sigma(eq)$ and $e_\pi(eq)$ which yields an increase in energy of all orbitals except $d_{Z}2$, while the d_{xy} orbital increases at twice the rate of the d_{xz} and d_{yz} orbitals, as one would expect. In terms of CLFSEs, this has the effect of decreasing the magnitude of CLFSE for the d^1, d^2 and d^3 configurations, while the d^4 CLFSE again increases as a function of elongation. However, the rate of d^4 CLFSE increase is now less than that in the absence of π bonding, for the converse of the reason outlined for the presence of axial π bonding. The reduction in $e_\sigma(ax)$ is now 'shared' between $e_\sigma(eq)$ and $e_\pi(eq)$, and consequently the $d_{X}2_{-y}2$ orbital increases in energy by $5/14\delta$, where δ is again the change in $e_\sigma(ax)$ and assuming that $e_\pi(eq) = 1/5\ e_\sigma(eq)$. This yields a change in d^4 CLFSE of $15/14\delta$.

4.2.3: Equatorial and Axial π Bonding

If a π bonding capability is introduced for both the axial and equatorial ligands one returns to the familiar octahedral orbital pattern. However, with the inclusion of π bonding one now has a mechanism by which the degeneracy of the t_{2g} orbital set may be raised, the d^1 and d^2 configurations both displaying potential Jahn-Teller activity. As for the e_g orbital set, this degeneracy may be lifted by axial elongation or compression. If the sum is maintained as the distortion progresses, the d^1, d^2 and d^4 CLFSEs all increase in magnitude as a function of both compression and elongation,

with the d^4 CLFSE being dependant only upon the magnitude of change of $e_\sigma(ax)$ rather than the sense of the distortion. This is not the case however for the d^1 and d^2 configurations. For d^1, compression is preferred over elongation as this gives a t_{2g} splitting pattern with the d_{xy} orbital reduced in energy whilst the d_{xz} and d_{yz} orbitals increase in energy. As the t_{2g} bari-centre is maintained this gives a larger CLFSE than for an elongation. The converse is true of the d^2 configuration, which shows a preference for elongation. These observations are as anticipated from simple Jahn-Teller predictions. The change in CLFSE for the d^1, d^2 and d^4 configurations may again be described in terms of δ, the change in e_σ for a notional octahedral precursor, for $e_\pi = 1/5\ e_\sigma$ and a constant sum.

d^1

compression

$$\begin{aligned} CLFSE &= 4e_\pi(eq) - 1/5\ (2e_\sigma(ax) + 4e_\sigma(eq) + 4e_\pi(ax) + 8e_\pi(eq)) \\ &= 4/5\ e_\sigma - 2/5\ \delta - 1/5\ (6e_\sigma + 12\ e_\pi) \end{aligned}$$

elongation

$$\begin{aligned} CLFSE &= 2e_\pi(eq) + 2e_\pi(ax) - 1/5\ (2e_\sigma(ax) + 4e_\sigma(eq) + 4e_\pi(ax) + 8e_\pi(eq)) \\ &= 4/5\ e_\sigma - 1/5\ \delta - 1/5\ (6e_\sigma + 12\ e_\pi) \end{aligned}$$

d^2

compression

$$\begin{aligned} CLFSE &= 4e_\pi(eq) + 2e_\pi(eq) + 2e_\pi(ax) - 2/5\ (2e_\sigma(ax) + 4e_\sigma(eq) + 4e_\pi(ax) \\ &\quad +8e_\pi(eq)) \\ &= 8/5\ e_\sigma - 1/5\ \delta - 2/5\ (6e_\sigma + 12\ e_\pi) \end{aligned}$$

elongation

$$\begin{aligned} CLFSE &= 2\ (2e_\pi(eq) + 2e_\pi(ax)) - 2/5\ (2e_\sigma(ax) + 4e_\sigma(eq) + 4e_\pi(ax) \\ &\quad +8e_\pi(eq)) \\ &= 8/5\ e_\sigma - 2/5\ \delta - 1/5\ (6e_\sigma + 12\ e_\pi) \end{aligned}$$

d^4

$$CLFSE = -\{3e_\sigma - 3/2\ \delta - 1/5\ (6e_\sigma + 12\ e_\pi)\}$$

The expression for the d^4 CLFSE is similar to that derived for the distortion in the absence of π bonding, and shows the same energetic gradients with respect to δ even though the overall magnitude of the CLFSE is smaller due to the inclusion of π bonding. A six coordinate species that includes metal-ligand π bonding will therefore show Jahn-Teller activity to the same extent as a σ-only complex, provided that the functional form of e_λ vs bond length is the same. This is because individual bari-centres are maintained for the e_g and t_{2g} orbital sets, rather than just the 'global' bari-centre as achieved for the cases displaying either axial or equatorial π bonding only.

Two main conclusions can be drawn from the observations so far. Firstly, it would appear that to reproduce a first order Jahn-Teller type distortion from a regular octahedral geometry one must keep the CLF sum constant as the distortion progresses. Within a Molecular Mechanics framework this would mean devising some mechanism by which the sum would remain constant from iteration to iteration. Implementation of such a scheme would be a mistake, however, as in the absence of π bonding the d^1, d^2 and d^3 CLFSEs are equal to the negative of the bari-centre. If the bari-centre remained constant from iteration to iteration then the CLFSE for these configurations would no longer increase as a function of shortening bond length, it would simply remain unchanged - an obviously erroneous result. In addition, the sum would remain at the value appropriate for the starting geometry, thereby placing an unacceptable constraint upon the starting coordinates for a Molecular Mechanics calculation. The distortion must therefore be allowed to follow the path determined by the CLFSE derivatives as calculated without any consideration of the sum. These derivatives, unlike the magnitude of the CLFSE, are independent of the sum and hence the starting geometry

will not influence the result of the minimisation of the force field energy terms as would be the case if the sum remained constant.

The second conclusion also concerns the Jahn-Teller effect. It has been shown that for all the coordination environments considered here, the d^4 CLFSE either shows no preference for either elongation or compression, or favours a compressed geometry, most notably when the distortion is considered as a function of bond length rather than axial e_λ . In contrast, almost all Cu(II) complexes display an axially elongated geometry. This does not represent a failing of the CLFSE term, however, nor is this observation unique to this treatment of metal centres. First order Jahn-Teller theory suggests that a compressed-tetragonal geometry is just as likely as the elongated stereochemistry, whilst more sophisticated treatments including the extension to second order of the electronic term in the total potential energy expression are found to stabilise a compressed rather than an elongated geometry[84,85]. A number of workers have independently suggested that the elongated-tetragonal geometry characteristic of six-coordinate copper(II) complexes results from configuration interaction between the 4s and $3d_{z^2}$ metal orbitals[86-88]. In the D_{4h} symmetry of planar complexes the 4s and $3d_{z^2}$ functions both transform as a_{1g} and so can mix, studies of Cu(II) systems[89] having demonstated that such mixing is extensive enough to depress the energy of the $3d_{z^2}$ orbital by up to 6000 cm^{-1} relative to its energy as predicted by various ligand field models based solely upon the 3d orbital basis. The CLF model is capable of modelling such effects by the use of negative values of $e_\sigma(L)$ for distant ligands that effectively form coordination voids, as described in chapter 2. It is therefore feasible, that the CLFSE term, with its ability to model the d-s mixing that is suggested to be responsible, at least in part, for the preference of octahedral Cu(II) species to show axial elongation rather than compression, will predict lower energies for elongated structures than for compressed structures despite the preference for compression indicated earlier on the basis of the CLFSE energy gradients.

What is clearly indicated here is that for a d^4 configuration, a regular octahedral geometry forms an energetic maximum in the CLFSE, indicative of the Jahn-Teller instability of such a system. Considering this distortion as a concerted mechanism may, however, be slightly misleading. The Jahn-Teller active vibrational mode of a d^9 metal ion, to first order, may be described as ligand movement such that the axial bond length increases at twice the rate at which the equatorial bond length decreases, this ratio of bond length change being maintained until an energetic minimum is reached. It is this type of ligand movement that is simulated in the preceding calculations. Such a movement of the ligands as the distortion proceeds cannot be reproduced within a Molecular Mechanics simulation, however. In the MM treatment, energy derivatives are calculated for each atom, either analytically or numerically, and the atomic coordinates are modified according to the sense and magnitude of those derivatives. Consequently, the active vibration mode will only be followed if the CLFSE derivative for the axial ligands is twice that of the equatorial ligands and opposite in sense. This is not the case however. If one considers a slightly axially elongated d^9 system, by way of example, the CLFSE derivatives may be evaluated for both the axial and equatorial ligands. A reduction in the axial e_σ parameter value , δ, yields an increase in CLFSE of 1/5 δ, as a consequence of lowering the bari-centre to which the highest energy orbital, $d_{x^2-y^2}$, is referred to. For the same change in the equatorial e_σ the $d_{x^2-y^2}$ orbital increases in energy by 3 δ whilst the bari-centre increases by 4/5 δ. This gives an increase in CLFSE of 9/5 δ. The equatorial bond lengths therefore shorten some nine times more quickly than the axial bond lengths lengthen. If this is related to a change in bond length rather than parameter value then the effect is even more dramatic as for a given magnitude of bond length change, the change in equatorial parameter will be larger than that for the axial parameter due to the r^{-5} parameter dependence upon bond length. It must be remembered, however, that these are the CLFSE derivatives only, and within a Molecular Mechanics treatment there will at least be a bond stretch term

derivative to consider in addition, which, for the Morse function appropriate to describe large deviations from equilibrium bond length, is asymmetric with respect to the deformation of a bond from its equilibrium value. The inclusion of such an asymmetric term may well produce net gradients that allow the movement of atoms within an energy minimisation to follow the Jahn-Teller active vibration mode more accurately, or at least to yield an appropriate structure when energy minimisation is complete.

By way of summary, the d^4 CLFSE increases in magnitude, becoming more negative, for both axial compression and elongation, and although it would appear that compression is favoured under certain circumstances it must be remembered that the CLFSE is not the only term to be considered. Other factors such as atomic charges, Van Der Waal's non-bonding interactions, traditional bond stretching terms and physical restraints upon the movement of ligands from the remainder of the molecule will also be important in determining the atomic derivatives and consequently the minimum energy geometry of a complex.

4.3: 5-coordination

The most relevant 5-coordinate geometry for these studies is trigonal bipyramidal. This geometry is considered here with and without metal-ligand π bonding, and the behaviour of the CLFSE for all d configurations is monitored as a function of axial elongation and compression. Potential Jahn-Teller distortions are also investigated. The only other 5-coordinate geometry that may be of interest is square pyramidal, but this geometry does not warrant special study here, not least because it may be considered as a special case of the octahedral based geometries already discussed.

For a trigonal bipyramidal geometry it is considerably more complex to write analytical expressions for the one electron orbital energies and consequently CLFSEs than for D_{4h} species. However, similar empirical relationships do emerge, which may also be

rationalised analytically. For example, the CLFSE for all configurations will again increase in magnitude as a function of shortening of the metal-ligand bond lengths, and the CLFSE for all d configurations is reduced if π bonding is included for all ligands. These observations will presumably be true of all geometries.

The effect of axial compression and elongation are now considered with and without ligand π bonding capability.

4.3.1: No π-bonding

Figures 4.4 and 4.5 show the effect upon CLFSE as the axial ligand moves from an elongated geometry to a compressed stereochemistry as monitored by $e_\sigma(ax)$. The sum is kept constant at 23,000 cm^{-1} so that the bari-centre remains constant. This may seem anomalous from the discussion of the results for six coordinate species, but this requirement is included here not so as to attempt reproduce any concerted distortion mechanism but to maintain the 'global' bari-centre to prevent any change of CLFSE as a consequence of changing bari-centre. The resultant energy gradients are therefore the result of the effect of changing parameter values upon the orbital energies, which in turn are not complicated by the effect of changing bari-centres.

As can be seen in figure 4.4, the d-orbitals split into three groups. The d_{xz} and d_{yz} orbital pair are at lowest energy, unperturbed by the ligand field in the absence of π bonding. The energy of these orbitals does not change as the distortion from an axially compressed to elongated geometry progresses. The next highest energy pair, the d_{xy} and $d_{x^2-y^2}$ orbitals, decrease in energy as the axial ligands donate more strongly and consequently the equatorial ligands donate less strongly to maintain the sum. The highest energy orbital, the d_{z^2} orbital, increases in energy as $e_\sigma(ax)$ increases, the rate of increase being twice the rate of decrease in energy of the d_{xy} and $d_{x^2-y^2}$ orbitals due to maintaining a constant sum through the distortion. Figure 4.5 shows the behaviour of the CLFSEs. The d^1 and d^2 CLFSEs do not change as a function of the axial parameter

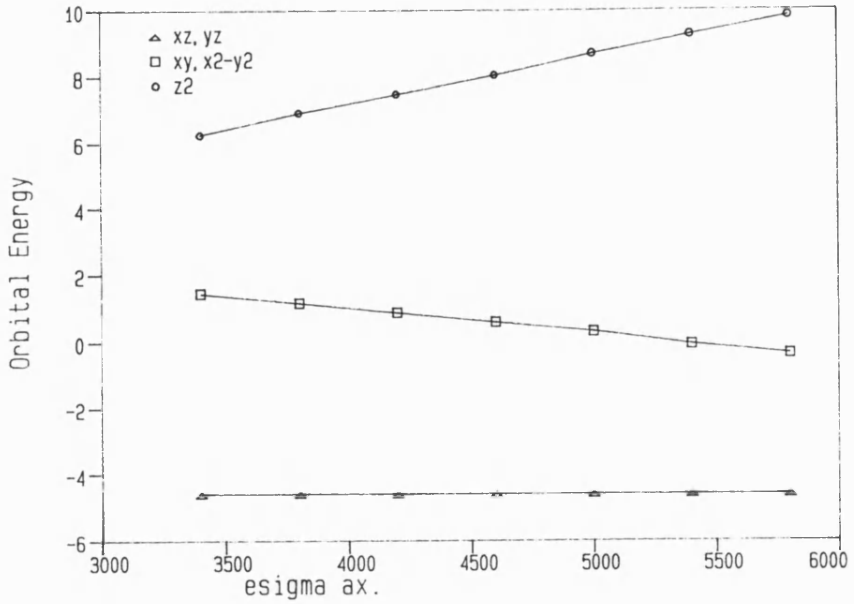

Figure 4.4: Orbital energies as a function of $e_\sigma(ax)$, for a trigonal bipyramidal species, without π bonding, with a constant CLF Σ value. Orbital energy scale in units of 1000 cm^{-1}, $e_\sigma(ax)$ in units of cm^{-1}.

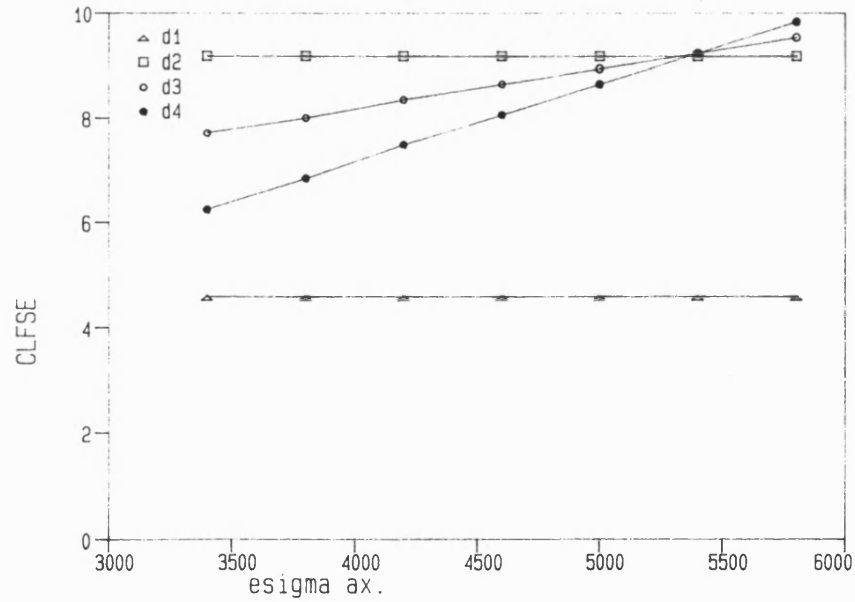

Figure 4.5: Magnitude of the CLFSE as a function of $e_\sigma(ax)$, for a trigonal bipyramidal species, without π bonding, with a constant CLF Σ value. CLFSE in units of 1000 cm^{-1}, $e_\sigma(ax)$ in units of cm^{-1}.

of course, since the two lowest energy orbitals do not change in energy, while the d^3 and d^4 CLFSEs increase in magnitude as the distortion progresses, reflecting the decrease in energy of the d_{xy} and $d_{x^2-y^2}$ orbitals. It is interesting to note that the d^2, d^3 and d^4 configurations have a common CLFSE value for $e_\sigma(ax) = 5400\ cm^{-1}$. This is of numerical rather than chemical interest however, as this occurs when the d_{xy} and $d_{x^2-y^2}$ orbitals have a zero energy. The d^2, d^3 and d^4 CLFSEs are equal to $2E_1$, $2E_1 + E_2$ and $2E_1 + 2E_2$ respectively where E_1 is the energy of the d_{xz} and d_{yz} orbitals and E_2 is the energy of the d_{xy} and $d_{x^2-y^2}$ orbitals. When $E_2 = 0$, the CLFSEs for these three configurations are obviously equal.

4.3.2: Axial or Equatorial π Bonding

If a positive axial π bonding capability is introduced the d_{xz} and d_{yz} orbitals are now perturbed by the ligand field. The immediate effect of this is to reduce the CLFSE for all configurations for a constant sum. As a function of axial compression and elongation, the most obvious difference that is made by the presence of axial π bonding is that the energy of the d_{xz} and d_{yz} orbitals increases as $e_\sigma(ax)$ increases. This causes the d^1 and d^2 CLFSEs to decrease as a function of increasing $e_\sigma(ax)$. The less obvious consequence of introducing axial π bonding is that the energy of the d_{xy} and $d_{x^2-y^2}$ orbitals decreases more quickly than in the absence of π bonding. As the $e_\sigma(ax)$ increases, so does $e_\pi(ax)$, and hence $e_\sigma(eq)$ must decrease in order to maintain the sum. Since the total axial contribution to the sum will increase more rapidly if π bonding is present, $e_\sigma(eq)$ must therefore decrease more rapidly than in the absence of π bonding. As a consequence, the d_{xy} and $d_{x^2-y^2}$ orbitals decrease in energy more quickly. The d^3 and d^4 CLFSEs are thus effected in two ways. If the orbital energies are again expressed as E_1 and E_2, the d^3 and d^4 CLFSEs are $2E_1 + E_2$ and $2E_1 + 2E_2$ respectively, these two CLFSEs are affected by both the increase in energy of E_1 and by the decrease in energy of E_2, but by differing amounts due to the different orbital

occupancies. As the rate of change in energy of the d_{xy} and $d_{x^2-y^2}$ orbitals is greater than twice that of the d_{xz} and d_{yz} orbitals, the d^3 CLFSE increases in magnitude as a function of axial elongation in the presence of axial π bonding, as does the d^4 CLFSE, albeit at a greater rate than d^3 due to the double occupancy of the d_{xy} and $d_{x^2-y^2}$ orbital pair. When compared with the rate of CLFSE increase in the absence of π bonding it is apparent that the d^3 and d^4 CLFSEs increase more slowly if axial π bonding is included than if there is no π bonding, as a function of $e_\sigma(ax)$. This is easily rationalised for the d^4 case as, due to the inclusion of axial π bonding, the $e_\sigma(eq)$ value falls more rapidly than in the absence of π bonding as $e_\sigma(ax)$ increases. Since $e_\sigma(eq)$ contributes to the energy of the d_{z^2} orbital, and the other contribution to the orbital energy, $e_\sigma(ax)$, is defined as increasing at the same rate, the energy of the d_{z^2} orbital increases more slowly if axial π bonding is present. Since this orbital is the highest in energy the d^4 CLFSE increases in magnitude at the same rate as that orbital. The d^3 configuration is more difficult to rationalise, but the d^3 CLFSE will increase more slowly in the presence of axial π bonding than in the absence of π bonding if the difference in the rate of decrease in energy as a function of $e_\sigma(ax)$ of the d_{xy,x^2-y^2} orbital pair for the two situations is less than twice the rate at which the $d_{xz,yz}$ orbital pair increase in energy as a function of $e_\sigma(ax)$ in the presence of axial π bonding. This may be expressed analytically, in terms of the change in $e_\sigma(ax)$, δ, again assuming that $e_\pi(L) = 1/5\ e_\sigma(L)$. The rate of change of orbital energies are 2/5 δ, -21/20 δ and 13/10 δ for the $d_{xz,yz}$, d_{xy,x^2-y^2} and d_{z^2} orbitals respectively. This gives CLFSE gradients for d^3 and d^4 configurations of 1/4 δ and 13/10 δ respectively compared with 3/4 δ and 3/2 δ in the absence of π bonding.

The effect of the introduction of equatorial π bonding is now considered. The d_{xz} and d_{yz} orbitals are again perturbed by the π bonding capability, as are the d_{xy} and $d_{x^2-y^2}$ orbitals, causing all CLFSEs to be smaller in magnitude than in the absence of π

bonding. However, when distortion is considered differences between the effect of the two types of π bonding emerge. As the axial bond length decreases and $e_\sigma(ax)$ increases, the sum is maintained by a decrease in both equatorial parameters. The result of this is to lower the energy of the d_{xz} and d_{yz} orbitals. This yields an increase in d^1 and d^2 CLFSE as a function of axial elongation. The d_{xy} and $d_{x^2-y^2}$ orbitals also decrease in energy, but at a lesser rate than in the absence of π bonding as the role of maintaining the sum is 'shared' between equatorial σ and π parameters, although $e_\pi(eq)$ also contributes to the energy of this orbital pair. Again, the d^3 and d^4 CLFSEs increase in magnitude as $e_\sigma(ax)$ increases, but more rapidly than in the absence of π bonding. This is again most easily rationalised for the d^4 CLFSE in terms of the rate of change of energy of the d_{z^2} orbital. As $e_\sigma(ax)$ increases the sum is maintained by both $e_\sigma(eq)$ and $e_\pi(eq)$. Thus, for a given increase in $e_\sigma(ax)$, the corresponding reduction in $e_\sigma(eq)$ is less than that in the absence of π bonding. Consequently the energy of the d_{z^2} orbital increases more rapidly yielding a greater increase in magnitude of d^4 CLFSE than in the absence of π bonding. The d^3 CLFSE will increase more rapidly in the presence of equatorial π bonding than without π bonding if the energy of the $d_{xz,yz}$ orbital pair increases at less than half the difference in the rate at which the d_{xy,x^2-y^2} orbital pair decreases in energy with and without equatorial π bonding. This may again be expressed analytically in terms of δ, the change in $e_\sigma(ax)$, assuming that $e_\pi(L) = 1/5\ e_\sigma(L)$. The rate of change of orbital energies are -1/7 δ, -19/28 δ and 23/14 δ for the $d_{xz,yz}$, d_{xy,x^2-y^2} and d_{z^2} orbitals respectively. This gives d^3 and d^4 CLFSE gradients of 27/28 δ and 23/14 d respectively, compared again with 3/4 δ and 3/2 δ in the absence of π bonding.

4.3.3: Equatorial and Axial π bonding

If π bonding is introduced for all ligands the resulting CLFSEs for all configurations are smaller in magnitude than for all the other situations considered here, due to an

overall reduction in the orbital splitting magnitudes. In terms of distortion, as $e_\sigma(ax)$ and consequently $e_\pi(ax)$ increase, the sum is maintained by both $e_\sigma(eq)$ and $e_\pi(eq)$. This causes the $d_{xz,yz}$ orbital pair to increase in energy and so the d^1 and d^2 CLFSEs decrease in magnitude accordingly. The d_{xy,x^2-y^2} orbital pair decreases in energy, but at a greater rate than in the absence of π bonding. In the absence of π bonding the rate of decrease in energy of this orbital is equal to 3/4 δ, where δ is the change in $e_\sigma(ax)$, whereas in the presence of π bonding for all ligands this relationship becomes 3/4 + 1/5 δ, from the change in $e_\sigma(eq)$ and $e_\pi(eq)$ respectively, assuming that $e_\pi(L) = 1/5\ e_\sigma(L)$. The energy of the d_z^2 orbital increases by 3/2 δ, the same rate as in the absence of π bonding. Consequently, the d^4 CLFSE changes at the same rate as without π bonding, whereas the d^3 CLFSE increases by $\{(3/4 + 1/5) - 2(2/5\text{-}1/5)\}\delta = 11/20\ \delta$, less than the rate of 3/4 δ in the absence of π bonding.

These calculations show that for all coordination environments considered here, axial compression is favoured for d^3 and d^4 configurations, and a regular trigonal bipyramidal geometry does not represent an energetic maximum, unlike the regular geometry for octahedral species. For d^1 and d^2 configurations the preference appears to be for either elongation or compression depending upon the particular coordination environment. This correlates well with previous CLF studies of 5-coordinate species[51]. The structures of the 5-coordinate complexes of Ni(II) and Cu(II) of the form $[M(Me_6tren)Br]^+$, where Me_6tren represents tris(2-dimethylaminoethyl)amine, have been rationalised in terms of axial 'holes' in the d-orbital electron density, due to the single occupation of the d_z2 orbital, leading to a preference for a compressed geometry. The same paper also reports CLF studies for analogous complexes of Fe(II) and Co(II), which display elongated geometries. These structures may be rationalised in terms of simple VSEPR theory which would suggest an elongated geometry in the absence of ligand field effects, but from the work reported here for axial π bonding the observed

geometry may also be attributed in part to the increase in CLFSE for d^1 and d^2 configurations for such a set of coordinating ligands.

The preferences for the sense of axial distortion reported here may be considered as being the result of maximising the CLFSE as a function of ligand displacement. However, there is also the potential for Jahn-Teller activity for d^1 and d^3 configurations as these systems display orbitally degenerate ground terms. This degeneracy is not raised as a consequence of axial distortion. For the d^1 configuration the orbitals in question are the d_{xz} and d_{yz}, for the d^3 configuration they are the d_{xy} and $d_{x^2-y^2}$ orbitals. Obviously the orbital degeneracy displayed by the d^3 configuration will be unaffected by the axial ligand field, whilst for the d^1 case, due to the effect of holohedral symmetry, the degeneracy will be unaffected by saturated or linear ligator axial ligand types. The only means by which the d_{xz} and d_{yz} orbital pair can be split is if the axial ligands have an asymmetric π bonding capability. Both orbital pairs may be split by an asymmetry in the equatorial field, however. The d_{xy} and $d_{x^2-y^2}$ orbitals will be split by an asymmetry of either equatorial σ or π bonding, whilst the d_{xz} and d_{yz} pair will be split only by a asymmetry of equatorial π bonding. This is shown below in figures 4.6 and 4.7 for σ bonding only, and figures 4.8 and 4.9 for the inclusion of π bonding. All calculations employ a sum of 23000 cm^{-1} which is kept constant as one equatorial parameter is adjusted in an attempt to model a concerted distortion, all other parameters are equal and $e_\pi = 1/5\ e_\sigma$ where appropriate.

Figure 4.6 shows the orbital energies as a function of $e_\sigma(eq)$ for the equatorial ligand that is adjusted. The d_{xz} and d_{yz} orbitals are unperturbed by the ligand field and so remain at a constant energy. The d_{xy} and $d_{x^2-y^2}$ orbitals do indeed split, the sense and magnitude of the splitting being dependant upon whether the unique $e_\sigma(eq)$ value has increased or decreased from the parent geometry in which all e_λ are equal. The unique equatorial ligand has been defined as lying on the global x-axis, and hence the change of $e_\sigma(eq)$ has most effect on the $d_{x^2-y^2}$ orbital. Since the sum is maintained equally by

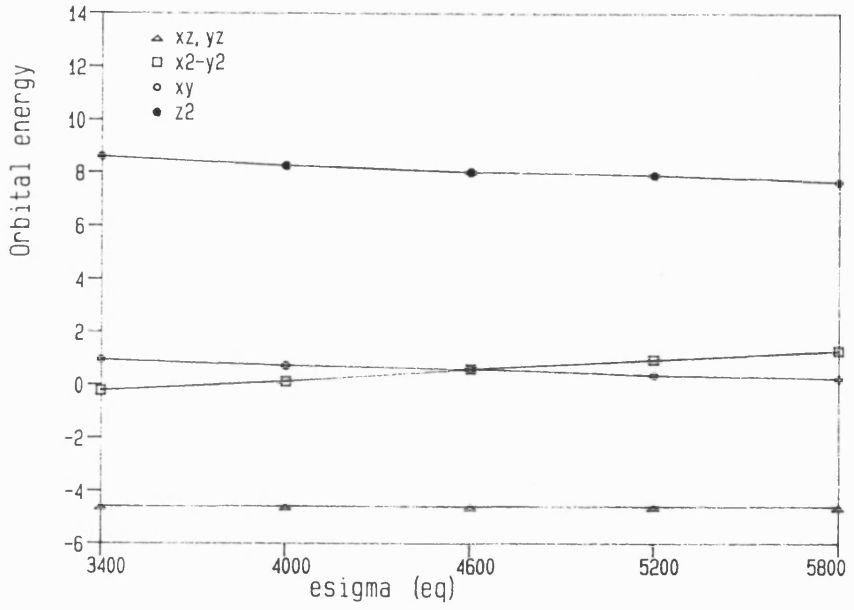

Figure 4.6: Orbital energies as a function of the unique e_σ(eq), for a trigonal bipyramidal species, without π bonding, with a constant CLF Σ value. Orbital energy scale in units of 1000 cm^{-1}, e_σ(ax) in units of cm^{-1}.

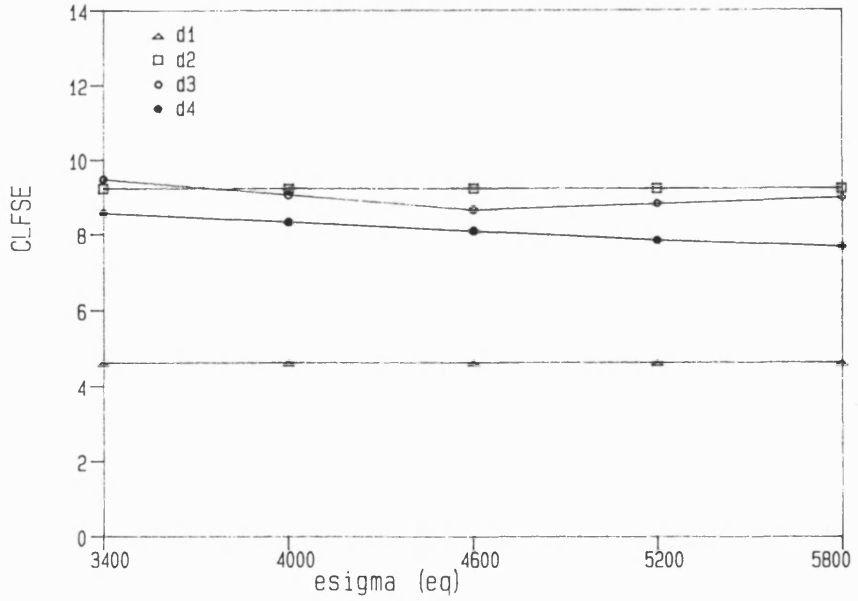

Figure 4.7: Magnitude of the CLFSE as a function of the unique e_σ(eq), for a trigonal bipyramidal species, without π bonding, with a constant CLF Σ value. CLFSE scale in units of 1000 cm^{-1}, e_σ(ax) in units of cm^{-1}.

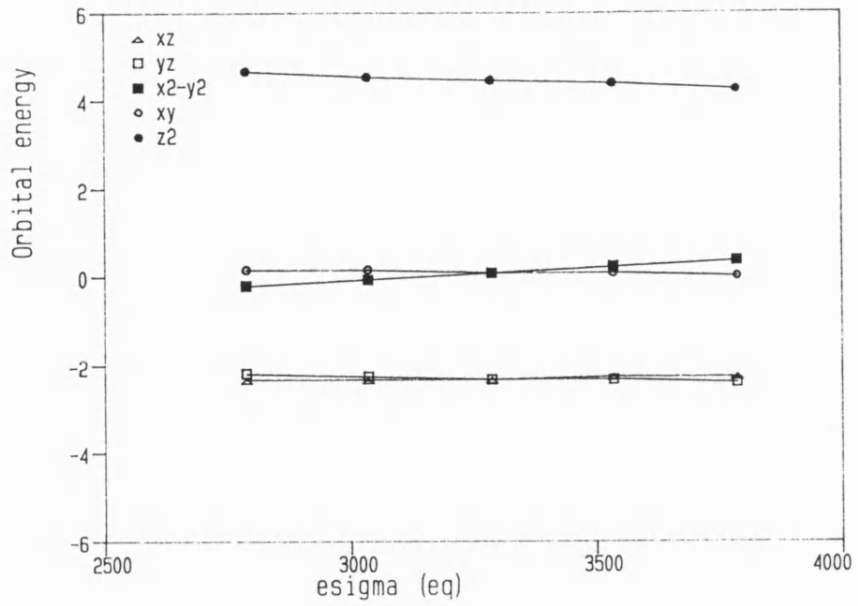

Figure 4.8: Orbital energies as a function of the unique e_σ(eq), for a trigonal bipyramidal species, with π bonding, with a constant CLF Σ value. Orbital energy scale in units of 1000 cm^{-1}, e_σ(ax) in units of cm^{-1}.

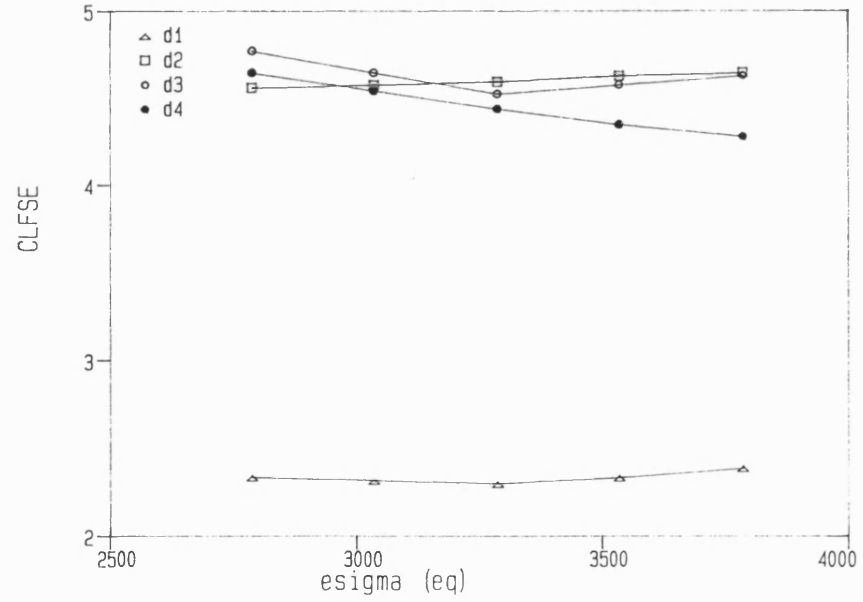

Figure 4.9: Magnitude of the CLFSE as a function of the unique e_σ(eq), for a trigonal bipyramidal species, with π bonding, with a constant CLF Σ value. CLFSE scale in units of 1000 cm^{-1}, e_σ(ax) in units of cm^{-1}.

all the other ligands, the d_{xy} and d_{z^2} orbitals decrease in energy as e_σ(eq) increases and it is for this reason that the bari-centre is not maintained for the parent d_{xy,x^2-y^2} orbitals, the $d_{x^2-y^2}$ orbital changing in energy more rapidly. If the sum were maintained by the other equatorial parameters alone then this bari-centre would be maintained. Figure 4.7 shows the CLFSEs. The d^1 and d^2 CLFSEs do not change, while the d^4 CLFSE is lowered in magnitude as expected from the orbital behaviour. The d^3 CLFSE increases in magnitude for both an increase and decrease of e_σ(eq). As the bari-centre for the d_{xy,x^2-y^2} orbital pair is not maintained, the d^3 CLFSE is asymmetric with respect to increase and decrease of e_σ(eq), a decrease being preferred corresponding to a lengthening of one equatorial bond. The same conclusion emerges if one considers the calculation of the d^3 CLFSE derivative within a Molecular Mechanics framework. Any ligand movement that will reduce the energy of one of the orbitals of the d_{xy,x^2-y^2} pair will yield an increase in CLFSE, and due to the orientation of the ligands with respect to the orbital axes it will be preferable to increase the bond length of the ligand that lies along or closest to an orbital axis as this will yield the largest change in orbital energy.

If π bonding is included the behaviour of the orbital energies, figure 4.8, and CLFSEs, figure 4.9, is largely the same with the important exception of the $d_{xz,yz}$ pair and consequently the d^1 and d^2 CLFSEs. As anticipated this orbital pair split as the unique e_σ(eq) deviates from the parent value. In contrast to the d_{xy,x^2-y^2} orbital splitting pattern, the d_{xz} orbital changes in energy less rapidly than the d_{yz} orbital, as highlighted by the d^2 CLFSE which increases in magnitude as e_σ(eq) increases, apparently due to the way in which the sum is maintained. If the unique e_λ(eq) values are reduced, for example, the sum is maintained by an increase in both the other equatorial parameters and the axial parameters. The increase in e_π(ax) will cause an increase in energy in both the d_{xz} and d_{yz} orbitals equally whilst the change in equatorial parameters will serve to decrease the energy of the d_{xz} orbital, as the unique

equatorial ligand is defined to lie in the x-direction, and to increase the energy of the d_{yz} orbital. The net result when these contributions are summed is to cause the d_{yz} orbital to increase in energy more rapidly than the d_{xz} orbital decreases in energy. This has the effect of giving a greater change in d^1 CLFSE for a shortening of the unique ligand bond length than for an equivalent lengthening. The converse is true however, if one considers the change of orbital energies in a Molecular Mechanics fashion. Again, any ligand movement that reduces the energy of one of the orbitals of the $d_{xz,yz}$ pair will yield an increase in d^1 CLFSE. By the same reasoning as before, this will be achieved most effectively by an increase in the bond length of the ligand that lies closest to the direction of one of the d orbital axes. These observations are in agreement with the theoretical studies reported by Bacci[90,91] which suggest that the potentially Jahn-Teller active vibration modes of a trigonal bipyramidal species are such as to reduce the symmetry of the complex to C_{2v} from the D_{3h} parent point group, corresponding to the movement of one of the equatorial ligands either towards or away from the metal.

The only other distortion from trigonal bipyramidal geometry of interest, other than those resulting from bending modes, is that of movement of the metal atom out of the plane of the equatorial ligands, a deformation which is of particular relevance for the $[M(Me_6tren)Br]^+$ compounds mentioned earlier. The crystal structures of these compounds show the metal to be some 0.4 Å out of the equatorial ligand plane, but it is not clear whether this is the result of ligand field effects, simple steric constraints imposed by the tren ligand or the consequence of the asymmetric axial ligation. Calculations have been performed in which the metal is moved out of the equatorial ligand plane along the z-axis without changing any $e_\lambda(L)$, for coordination environments of sigma only, axial π, equatorial π and π bonding for all ligands. Such a metal movement does not raise the orbital degeneracies, but does affect the CLFSEs. The four sets of calculations all display a decrease in magnitude of d^3 and d^4 CLFSE,

at various gradients for the different environments. The rate of decrease of d^4 CLFSE is always greater than that for the d^3 configuration. All calculations show a decrease in energy of the d_z2 orbital and an increase in energy of the d_{xy,x^2-y^2} orbital pair, while in the absence of π bonding the $d_{xz,yz}$ orbital pair are not affected by the distortion. This not the case however if any π bonding capability is introduced. In the presence of axial π bonding the energy of the $d_{xz,yz}$ orbital pair decreases as the metal moves away from the equatorial plane, although the rate of decrease is less than the rate of increase of the d_{xy,x^2-y^2} orbital pair. This yields an increase in magnitude of d^1 and d^2 CLFSE whilst the d^3 and d^4 CLFSEs decrease. Equatorial π bonding shows the converse effect. The $d_{xz,yz}$ orbitals increase in energy, as do the d_{xy,x^2-y^2} orbitals, and so an decrease in the magnitude of the CLFSEs for all configurations is observed. If π bonding is included for all ligands, the orbital behaviour is rather similar to that observed for axial π bonding only. The $d_{xz,yz}$ orbital pair decreases in energy whilst the d_{xy,x^2-y^2} orbital pair increases in energy again causing an increase in magnitude of the d^1 and d^2 CLFSE and a decrease in the d^3 and d^4 CLFSE. These calculations suggest that the observed behaviour of the tren complexes with respect to the movement of the metal out of the equatorial plane is not as a consequence of LFSE effects, as the d^3 and d^4 CLFSEs decrease for all ligand types considered here and although the d^1 and d^2 CLFSEs increase in magnitude as the metal moves out of the plane for the case of axial π bonding only, the CLFSE energy gradients are small and are therefore unlikely to cause the relatively large distortions that are experimentally observed.

4.4: 4-coordination

The obvious 4-coordinate geometries that require study are tetrahedral and square planar. The square planar geometry may, as for the 5-coordinate square pyramidal geometry, be considered as a special case of octahedral based coordination. However, this geometry has a special relationship to tetrahedral coordination, especially in terms of the Jahn-Teller effect, and so does warrant consideration here. The Jahn-Teller distortion of a d^4 system from tetrahedral geometry is one of flattening, and as such is an angular rather than radial distortion in contrast to the Jahn-Teller distortions studied so far in this chapter. It is with this in mind that the square planar geometry bears relevance as the limiting case of a flattened tetrahedron.

The effect of tetrahedral flattening is now considered in terms of orbital energies and CLFSEs as a function of the degree of flattening as measured by the L-M-L angle shown in figure 4.10, both with and without ligand π bonding capability.

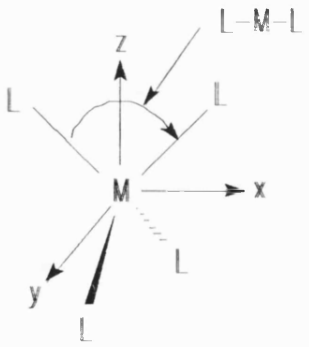

Figure 4.10: Angle and axis definition for tetrahedral species.

4.4.1: No π-bonding

Figures 4.11 and 4.12 show the behaviour of the orbital energies and CLFSEs respectively as a function of the angle of flattening in the absence of π bonding. All $e_\sigma(L)$ parameters are equal and remain unchanged as, therefore, does the sum.The orbital energies show the familiar arrangement for an angle of 110^o, essentially a regular tetrahedron, with the t_2 orbital set higher in energy than the e set. The only difference from traditional schemes is that the $d_{x^2-y^2}$ orbital is defined as being of the t_2 set rather than the e set, the converse being true of the d_{xy} orbital. This is the result of the definition of axis frame. Traditional schemes place the ligands at the corners of a cube with the metal axes defined as pointing to the centre of the faces of the cube, whereas for these calculations the axis frame is as defined in figure 4.10. This is only a labelling difference, however, the behaviour of the orbitals is independent of axis frame definition, as one would expect if this method of calculating CLFSEs is to be applied successfully in general. As the tetrahedron flattens, the d_{xy} orbital remains unchanged in energy and indeed remains unperturbed by the ligand field due to the absence of π bonding. The d_{z^2} and $d_{x^2-y^2}$ orbitals both increase in energy, the latter increasing more rapidly, as the ligands approach the equatorial plane. This is accompanied by a decrease in energy of the d_{xz} and d_{yz} orbitals. The d^1 CLFSE remains unchanged as the tetrahedron flattens because the energy of the d_{xy} orbital remains constant. The d^2 CLFSE initially decreases in magnitude, as the d_{z^2} orbital increases in energy, but at an angle of ca 145^o begins to increase and continues to do so until an angle of 180^o is reached. This increase of d^2 CLFSE coincides with the 'cross-over' of the $d_{xy,yx}$ orbital pair and the d_{z^2} orbital, the $d_{xz,yz}$ pair becoming the second lowest energy orbitals and hence are occupied rather than the d_{z^2} orbital. As this orbital pair is decreasing in energy the d^2 CLFSE increases in magnitude. Similar behaviour is observed for the d^3 CLFSE although this CLFSE increases initially as the $d_{xz,yz}$ orbital pair decrease in energy more rapidly than the d_{z^2} orbital increases in energy.

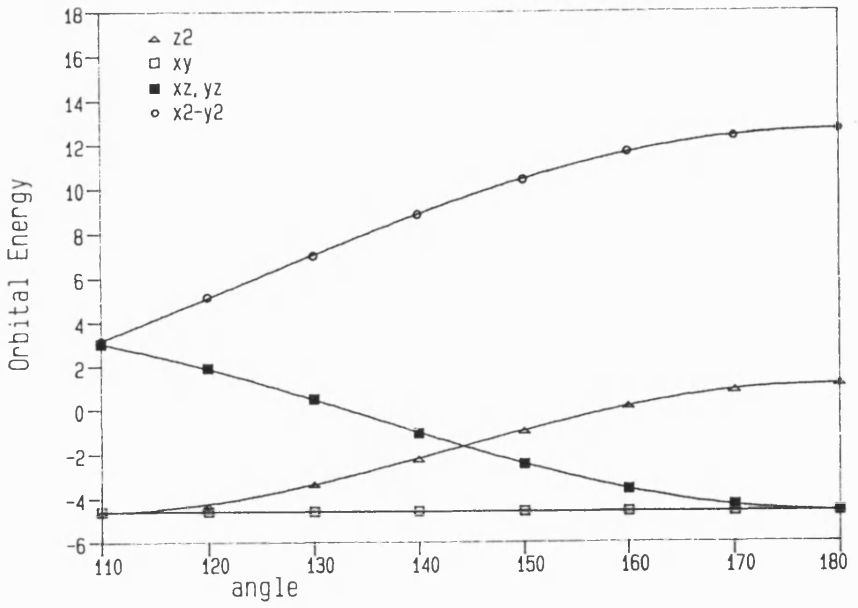

Figure 4.11: Orbital energies as a function of the flattening angle, for a tetrahedral species, without π bonding, without void cell contributions, with a constant CLF Σ value. Orbital energy scale in units of 1000 cm^{-1}.

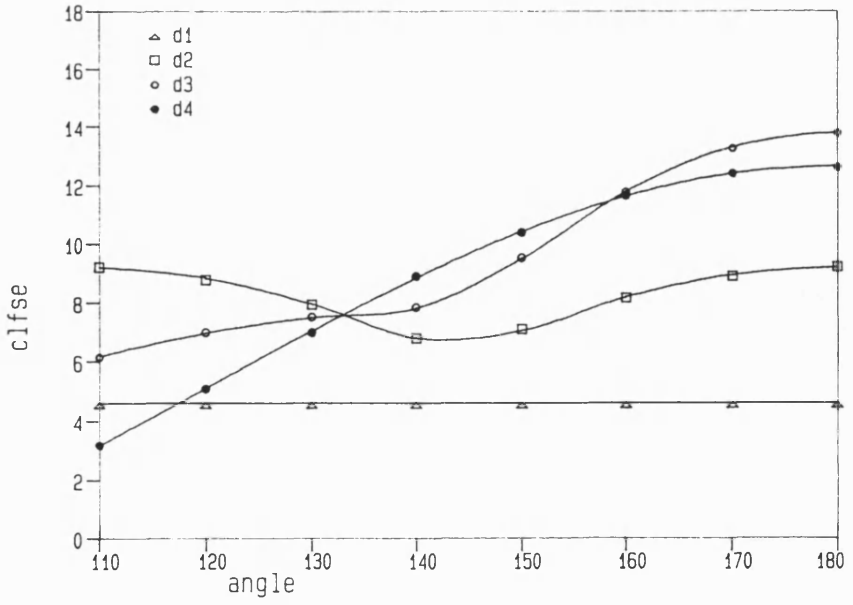

Figure 4.12: Magnitude of the CLFSE as a function of the flattening angle, for a tetrahedral species, without π bonding, without void cell contributions, with a constant CLF Σ value. CLFSE energy scale in units of 1000 cm^{-1}.

However, once the $d_{xz,yz}$ pair becomes the second lowest energy orbital the d^3 CLFSE increases more rapidly, and due to the double occupancy of this orbital pair the d^3 CLFSE increases at twice the rate of the d^2 CLFSE from an angle of 145^o onwards. The d^4 CLFSE increases in magnitude smoothly as the tetrahedron flattens, the gradient decreasing as a square planar geometry is approached. The behaviour of the CLFSEs are according to the predictions of the Jahn-Teller effect. The d^1, d^3 and d^4 configurations are all potentially Jahn-Teller active and so should show an energetic maximum, i.e. a minimum in the magnitude of CLFSE, for a tetrahedral geometry. This is indeed the case with the exception of the d^1 configuration for which the CLFSE remains constant. For a d^2 configuration a tetrahedral geometry represents a maximum in the magnitude of the CLFSE, again as one would anticipate from the lack of Jahn-Teller activity for such a species. It is interesting to note that for a tetrahedral elongation, as represented by an angle of 100^o, the change in d^3 CLFSE is greater than for a flattening of equal magnitude. The same is not the case for the d^4 CLFSE which shows a preference for flattening. This correlates well with the experimental observation that high spin four coordinate Ni(II) complexes generally adopt an elongated tetrahedral geometry.

The orbital energies for an angle of 180^o, a square planar arrangement, are again as one would expect with one important exception. For a square planar geometry a coordination void exists which must be accounted for in the parameterisation, a failure to do so results in an overestimation of the energy of the d_z2 orbital energy of about 6000 cm^{-1} with obvious consequences for the computed CLFSEs and, perhaps more importantly, the CLFSE gradients. Previous CLF studies have suggested that the magnitude of the void cell contribution is related to the angle that the void 'occupies'. Thus, in the first instance, it would seem reasonable to include void cell contributions as a linear function of the angle of flattening, employing an interpolation of values from a zero value for an angle of 110^o to a value of 3000 cm^{-1} for an angle of 180^o.

The result of such an inclusion of void cells upon orbital energies and CLFSEs is shown in figures 4.13 and 4.14. The $e_\sigma(L)$ values remain unchanged as the void cell contribution increases.

The most significant modifications to the behaviour of the orbital energies due to the inclusion of void cell contributions are those to the d_{xy} and d_{z^2} orbitals. The d_{xy} orbital increases in energy in a linear fashion which reflects the gradual decrease in energy of the bari-centre. This is due to the increasing magnitude of the negative void cell contribution while the other parameters remain unchanged, which results in a decrease in the CLF sum and consequently in the bari-centre. Similar changes in the behaviour of the d_{xz}, d_{yz} and $d_{x^2-y^2}$ orbitals are observed for the same reason. The d_{z^2} orbital initially decreases in energy, then increases in energy and finally decreases again as a square planar geometry is approached. This is the result of summing a linear change in energy as a result of the inclusion of a void cell contribution with the non-linear change in energy as a result of ligand movement as seen in figure 4.11. This initial decrease in energy of the d_{z^2} orbital has important consequences for the CLFSE behaviour when considered in terms of the Jahn-Teller predictions outlined above. As shown in figure 4.14, the d^1 CLFSE initially increases in energy and then decreases, as does the d^2 CLFSE as the d_{z^2} orbital initially decreases in energy more rapidly than the d_{xy} orbital increases in energy. The latter observation is clearly undesirable in terms of the Jahn-Teller effect. The d^3 CLFSE shows rather smoother behaviour than in the absence of void cells as there is no longer the cross-over of orbital energies which caused the CLFSE to increase in magnitude, but again shows that a tetrahedral arrangement is unstable. The d^4 CLFSE is qualitatively unchanged, but does increase more rapidly if void cells are included due to the effect upon the $d_{x^2-y^2}$ orbital of the decrease in the bari-centre.

The inclusion of void cells in this fashion appears rather inconclusive, due to the effect of changing bari-centre. Although it is rather contrary to the conclusions drawn from

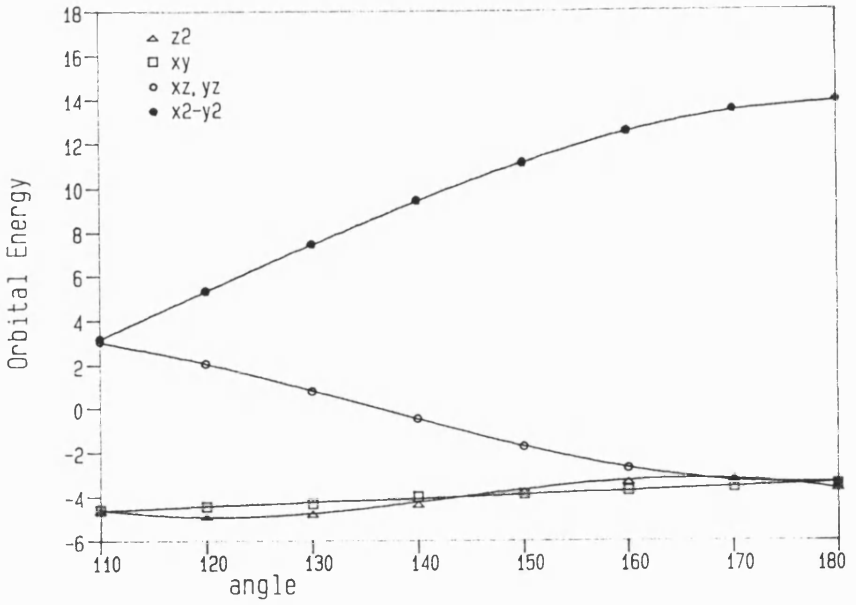

Figure 4.13: Orbital energies as a function of the flattening angle, for a tetrahedral species, without π bonding, with void cell contributions, without a constant CLF Σ value. Orbital energy scale in units of 1000 cm^{-1}.

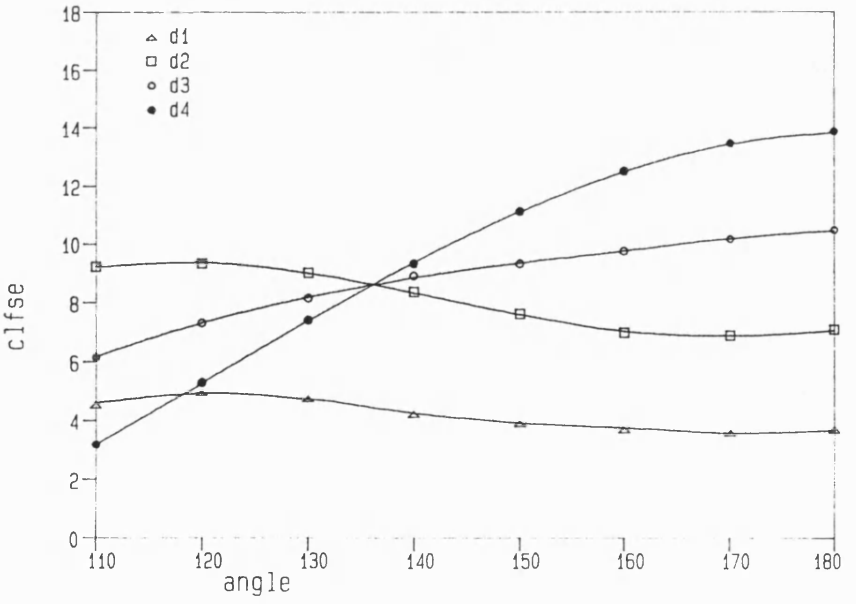

Figure 4.14: Magnitude of the CLFSE as a function of the flattening angle, for a tetrahedral species, without π bonding, with void cell contributions, without a constant CLF Σ value. CLFSE energy scale in units of 1000 cm^{-1}.

the six coordinate species, this may be alleviated if the CLF sum is kept constant and hence the bari-centre remains unchanged by increasing the $e_\sigma(L)$ as the void cell contribution increases. The effect of this treatment of void cells is shown in figures 4.15 and 4.16 below for a sum of 23000 cm^{-1}.

Figure 4.15 shows that the energy of the d_{xy} orbital remains constant, so the bari-centre has indeed remained unchanged, so changes in orbital energies and CLFSEs may be considered as 'real' consequences of the inclusion of the void cell contributions rather than as artefacts of a changing CLF sum. The d_{xz} and d_{yz} orbitals behave much as in the absence of void cells while the $d_{x^2-y^2}$ orbital increases in energy considerably more quickly due to the increase in equatorial parameter values. The d_{z^2} orbital behaves in much the same way as shown in figure 4.13 with the exception that it initially decreases in energy more rapidly and then increases to a higher energy at 180^o. This may be rationalised in terms of a combination of the increase in $e_\sigma(eq)$ and that the bari-centre remains constant. The behaviour of the CLFSEs is generally similar to those shown in figure 4.14. The d^1 and d^2 CLFSEs again initially increase in magnitude before decreasing, the initial gradient for the d^2 CLFSE being the same as that for d^1. The d^3 CLFSE increases steadily, the gradient increasing sharply at ca 160^o when the $d_{xz,yz}$ orbital pair becomes lower in energy than the d_{z^2} orbital. The d^4 CLFSE again shows a smooth increase in magnitude with a reduction in gradient as an angle of 180^o is approached. However, due to the increase in the equatorial parameters the rate of increase of the d^4 CLFSE and the magnitude for an angle of 180^o are both larger than observed in either the absence of void cells or with void cells but without a constant sum.

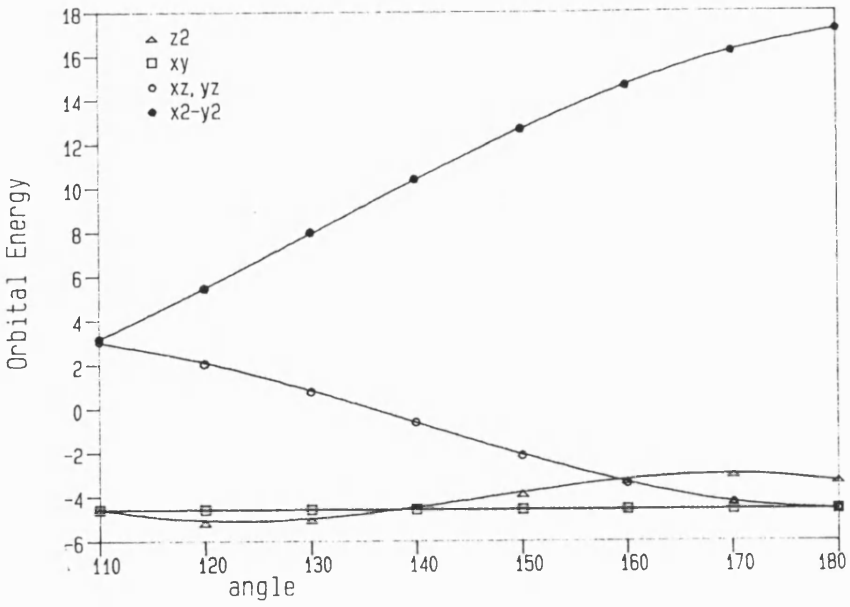

Figure 4.15: Orbital energies as a function of the flattening angle, for a tetrahedral species, without π bonding, with void cell contributions, with a constant CLF Σ value. Orbital energy scale in units of 1000 cm^{-1}.

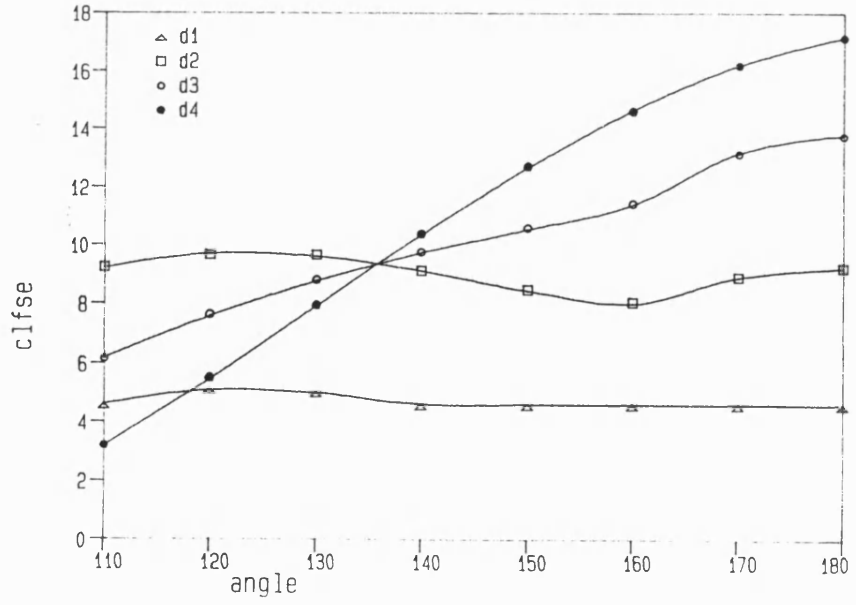

Figure 4.16: Magnitude of the CLFSE as a function of the flattening angle, for a tetrahedral species, without π bonding, with void cell contributions, with a constant CLF Σ value. CLFSE scale in units of 1000 cm^{-1}.

4.4.2: With π-bonding

The effect of introducing π bonding is now considered for the same flattening process. Initially void cells are omitted, with the $e_\lambda(L)$ remaining constant and $e_\pi = 1/5\ e_\sigma$. For a sum of 23000 cm^{-1} the behaviour of orbital energies and CLFSEs are shown in figures 4.17 and 4.18 below.

The qualitative behaviour of the orbital energies shown in figure 4.17 are as seen in the absence of π bonding, with the exception that the d_{xy} orbital increases in energy as the tetrahedron flattens rather than remaining at a constant energy. The d_z2 orbital is also seen to initially decrease in energy although the initial rate of decrease of this orbital is less than the rate of increase of the d_{xy} orbital. This behaviour results in an increase in magnitude of the d^1 CLFSE as the tetrahedron flattens, but a decrease in the d^2 CLFSE as one would expect from a Jahn-Teller rational. The d^1 CLFSE decreases after the initial increase, but begins to increase again, as does the d^2 CLFSE, at an angle of 145^o when the d_{xy} and d_z2 orbitals become higher in energy than the $d_{xz,yz}$ orbital pair. This 'cross-over' of orbital ordering also causes the d^3 CLFSE to increase more rapidly at 145^o. The d^4 CLFSE again increases smoothly as the tetrahedron flattens, but at a lesser rate and magnitude than in the absence of π bonding. For an angle of 100^o, a tetrahedral elongation, similar behaviour of the CLFSEs is observed. The d^1, d^3 and d^4 CLFSEs increase in magnitude while the d^2 CLFSE decreases. It is interesting to note that the d^1 and d^3 CLFSE both show a preference for elongation in terms of the gradient of the CLFSE, while the d^4 CLFSE shows a preference for flattening.

If a void cell contribution is included as before, initially without modifying the $e_\lambda(L)$ to maintain the sum, the behaviour of the orbital energies and CLFSEs are shown in figures 4.19 and 4.20. Due to the introduction of a void cell contribution the behaviour of the d_z2 orbital is affected profoundly. The energy of this orbital steadily decreases throughout the distortion, and decreases at a greater rate than the d_{xy} orbital increases

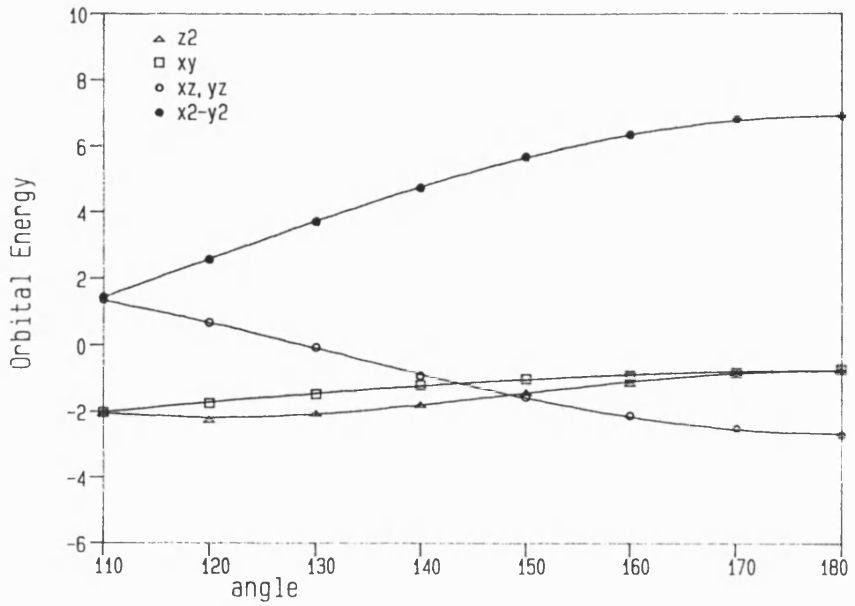

Figure 4.17: Orbital energies as a function of the flattening angle, for a tetrahedral species, with π bonding, without void cell contributions, with a constant CLF Σ value. Orbital energy scale in units of 1000 cm^{-1}.

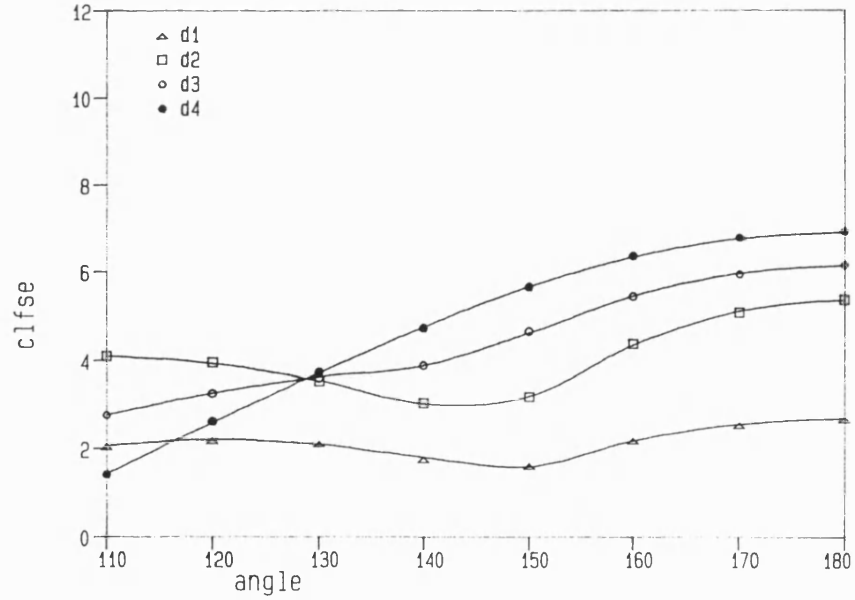

Figure 4.18: Magnitude of the CLFSE as a function of the flattening angle, for a tetrahedral species, with π bonding, without void cell contributions, with a constant CLF Σ value. CLFSE scale in units of 1000 cm^{-1}.

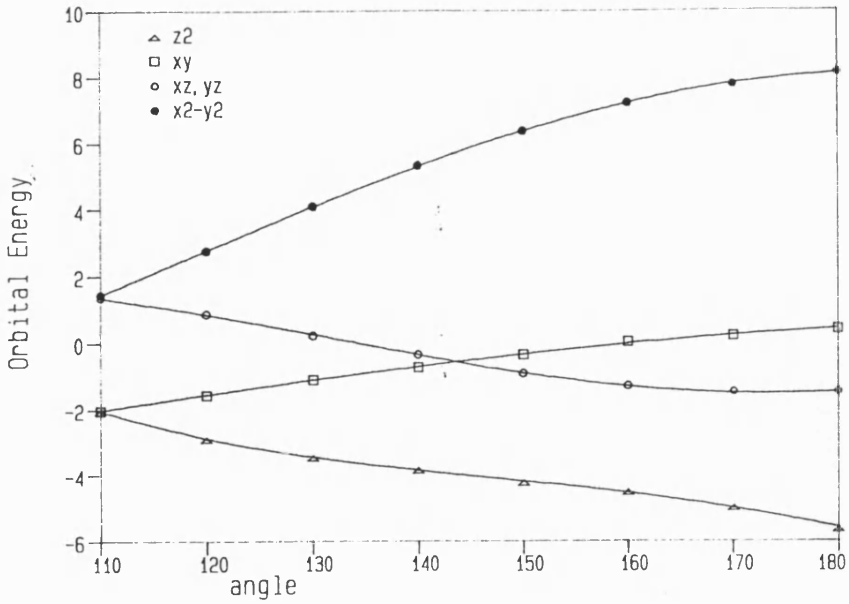

Figure 4.19: Orbital energies as a function of the flattening angle, for a tetrahedral species, with π bonding, with void cell contributions, without a constant CLF Σ value. Orbital energy scale in units of 1000 cm^{-1}.

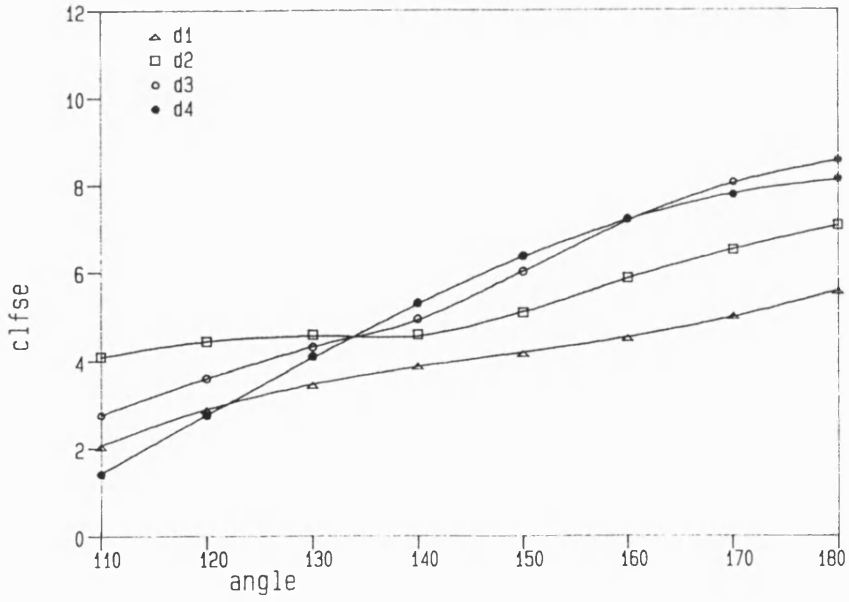

Figure 4.20: Magnitude of the CLFSE as a function of the flattening angle, for a tetrahedral species, with π bonding, with void cell contributions, without a constant CLF Σ value. CLFSE scale in units of 1000 cm^{-1}.

in energy. The $d_{xz,yz}$ orbital pair and the d_z2 orbital behave in much the same fashion as without void cells. The consequence of the behaviour of the d_z2 orbital is that the CLFSE for all d-configurations increases as a function of tetrahedral flattening. This is obviously an unsatisfactory situation.

Figures 4.21 and 4.22 show the effect of maintaining a constant sum by increasing $e_\lambda(L)$ as the void cell contribution becomes more negative. The orbital energy behaviours are essentially the same as those shown in figure 4.19, and consequently the CLFSEs are not greatly modified by maintaining the sum. An increase in CLFSE again occurs for all configurations as the tetrahedron is flattened. The only significant difference is that the d^3 and d^4 CLFSEs are larger in magnitude and increase more rapidly than if the sum is not maintained.

It is apparent that this method of introducing a void cell contribution is not appropriate. Regardless of whether the sum is constant or not and independent of π bonding parameters, if a void cell is included as a linear function of flattening angle then these results show that a high spin d^2 or d^7 tetrahedral complex will not be stable with respect to tetrahedral flattening. This is, of course, contrary to the Jahn-Teller theorem. This does not preclude the inclusion of void cells in other ways however. The results reported here simply indicate that more selective criteria for parameterising the void cell contribution are required. It is clear that the cause of the increase in the d^2 CLFSE is due to the behaviour of the energy of the d_z2 orbital between a flattening angle of 110^o and *ca*135^o. If void cells are included the d_z2 orbital appears to fall in energy rather too quickly and so one might suggest that voids should only included when an angle of 135^o is reached. This approach finds some justification from previous CLF analyses[47] which indicate that for angles less than 130^o any void cell contribution is negligible. The results presented here also suggest that the CLFSE gradient for a d^4 or d^9 configuration, the configurations most likely to undergo significant distortion, is not

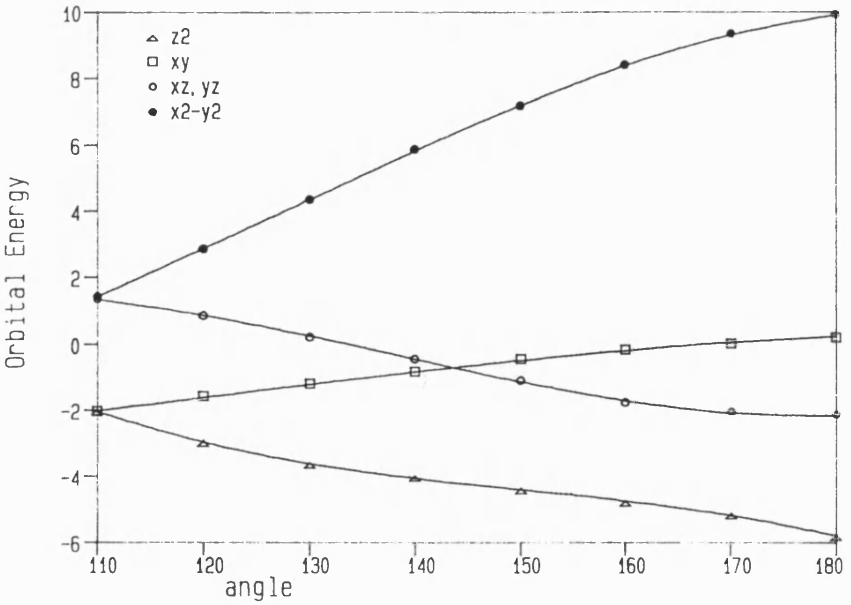

Figure 4.21: Orbital energies as a function of the flattening angle, for a tetrahedral species, with π bonding, with void cell contributions, with a constant CLF Σ value. Orbital energy scale in units of 1000 cm^{-1}.

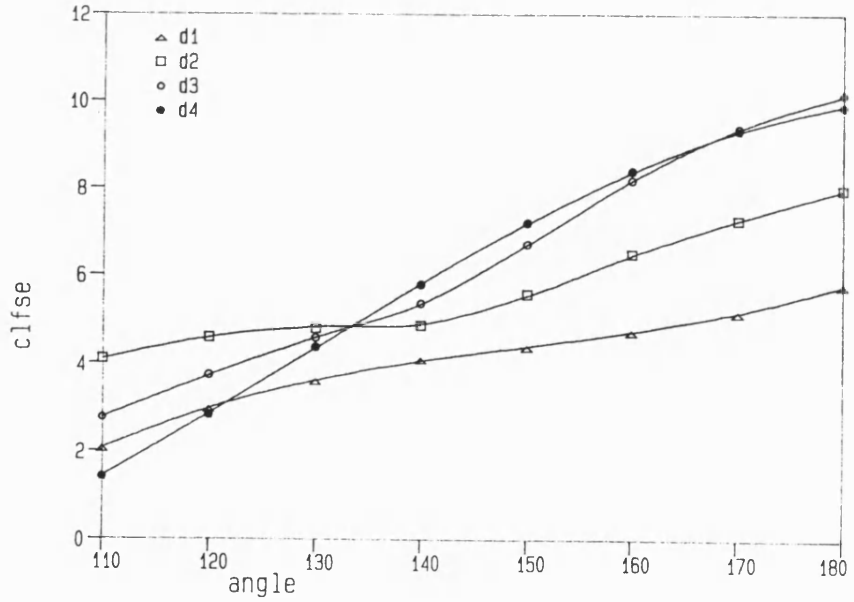

Figure 4.22: Magnitude of the CLFSE as a function of the flattening angle, for a tetrahedral species, with π bonding, with void cell contributions, with a constant CLF Σ value. CLFSE scale in units of 1000 cm^{-1}.

greatly affected by inclusion of void cells in the range 110-135^{o}, for void cell contributions calculated in a linear fashion. For distortions of a larger magnitude, the inclusion or otherwise of void cells is significant, but only if the CLF sum is maintained. Given that the d^4 CLFSE is equal to the negative of the energy of the highest energy orbital, for this geometry the $d_{x^2-y^2}$ orbital, it is obvious that if the sum is not maintained as the void cell contribution increases then the energy of the $d_{x^2-y^2}$ orbital, and hence the d^4 CLFSE, is only affected in so much as the increasingly negative value of the void cell parameter reduces the bari-centre and hence increases the relative energy of the $d_{x^2-y^2}$ orbital. If the sum is maintained by increasing the $e_\lambda(L)$ then the $d_{x^2-y^2}$ orbital increases in energy considerably more rapidly and a significant difference in the magnitude and gradient of the d^4 CLFSE is observed when compared to that in the absence of void cell contributions. It would appear, therefore, that in order to reproduce the d^4 CLFSE gradient appropriately then one must include void cells and keep the sum constant as the distortion progresses. This poses a problem, however. As previously found for octahedral distortion, it is incorrect in general to maintain the sum as a distortion progresses. Even if this were not the case there would be no obvious way of maintaining the sum, due to the angular rather than radial nature of the tetrahedral distortion. There is notionally no change in metal-ligand bond length as the tetrahedron flattens, so one cannot justifiably increase the $e_\lambda(L)$ without deviating from the base assumption that the CLF parameters are related to bond length.

4.5: Conclusions

The calculations described in this chapter have illustrated that the CLFSE term is capable of producing CLFSE energy gradients that are appropriate in sense for the four, five and six coordinate geometries considered here with a variety of ligand types. The CLFSE term has correctly highlighted the Jahn-Teller instability of a regular octahedral arrangement of six identical ligands with respect to axial elongation and

compression for a d^4 configuration, as well as for the d^1 and d^2 configurations when the coordinated ligands show a π bonding capability. The Jahn-Teller effect within tetrahedral species has also been considered, the d^4 configuration again being of prime concern, and the significance of void cell contributions, along with the inherent difficulties of including these effects, have been discussed. The CLFSE term is also capable of reproducing the more general effects of Ligand Field Stabilisation Energies. These include the familiar "double hump" behaviour of the heats of hydration of the first row transition series, which is treated implicitly within the CLFSE term as the radial part of the metal-ligand bond that gives rise to this additional energy is accounted for within the radial dependence of the CLFSE. The general effects of LFSEs also include the stereochemical activity of d-orbital "holes" apparent in trigonal bipyramidal coordination environments for d^3 and d^4 configurations. This effect has been shown to be appropriately handled by the CLFSE term, and the CLFSE term also illustrates the potential Jahn-Teller activity of such species for d^1 and d^3 configurations.

The calculations reported for the tetrahedral species illustrate the implicit treatment of ligand-metal-ligand angles within the CLFSE term, and this treatment of L-M-L angles is general to all coordination environments. For example, the CLFSE term provides a restoring force to prevent angular distortions from octahedral geometries for d^1, d^2 and d^3 configurations, while for a d^4 configuration the CLFSE term favours movement of the ligands along the metal-ligand axis rather than movement of an angular as opposed to a radial nature. It is likely, therefore, that the CLFSE term, along with suitable ligand-ligand repulsion terms of a Van der Waals or Coulombic form where necessary, will be capable of treating the angular potential around metal centres without recourse to the harmonic or fourier potentials that are both common and problematic in conventional Molecular Mechanics force fields. Although it is beyond the scope of this work, the CLFSE term is also capable of handling M-L-N angles, where N represents the next atom bonded to the ligating atom, through the mechanism of missdirected

valence. Any missalignment of ligand bonding orbitals as a consequence of non-ideal M-L-N angles will result in a degree of missdirected valence, and appropriate parameterisation of these effects will result in a modification of the CLFSE. The resultant energy gradient will act such as to either restore the ideal M-N-L angle or to favour such a distortion depending upon the particular coordination circumstances.
It is clear then that the CLFSE term is able to produce energy gradients that accord well with Jahn-Teller and LFSE predictions in a qualitative fashion. However, if the CLFSE term is to successfully model transition metals within a Molecular Mechanics framework then the magnitudes of the computed energy gradients must also be appropriate. Much of the discussion of the magnitude of the CLFSE energy gradients in this chapter has involved the CLF sum rule, and the way in which sum is maintained in order to reproduce Jahn-Teller type effects in six and four coordinate species, especially for a d^4 configuration. The apparent need to maintain the sum at a constant value is the result of attempting to satisfy the requirements of the Jahn-Teller theorum as regards maintaining a bari-centre for the orbitals that show the parent degeneracy. This in turn is related to the change in metal-ligand bond lengths which, if a bari centre is to be maintained and assuming an essentailly linear relationship between e_λ and bond length, will model ligand movements along the Jahn-Teller active vibration mode in a first order fashion. It would be incorrect to maintain a constant sum from iteration to iteration within a Molecular Mechanics scheme, however, and so the sum rule has only been used in this chapter so as either to reproduce Jahn-Teller effects or to simplify the calculations by preventing changes in CLFSE as a consequence of changing bari-centre. Within a Molecular Mechanics calculation it would be over-ambitious to expect to be able to not only reproduce the experimentally observed structure of a species as the result of energy minimisation, but also the concerted distortion that gave rise to that structure. Provided that the CLFSE term in combination with the appropriate Molecular Mechanics terms produce net energy gradients that result an energy minimised structure

that agrees closely with the experimentally observed structure, then that is sufficient. It is, therefore, impossible to predict from the work reported in this chapter whether or not the CLFSE term will provide metal centred energy gradients that will balance suitably with traditional Molecular Mechanics terms. This may only be determined from the success or otherwise of the CLFSE term operating within a Molecular Mechanics routine for modelling the known structures of transition-metal species.

Chapter 5

Results of Molecular Mechanics: 1

5.1: Introduction

This chapter describes the molecular modelling of three series of compounds, all of essentially octahedral coordination of mostly saturated nitrogen donors. In order to reduce the complexity of the Molecular Mechanics treatment and parameterisation, and to provide a computationally transparent test bed for the CLFSE term, these calculations employ a minimal parameter set. The initial aim of these calculations is solely to reproduce the observed crystal structures, rather than to attempt a chemically complete treatment. However, despite the relative simplicity of the molecular mechanics treatment, it will be seen that a useful chemical insight can be gained into some of the species studied here.

5.2: $M(NH_3)_6^{2+}$

The crystal structures of the hexamine complexes of the second half of the first row of the transition series have been reported from Mn to Cu[92-94]. Unfortunately Zn does not form a hexamine complex but forms a tetramine[95], so for the purposes of these calculations an estimate of the hexamine structure is employed. It is these structures that this set of calculations seeks to reproduce, the structural details of which are summarised in table 5.2. This series of complexes is modelled here with the minimum possible parameter set. The only traditional Molecular Mechanics terms employed are Morse potential terms to describe the metal-ligand bond and the amine N-H bond, along with a theta term to describe the H-N-H angle. The parameter values employed to describe the 'organic' part of the molecule are listed in the appendix. No angle terms that involve the metal, such as the M-N-H and N-M-N angles, are included as these are treated implicitly by the CLFSE term. Similarly, no torsion terms are required, whilst non-bonding terms are omitted for simplicity. A Morse potential is employed to

describe bond deformations rather than a harmonic term, more commonly used for traditional Molecular Mechanics force fields, in recognition of the anticipated large distortions from equilibrium bond length for metal-ligand bonds. It is considered that a Morse potential treats such distortions in a more appropriate fashion and so is employed for all the work reported here. The calculated structures, in terms of metal-ligand bond lengths, are therefore the result of a balance between the CLFSE term and the Morse potential terms. The Morse potential requires three input values, D_o, b_o, and α, D_o representing the heat of formation of the bond and b_o the equilibrium bond length. The value of α determines the energy gradient of the Morse potential for displacement from the equilibrium bond length and is adjusted to reproduce the observed structures. The D_o values are derived from a linear interpolation of the heats of formation of Mn and Zn amines[96] while the b_o values are gained from a similar interpolation of the Mn and Zn bond lengths. The CLF e_λ versus bond length dependence for these systems is derived from the database values of chapter 2. The functional form of

$$e_\lambda = A/(r-\delta)^5 - B(r-\delta) \qquad \text{Eqn. 5.1}$$

is employed, A and B define the gradient of the curve, remaining constant for all metals except Cu, while δ is adjusted to translate the curve to ensure that the CLF sum is equal at 21000 cm^{-1} for all metals at the observed bond lengths. The implication of this use of delta is that the e_λ versus bond length gradient is the same for all metals at the observed bond length. The input parameters are summarised in table 5.1.
The structural results shown in table 5.2 show that, with the exception of Cu, the observed structures are all accurately reproduced in terms of both bond lengths and angles at the metal, and all show a regular octahedral geometry. The α values appear to be of reasonable magnitude, although there is no linear trend along the series. The values of alpha for Mn and Zn are arbitrary, however, as in the absence of a CLFSE

for high-spin d^5 and d^{10} configurations the metal-ligand bond lengths will minimise to the equilibrium bond length, b_o, regardless of the value of α. It is also important to note that although the reported minimised structures for Mn and Zn show regular octahedral geometries in terms of angles around the metal, this is due to employing octahedral starting coordinates rather than being due to any force field term enforcing this geometry. In order to gain an octahedral geometry from any set of starting coordinates some form of non-bonding term is required, and this topic is considered in detail in the next chapter. The same is not true, however, for the metals that show a non-zero CLFSE. The CLFSE term treats L-M-L angles implicitly and hence the calculated regular octahedral geometries are the consequence of the CLFSE term showing a maximum magnitude at such a geometry.

Metal	D_o, kcal	b_o, Å	CLF A	CLF B	CLF δ
Mn	100.0	2.28	-----	-----	-----
Fe	102.0	2.24	225800	900	0.12
Co	104.0	2.20	225800	900	0.0
Ni	106.0	2.16	225800	900	-0.08
Cu	108.0	2.26	336170	1400	0.0
Zn	110.0	2.08	-----	-----	-----

Table 5.1: Input parameters for Morse potential and CLFSE terms used in the structural calculations of the $M(NH_3)_6^{2+}$ species.

In contrast to the behaviour of Mn and Zn, the Morse potential alpha values for Fe, Co and Ni are of significance. For these metals the CLFSE term favours a decrease in metal-ligand bond length, while the energy of the Morse potential will increase for any

displacement from the equilibrium bond length, b_o. An energetic minimum therefore exists when the value of the CLFSE gradient is equal but opposite to the Morse potential gradient, the position of this minimum in terms of bond length being defined by the value of α as this is the only input parameter that is varied. As the gradients of the CLF e_λ vs bond length expressions are defined as being equal at the observed bond lengths due to the inclusion of delta in equation 5.1, then the rate of change of the octahedral t_{2g} - e_g one electron orbital splitting, defined as Δ_{oct} in classical crystal field theory, as a function of bond length is equal for these three metals at the appropriate bond length. Therefore, the difference in the CLFSE gradients for these three metals is simply due to the differing d-orbital populations. The CLFSE gradients may then be defined as

$$\text{CLFSE gradient} = n\, d(3e_\sigma)/dL \qquad \text{Eqn. 5.2}$$

where n=no. of d electrons, and $d(3e_\sigma)/dL$ is the rate of change of Δ_{oct} as a function of bond length, as $\Delta_{oct} = 3e_\sigma$ if $\pi-$bonding is not included. Thus, the CLFSE gradient for Co at the observed bond length is twice that of Fe at the observed bond length, and similarly the CLFSE gradient for Ni is three times that of Fe. In order that the energetic minimum will occur at the observed bond lengths, a value of α must be chosen such that for each metal the Morse potential gradient will be equal in magnitude but opposite in sense to the CLFSE gradient at this bond length. The energy of the Morse potential is defined as

$$E_{bond} = D_o[1-e^{-\alpha(b-b_o)}]^2 - D_o \qquad \text{Eqn. 5.3}$$

where D_o and b_o are invariant for a given metal. The gradient is therefore dependant upon the value of α and the value of $(b-b_o)$, the magnitude of deviation from the equilibrium bond length. as shown in equation 5.4.

$$dE/db = 2\alpha D_o\{e^{-\alpha(b-b_o)} - e^{-2\alpha(b-b_o)}\} \qquad \text{Eqn. 5.4}$$

Given the non-linear variation in the value of $b-b_o$ along the series and the linear variation of D_o coupled with the exponential nature of the Morse potential derivative, it is not surprising that a linear trend in the α values required to reproduce the observed structures is not observed.

Metal	α	Bond Lengths				L-M-L angles	E_{min} kcal
		equatorial calc Å	equatorial *obs* Å	axial calc Å	axial *obs* Å		
Mn	2.50	2.28	2.28	2.28	2.28	90.0°	0.000
Fe	1.90	2.23	2.23	2.23	2.23	90.0°	-11.783
Co	0.87	2.11	2.11	2.11	2.11	90.0°	-19.878
Ni	0.85	2.03	2.03	2.03	2.03	90.0°	-27.343
Cu elong.	0.845	2.08	2.08	2.31	2.62	90.0°	-21.821
comp.	0.845	2.25	2.08	1.93	2.62	90.0°	-24.230
Zn	4.00	2.08	2.08	2.08	2.08	90.0°	0.000

Table 5.2: Results of energy minimisations for the $M(NH_3)_6^{2+}$ species.

The total energies for the minimised structures are also shown in table 5.2. If the Morse potential bond terms are expressed as total energies rather than strain energies

then an estimate of the heats of formation can be made, and these are plotted in figure 5.1 below.

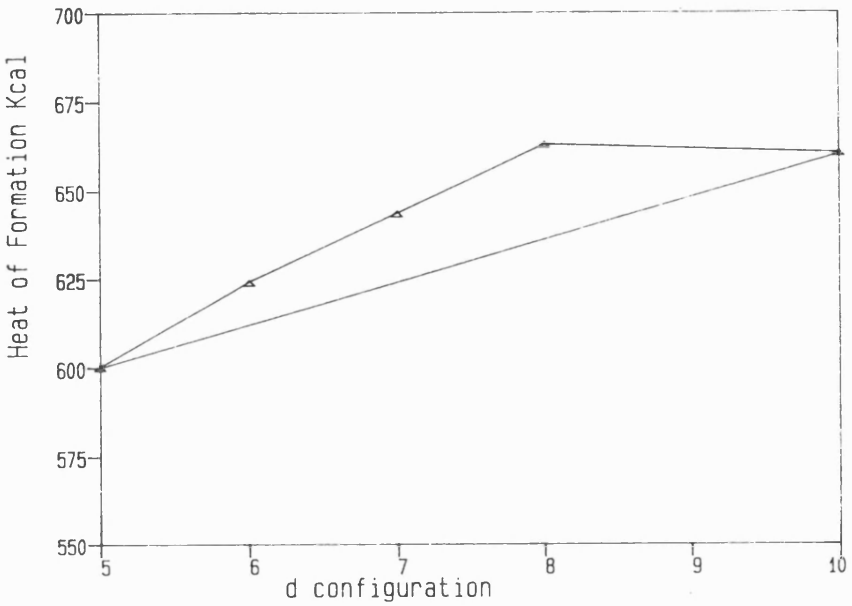

Figure 5.1: Calculated heats of formation for the $M(NH_3)_6^{2+}$ species.

These heats of formation show excellent agreement with the familiar 'double hump' behaviour of many of the thermodynamic properties of the first row transition series[96]. Traditional ligand field theory suggests that the heats of formation should increase essentially linearly from Mn to Ni, and at a greater rate than an interpolation between Mn and Zn, which is shown to be the case in figure 5.1.

Table 5.3 shows the effect of the variation of α upon the resultant minimised structures for the Fe, Co and Ni complexes. The minimised metal-ligand bond lengths are shown

for 10% variations of α either side of the value of α required to give the observed structure. It is immediately apparent that the effect upon calculated bond length of the change in α increases from Fe to Ni. This is due to the increasing magnitudes of the CLFSE and Morse potential derivatives. The CLFSE gradient for Ni at the observed bond length is three times that of the equivalent gradient for Fe, and consequentially a 10% change in the α value for Ni will yield a larger change in calculated bond length and consequently a larger change in total energy than for Fe. For all three metals, however, the calculated bond lengths show a reasonable sensitivity to changes in α, and this observation suggests that the CLFSE term generates gradients that are compatible with those calculated from the Morse potential with neither term dominating the overall force field.

Metal	α	Bond Lengths	E_{min}
	1.71	2.2272	-11.841
Fe	1.90	2.23	-11.783
	2.09	2.2315	-11.741
	0.783	2.0854	-20.906
Co	0.87	2.11	-19.878
	0.957	2.1294	-19.191
	0.765	1.9853	-29.715
Ni	0.85	2.03	-27.343
	0.935	2.0580	-25.852

Table 5.3: Effect of the variation of α upon the energy minimised structures.

The most challenging complex of this series is without doubt the copper compound. The crystal structure[94] reports a severely tetragonally distorted geometry, with equatorial ligand bond lengths of 2.08 A and axial bond lengths of 2.62 A. For this species an interpolated value for b_o is not employed, but a value of 2.26 A is used as this is the value from which a notional parent octahedral geometry would yield the observed bond lengths as a result of a distortion along the Jahn-Teller active vibration mode. The CLF input parameters, A and B, are chosen such that reasonable CLF e_λ values are gained for the observed bond lengths, and that the CLF sum is 21000 cm^{-1} at these bond lengths. The δ parameter is set to zero.

The results listed in table 5.2 show that the minimised geometry for the Cu complex is indeed tetragonally elongated, although the axial bond lengths are not as long as experimentally observed. As was described in Chapter 4, it is apparent that the CLFSE derivatives show a much greater preference for shortening of the equatorial bond lengths than for lengthening of the axial bond lengths, as indicated by the larger deviation from b_o for the equatorial ligands. It is also important to note that the minimised structure is dependant upon the starting coordinates with regard to elongation or compression. As an octahedral geometry represents a global energetic maximum, then a steepest descent minimisation routine, as employed here, will yield either a compressed or an elongated geometry depending upon whether the starting coordinates show a compression or elongation respectively. The most significant result of this calculation is, however, that different Cu-N bond lengths result from identical parameterisation of all the ligands. This appears to be a result unique to this method of modelling transition metal species and, although the extent of elongation is underestimated, this is a most encouraging success for the CLFSE term.

It can be seen that the axial bond lengths increase from the initial coordinates, and are greater than b_o, so it is apparent that the CLFSE derivatives do favour axial elongation. However, the CLFSE derivatives are obviously insufficient to overcome the Morse

potential term acting against such a distortion resulting in an underestimation of the axial elongation. This problem may be solved in one of two ways; one could employ an artificially large b_o, against Jahn-Teller rationale, or one can make use of the CLF 'sum rule' to increase the derivatives favouring axial elongation. The CLF sum, Σ, for the calculated structure listed in table 5.2 is about 25000 cm^{-1}, some 4000 cm^{-1} larger than the empirically observed value[44]. The source of this discrepancy is the underestimation of the axial bond lengths and hence an overestimation of the axial e_λ. If the system is obliged to yield a sum closer to the empirical value, Σ_o, then a mechanism is provided by which the axial ligands may be forced to move away from the metal.

The sum rule is implemented by means of a sum strain energy and hence derivative, calculated as below:

$$E_\Sigma = kS(\Sigma_o-\Sigma)^2 \qquad \text{Eqn. 5.5}$$

where Σ_o is the input optimum sum value, Σ is the calculated sum, S is an adjustable multiplication factor and k is a constant scaling factor to give consistent units. In this instance the sum derivative is applied after an initial minimisation in which the Morse potential alpha value is adjusted to give the appropriate equatorial bond lengths, as per table 5.2. The sum derivative is then applied to all ligands that have bond lengths longer than a specified distance, in this case the b_o value. The axial bond lengths are therefore adjusted such that the optimum sum is attained, or an energetic minimum is reached, without modification of the remainder of the molecule. The results of including this additional term for varying values of S are shown in table 5.4.

Table 5.4 shows the minimised bond lengths along with the CLFSE, the sum for the minimised structure, the sum strain energy and the total energy of the minimised structure. The inclusion of the sum strain energy term allows the problem of

underestimating the axial bond lengths to be overcome by introducing another energy term to be minimised, which in combination with the CLFSE produces a gradient favouring axial elongation sufficient to balance the Morse potential and yield the observed metal-ligand bond lengths.

S	Bond Lengths		CLFSE	Σ	E_{sum}	E_{min}
	equatorial	axial	cm^{-1}	cm^{-1}	kcal	kcal
0.0	2.08	2.310	-11813	26620	0.000	-21.821
0.5	2.08	2.581	-12836	21498	1.014	-11.934
1.0	2.08	2.597	-12882	21265	0.583	-11.387
1.5	2.08	2.604	-12901	21180	0.400	-11.183
2.0	2.08	2.607	-12906	21138	0.312	-11.087
3.0	2.08	2.610	-12918	21095	0.211	-10.975
4.0	2.08	2.612	-12924	21070	0.162	-10.917

Table 5.4: Effect of the value of S upon the energy minimised geometry of $Cu(NH_3)_6^{2+}$

The inclusion of this sum strain energy may be justified within the CLF formalism. The sum rule has emerged as powerful tool in CLF studies, both as a means of assessing the 'reasonableness of fit' of a given parameter set resulting from a ligand field analysis, as employed in chapter 3, and as a means of reducing the frequent problem of over-parameterisation in ligand field analyses. Previous CLF studies, along with those reported in this work, show that the sum is remarkably constant for a given ligand set and, within a row of the transition series, is essentially independent of both coordination number and metal, at least for a formal 2^+ oxidation state. These

observations seem entirely reasonable in terms of the Pauling Electroneutrality Principle in that a metal in a given oxidation state requires a certain of amount charge to be donated to it from the surrounding ligands. The amount of charge donated by each ligand will evidently be dependant upon the nature of the coordinating ligand itself and the ability of that ligand to donate charge, along with the nature and the number of other coordinated ligands, but a certain total amount of charge must be donated to satisfy the demands of electroneutrality. Since the e_λ for a given ligand reflects the amount of charge donation from the ligand to the metal then the sum of all such contributions to the metal will reflect the total charge donation to the metal. Thus, for a given type of ligand set, it would seem reasonable to expect an essentially constant sum, and indeed this has also been rationalised theoretically[58].

The sum rule can therefore be seen to provide a mechanism by which the observed structure of $Cu(NH_3)_6^{2+}$ may be reproduced. However, it may be argued that by the inclusion of an additional energy term that is specific to ligands that show bond lengths greater than a pre-defined value, in this case the axial ligands, these ligands are no longer treated in the same way as the other ligands. By this reasoning the method is therefore no more valid than traditional Molecular Mechanics treatments which have attempted to reproduce the structure of $Cu(NH_3)_6^{2+}$ [26] by defining large values of b_o for the axial ligands compared with those employed for the equatorial ligands. However, the CLF sum rule is valid within a CLF context and, in the same way as it has provided a useful tool for CLF analyses of ligand field properties, it is also capable of playing a useful role in the CLFSE force field within Molecular Mechanics. The parametric dependences of e_λ upon bond length used to assign CLF parameters to ligands are derived from the values gained from previous CLF analyses described in chapter 2. They are, therefore, appropriate for a given ligand in an average ligand field environment in terms of coordination number and other ligand types, as is appropriate for general treatment of transition metals within molecular modelling. Within a

complex however, ligands cannot be considered as discrete and invariable units as their behaviour, specifically in terms of charge donation to a metal, is also dependant upon the remainder of the complex. For example, the nickel macrocycle species discussed in chapter 3 show axial charge donation that is stronger than expected from consideration of the axial bond length due to steric constraints imposed by the macrocyclic ligand. If the equatorial donation is reduced by the constraint of increasing the size of the macrocycle, the axial ligands donate more strongly, often without a significant reduction in bond length. Such an increase in axial donation cannot be reproduced by recourse to a dependence of e_λ upon bond length. The charge donation behaviour of a ligand may also be dependant upon the site occupied by that ligand within the complex. The stereochemical activity of d-orbital 'holes' has provided rational for both the structural and ligand field properties displayed by many Cu(II) species. For example, Gerloch and Deeth[45] have reported a CLF analysis of a Cu(II) complex in which a bipyridyl ligand bridges both axial and equatorial sites. A difference of 4000 cm^{-1} in the $e_\sigma(N)$ value for the two coordinating nitrogen atoms was evaluated despite a bond length difference of only 0.05 Å. This difference was attributed by the authors to the 'hole' in d-orbital electron density along the global z-axis, thereby allowing the axial ligand to donate more strongly. Complexes in which such deviations from an average dependence of e_λ vs bond length occur may well prove to be uncommon, but by use of the sum rule such anomalies may be detected. By modification of the sum rule algorithm the e_λ may be modified in a 'second pass' calculation, without necessarily modifying metal-ligand bond lengths, such that a more appropriate sum may be gained from more appropriate e_λ values. The advantage of such a method is that a better estimate of the ligand field properties of such a species would be gained, such as d-d spectra and esr g-values, for comparison with experimentally measured values. Given the potential utility of the sum rule, it would be foolish to discount it's use on the grounds of the way in which it has been employed here to enhance the CLFSE

derivatives favouring axial elongation of $Cu(NH_3)_6^{2+}$. Evidently a rather more sophisticated algorithm is required to implement the sum rule appropriately, but such an algorithm undoubtedly has a valid role to play in future applications of the CLFSE term.

The accurate reproduction of the reported structures of this series of first row transition metal hexamine complexes has illustrated that the CLFSE term is appropriate for use within a Molecular Mechanics force-field for the modelling of such compounds. Although some of the reported structures appear dubious, especially that of the nickel complex and possibly that of the cobalt complex, and the absence of a zinc hexamine structure from the literature allows only an approximate interpolation of b_o values, it is clear that form of the CLFSE term is correct. For d^1, d^2 and d^3 species, provided that the bond length that is to be reproduced is shorter than the corresponding value of b_o, then the observed structure may be reproduced simply by adjusting the value of the Morse potential alpha value. The definition of b_o as the notional bond length in the absence of the CLFSE ensures that this condition is always met, as for d^1, d^2 and d^3 species the CLFSE will always favour the shortening of the metal-ligand bond lengths and hence the observed bond lengths will always be less than in the absence of a ligand field stabilisation energy. As some of the reported structures do appear questionable, it is unwise to attempt to place too much importance upon the parameters employed to reproduce these structures. However, it appears that the CLFSE term calculates CLFSEs of appropriate magnitude and generates gradients that balance well with a Morse potential description of the metal-ligand bond in the absence of a CLFSE.
It is necessary to invoke the CLF sum-rule in order to reproduce the observed structure of the copper complex, and this may be considered to be a failing of this technique as the ligands are no longer treated in an identical manner. It is significant however, that in the absence of this additional energy term the energy minimised structure shows two

different bond lengths for axial and equatorial bonds resulting from identical parameterisation of all ligands, although the axial bond length is underestimated. Interestingly, when this complex is treated in a more chemically complete fashion, as described in the next chapter, the observed structure may be gained without recourse to this additional energy term.

5.2: M $(H_2NCH_2CH_2NH_2)_3^{2+}$

The crystal structures of only three trisethylenediamine complexes of the second half of the first transition series have been reported, those of Ni, Cu and Zn[97-99]. All three complexes are reported as showing essentially octahedral coordination geometries, with each complex having six equivalent metal-ligand bonds. This is unsurprising for the nickel and zinc compounds, but rather unlikely in the copper complex. It is more likely that the structure of the copper complex is, at best, a time averaged structure of a dynamic Jahn-Teller tetragonally distorted species and so only provides an average value for the metal-ligand bond lengths.

As for the hexamine series, this set of calculations seeks only to reproduce the observed structures reported for the Ni and Zn complexes, and to investigate the Cu complex in a relatively simplistic fashion. The organic backbone of the ethylenediamine ligands is treated by using the traditional Molecular Mechanics force field terms appropriate for such a species, including terms describing bond, angle, and torsion strain energies along with van der Waal's non-bonding interactions. In accord with previous Molecular Mechanics treatments of these species[26], no atomic charges are included. No attempt is made to optimise these parameters, and the values listed in the appendix are employed unchanged. The conformation of the ethylenediamine ligands within the complex is not studied in detail here, but the calculated conformations are as experimentally observed. Table 5.5 lists the input values employed for the metal centre. The D_o and b_o values are identical to those employed for the hexamine compounds, but the CLFSE input

values show some differences. The nickel complex is modelled using identical CLFSE e_λ A and B values, but employs a different value for δ. This is so as to give a sum of 21000 cm^{-1} at the observed bond length of 2.124 Å rather than 2.03 Å for the hexamine species. Previous CLF studies[55] have shown that the CLF sum for the hexamine and trisethylenediamine complexes are essentially the same, based upon the analyses of the mull and single crystal polarised spectra respectively, and so this would seem a reasonable modification to the parameterisation. The copper complex is parameterised in identical fashion to the corresponding hexamine complex.

Metal	D_o, kcal	b_o, Å	CLF A	CLF B	CLF δ
Ni	106.0	2.16	225800	900	0.014
Cu	108.0	2.26	336170	1400	0.0
Zn	110.0	2.08	-----	-----	-----

Table 5.5: Input parameters for Morse potential and CLFSE terms used in the structural calculations of the M $(H_2NCH_2CH_2NH_2)_3^{2+}$ species.

The structural results of full energetic minimisation for the nickel and zinc complexes are shown in table 5.6, along with the corresponding experimentally observed values, as are the employed parameter values and the appropriate calculated energies. The structural results are shown schematically in figures 5.2 and 5.3. For both complexes the observed metal ligand bond lengths are accurately reproduced and the experimentally reported angles are all reproduced to within 3^o. Both complexes show a three fold rotational axis, again as experimentally observed, this axis lying through the metal atom and perpendicular to the plane of the paper for the projection of the nickel complex shown in figure 5.4.

It is interesting to note that for the zinc complex, an increase in the Morse potential α value causes a shortening of the Zn-N bond length, as one would anticipate given that the calculated bond length is greater than b_o for this complex. However, this shortening of bond length is accompanied by a significant increase in the bite angle of the ethylenediamine ligand. This observation is consistent with the organic backbone of the ligand behaving as a rigid structure, and hence as the bond lengths shorten then the bite angle increases. The ligand is able to behave in such a rigid way because the angles that must change as the metal-ligand bond length changes are the N-M-N 'bite angle', and the M-N-C angle, neither of which are either explicitly or implicitly parameterised in this treatment as the CLFSE is zero, and so no strain energy results from a change in these angles. The ligand itself shows a slight angle strain, as the C-C-N angle is some 0.5^{o} larger than the unstrained value. This appears to be due to repulsive non-bonding interactions that occur due to the conformation imposed upon the ligand by being bound to the metal.

Metal	α	Bond Lengths		Bite Angle		E_{min}
		calc. Å	*obs.* Å	calc	*obs*	kcal
Ni	1.32	2.124	2.124	84.6	82.1	-28.081
Zn	0.40	2.219	2.216	80.5	81.1	3.750

Table 5.6: Results of energy minimisations for the $M(H_2NCH_2CH_2NH_2)_3^{2+}$ species.

The calculated structure of the nickel complex shows a bite angle of 84.6^{o}, some 2.5^{o} larger than the experimentally observed value, while this angle is 4^{o} larger than that calculated for the zinc complex, compared with an experimental difference of only 1^{o}. This slight overestimation may again be rationalised by assuming that the rigid

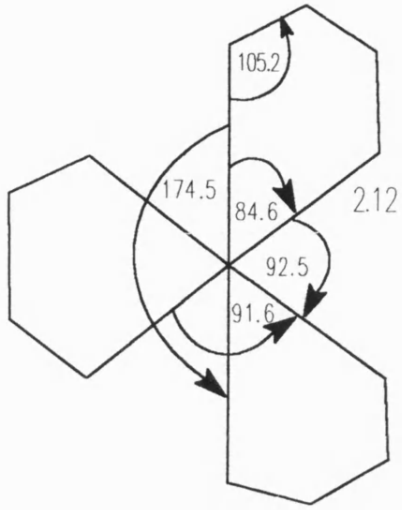

Figure 5.2: Schematic representation of the energy minimised structure of $Ni(en)_3^{2+}$.

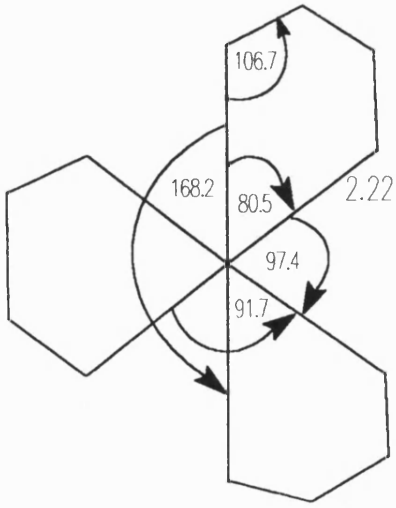

Figure 5.3: Schematic representation of the energy minimised structure of $Zn(en)_3^{2+}$.

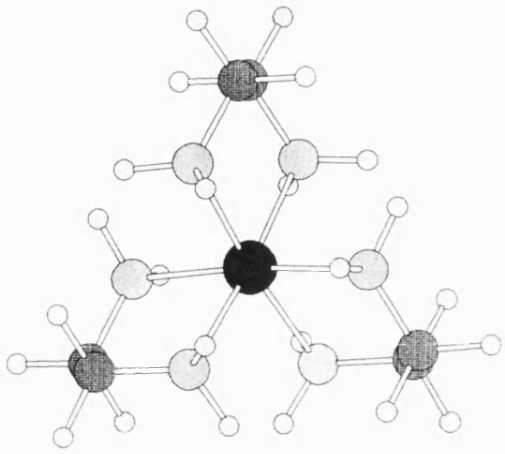

Figure 5.4: Projection of $Ni(en)_3^{2+}$ species along the C_3 rotation axis.

behaviour of the ligand causes the bite angle to increase as the metal-ligand bond lengths shorten. The organic backbone has undergone slight modification when compared with the zinc analogue, but the differences are small. The C-C-N angle is closer to the unstrained value than in the zinc analogue, showing an increase of only 0.2^{o}, and the N-C-C-N torsion angle is 58.35^{o} compared with 59.16^{o}, however the net effect of these two modifications is to reduce the span of the ligand by only 0.02Å, to 2.85Å. The most significant difference between the calculated structures is in the M-N-C angle which takes a value of 105.2^{o} compared with 106.7^{o} for the nickel and zinc complexes respectively. Again, this angle is not parameterised explicitly within the Molecular Mechanics force field and so there is no conventional increase in strain energy if this angle is reduced in order to accommodate the demands placed upon the ligand by shorter metal-ligand bond lengths. It is this angle in the nickel complex, therefore, that shows the largest deviation from the experimentally observed value, a difference of 3^{o}, although agreement between calculated and observed structures is still within acceptable bounds.

The cause of the overestimation of the N-M-N bite angle and underestimation of the M-N-C angle lies within the means by which these two angles are treated within the CLFSE term. The N-M-N angle is treated implicitly by the CLFSE, as illustrated in Chapter 4. For a d^8 species coordinated by six sigma-donating ligands the magnitude of the CLFSE shows a maximum when the six ligands adopt an octahedral arrangement, and deviation from this geometry results in a decrease in the CLFSE. Consequently, for a complex in which the ligands are under no steric constraint, such as $Ni(NH_3)_6^{2+}$, an octahedral geometry results. The trisethylenediamine complex will therefore minimise to give a geometry in which the bite angle is as close as possible to 90^o within the constraints imposed by the metal-ligand bond lengths and the strain energies of the ligand itself. The CLFSE energy gradient for the calculated deviation from octahedral geometry is small however, and so is insufficient to modify the arrangement of the ligand significantly so as to yield an octahedral arrangement of coordinating nitrogen atoms.

Although not included in these calculations, the M-N-C angle may also be treated within the CLFSE term. The effect of misdirected valence has long been recognised within the CLF formalism[40] as an important factor when analysing ligand field properties of complexes in which steric constraints prevent the notional bonding orbitals of a ligand from being directed along the ligand-metal axis. It is through the recognition and parameterisation of such effects that M-L-X angles, where X represents the next atom bonded to the ligand, may be treated implicitly within the CLFSE term. Due to the constraints already discussed, the calculated nickel structure shows a M-N-C angle of 105.2^o, compared with a notional 'ideal' angle of ca 109.5^o and such a deviation from ideal bond angle may be expected to give rise to some degree of misdirected valency. Inclusion of this misdirected valency within the CLF parameterisation would have the effect of reducing the CLFSE, the reduction being proportional to the extent of the deviation from 'ideal' of the M-N-C angle, and hence

a CLFSE 'strain energy' may be produced for this angle. In terms of the calculated structure, this would have the effect of increasing the M-N-C angle with respect to the calculated structure reported here, as in the absence of a M-N-C term this must represent a minimum value for this angle. The subsequent minimised geometry would therefore be the result of a balance between this term, the N-M-N term and the 'organic' force field, and so to reproduce the observed bond lengths the ethylenediamine ligand would be obliged to adopt a bite angle and a M-N-C angle closer to the experimentally observed values.

The copper complex is reported as showing six equivalent bond lengths of 2.15 Å. This is, however, unlikely to be the true structure as one would anticipate some form of tetragonal distortion for this species. The reported structure is, therefore, probably a time averaged structure of a dynamic Jahn-Teller distorted complex that oscillates between a tetragonally elongated and compressed geometry. These calculations seek to investigate the effect of the ethylenediamine ligands upon the species with respect to the copperhexamine complex previously discussed. These calculations therefore employ the same parameter set as were used to gain the calculated structure of $Cu(NH_3)_6^{2+}$ reported in table 5.2., and the results are shown in table 5.7 below, and the structural details are shown schematically in figure 5.5.

Metal	α	Bond Lengths		Bite Angle		E_{min}
		calc. Å	*obs.* Å	calc	obs	kcal
Cu	0.845	2.012,2.012, 2.266,2.278, 2.251,2.295	2.15	82.2, 86.2, 82.6	80.9	-20.867

Table 5.7: Results of energy minimisation for $Cu(H_2NCH_2CH_2NH_2)_3^{2+}$.

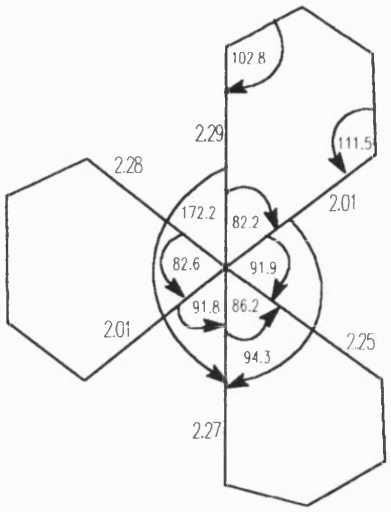

Figure 5.5: Schematic representation of the energy minimised structure of $Cu(en)_3^{2+}$.

The most significant aspect of the energy minimised geometry of the $Cu(en)_3$ species is that, despite using slightly elongated starting coordinates, the complex shows a tetragonally compressed geometry rather than an elongated geometry as calculated for the corresponding hexamine. This would appear to be due to the steric constraints imposed by the ethylenediamine ligands. In order to accommodate an elongated structure, the ethylenediamine ligands must span a rather larger distance than for a compressed structure, and, due to the relatively stiff nature of the ligands, the compressed structure is therefore favoured. This assertion is supported by calculations employing the "sum rule" derivatives that were used to show appropriate axial elongation for the hexamine complex. If the sum rule is included, a compressed geometry still results from an initially elongated coordinate set, but the course of the minimisation appears to be rather different. Due to the larger derivatives favouring axial elongation that result from employing the sum rule term, the species does show an initial preference for elongation to the extent that, after *ca* 100 iterations of the

minimisation routine, the complex shows a significant degree of elongation, the axial bond lengths being *ca* 2.4 Å and the equatorial bond lengths all being approximately equal at *ca* 2.0 Å. Thereafter, however, the extent of elongation decreases until the energetic minimum is reached, at which the species shows a compressed geometry. The implication is that the CLFSE term dominates while a suitable value of the sum is reached, but once this value is attained then the organic part of the force field becomes dominant, and will remain so provided that the sum does not deviate greatly from the ideal value. The organic terms may therefore reimpose their preference for the geometry of the complex, which would seem to be for an axial compression.

It is apparent then, that for the parameterisation employed for these calculations, a compressed geometry for $Cu(en)_3$ is favoured. It is less clear, however, as to whether this preference is due to the parameterisation of the organic part of the ethylenediamine ligand causing the ligand to be too stiff, or whether the complex does indeed show a compressed geometry experimentally. It is entirely feasible that the organic parameters are not appropriate for such a system, and no attempt is made to optimise these parameters, but in the absence of any treatment of the M-N-C angle one might expect these calculations to allow the ethylenediamine ligand the greatest flexibility as regards the ligand span. It can been seen from figure 5.5 that where one of the bidentate ligands spans both an axially compressed and a "normal" equatorial metal ligand bond then a large asymmetry of M-N-C angles occurs. If the ligand were to span an axially elongated and an equatorial bond then a larger asymmetry of M-N-C angle within the ligand would result. This asymmetry, and the large deviations from the ideal M-N-C angle, is facilitated in the absence of a term, either explicit or implicit, to describe deviations from this angle. One might expect, therefore, that if an elongated structure were to be favoured, then that structure would be reproduced by the parameterisation employed here.

The experimental evidence for this complex is rather unclear. The authors of the structural report recognise that apparent violations of the Jahn-Teller effect may occur for one of two reasons. Firstly, a regular octahedral geometry may seem apparent due to the complex oscillating between three equivalent distortions along each of the molecular axes, and hence the structure appears regular on a time average basis, known as the dynamic Jahn-Teller effect. Secondly, each molecule may be trapped in one of several such distortions, but these molecules are randomly distributed through the crystal and so the structure appears regular on a space average. However, the thermal factors for the nitrogen atoms are suggestive of a dynamic Jahn-Teller effect as, although the difference in the sizes of the thermal ellipsoids between the copper species and the nickel analogue is small, the direction of the thermal motion in the copper species is oriented along the metal-ligand axis, contrary to expectation. Unfortunately the experimental evidence is then insufficient to allow firm conclusions to be drawn from these calculations.

5.3: Ni X_2[n]ane

This section reports the results of Molecular Mechanics calculations performed upon the six nickel macrocyclic species that were the subject of the CLF study reported in chapter 3, of general form NiX_2[n]ane, where X represents Cl^- or NCS^-, n=14,15 or 16 and [n]ane represents a fully saturated n-membered tetraaza macrocyle. The single crystal X-ray structures have been reported by Ito *et al*[78] for all six complexes, and it is these structures that the calculations reported here seek to reproduce. The complexes all show an essentially tetragonal geometry, with saturated nitrogen equatorial ligands and axial ligands that show isotropic π-bonding capabilities. As for the trisethylenediamine complexes, the organic skeleton of the macrocylic ligand is modelled using the appropriate traditional Molecular Mechanics terms, parameter values for which are listed in the appendix, and again no terms describing atomic

charges are included. No attempt is made to optimise these parameters, with the exception of the van der Waals non-bonding parameterisation of the axial ligands. The invariant input values for the metal centre are shown in table 5.8. The Ni-N b_o and D_o values employed for the hexamine and trisethylenediamine complexes are used here to describe the Morse potential for both the saturated equatorial nitrogen donors and the axial isothiocyanate donor, while equivalent values for the chloride ligands are estimated from literature values. The CLF parameterisation for the saturated nitrogen ligands differs from that employed for the previous complexes. The CLF analyses reported in chapter 3 provide six independent values for $e_\sigma(N)$ which correspond to six different Ni-N bond lengths, and so it is possible to define CLF A and B parameters that provide a close fit to these six defined points. The parameterisation is therefore capable of not only providing accurate estimates of $e_\sigma(N)$ for a given bond length but also of producing appropriate $e_\sigma(N)$ vs bond length gradients for this set of compounds. Such a derivation of CLF parameters is possible for the equatorial nitrogen donors as there is no indication from the CLF analyses that there is any significant deviation from a normal form of e_λ vs M-N bond length dependence. However, the same is not true of the axial donors which show an increase in e_λ as the equatorial donation decreases as the macrocyclic ring size increases that is not accompanied by a corresponding decrease in axial bond length. If the axial ligand CLF parameters were derived in the same fashion as those for the equatorial nitrogen ligands then an inappropriately large e_λ vs M-X bond length gradient would result. The axial ligand parameters are therefore derived from the CLF database values reported in chapter 2, with π-bonding parameters defined as 0.2 e_σ and 0.140 e_σ for Cl^- and NCS^- respectively.

Ligand	D_o kcal	b_o Å	CLF A	CLF B	CLF δ	v.d.W. A	v.d.W. B
N(eq)	106	2.16	203807	206.5	0.00	86900	2020
Cl^-	104.8	2.466	420000	900	0.00	500000	3000
NCS^-	106	2.16	215000	900	0.00	250000	3000

Table 5.8: Input parameters for Morse potential and CLFSE terms used in the structural calculations of the NiX_2[n]ane species.

Figure 5.6 schematically shows the minimised structures of the three macrocyclic ligands without the presence of the nickel atom. The [14]ane ligand displays a plane of symmetry, along with a c_2 axis that lies perpendicular to this plane. The four nitrogen atoms form an almost square arrangement and are coplanar. The organic backbone shows an alternating chair and gauche conformation for the notional six and five membered rings respectively when the metal atom is included, as is experimentally observed in the presence of the nickel atom, but despite this stable arrangement the ligand shows a relatively high strain energy, as indicated by the significant deviations of the internal angles from unstrained values. The [15]ane ligand shows the lowest symmetry of the three macrocyclic ligands. The three six and one five membered rings show a chair-skew-chair-gauche conformational sequence, again as observed experimentally. The nitrogen atoms are not coplanar but form a pseudo-tetrahedral arrangement, each nitrogen showing a mean deviation of *ca* 0.3 Å from the plane defined by the other three nitrogen atoms. The ligand also minimises to give a slightly higher total strain energy than the [14]ane ligand. The minimised structure of the [16]ane ligand yields the lowest total strain energy of the three ligands, and shows the

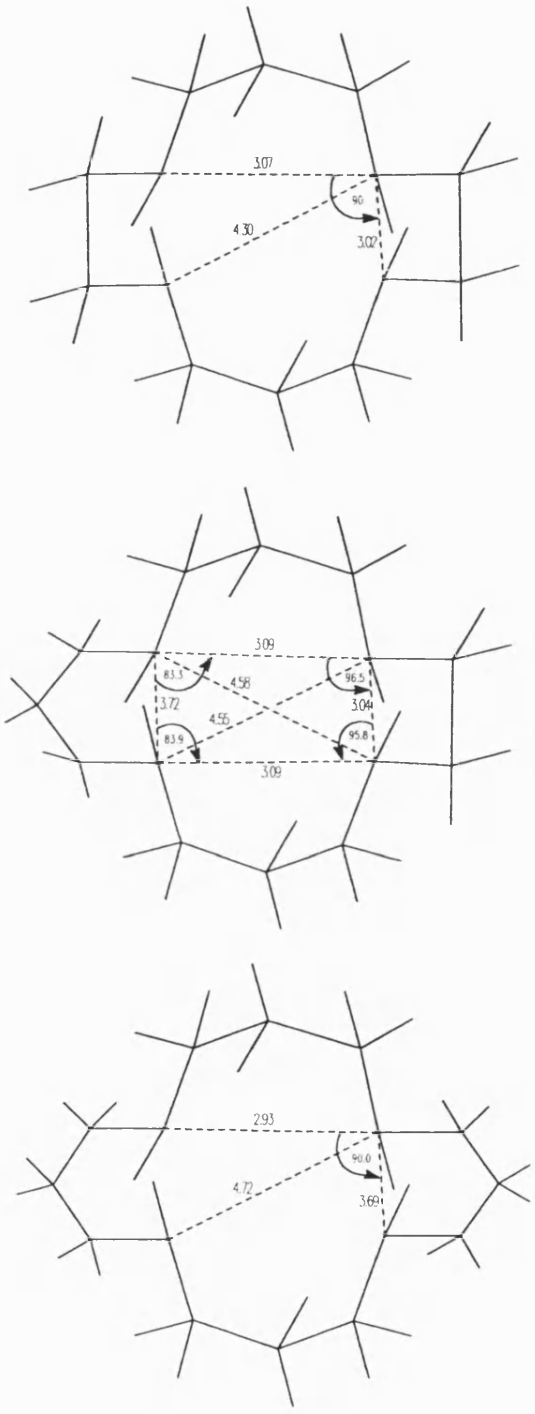

Figure 5.6: Schematic representation of the energy minimised structures of the [14]ane, [15]ane and [16]ane ligands without the metal atom.

same symmetry as the [14]ane ligand, with the four six membered rings adopting a stable chair-skew-chair-skew conformational arrangement. Interestingly, this conformation is not as experimentally observed, the observed structure showing a chair-chair-skew-skew arrangement which made up the starting coordinates for this calculation. The most significant aspect of the [16]ane structure is the difference in the bite size of the chair and skew ring conformations, 2.93 and 3.69 Å respectively, which yields two different notional bite angles of 76.7^{o} and 102.8^{o} respectively.
The energy minimised structures of the six nickel complexes are now described. Where possible, these calculations employ the experimentally observed structures as starting coordinates for the minimisation.

5.3.1: $NiCl_2$[14]ane

The [14]ane complex minimises to give the same ligand conformation as was observed both experimentally and when energy minimised in the absence of the metal atom. Again, the macrocyle shows an alternating chair and gauche conformation of six and five membered rings, and displays the same symmetry as described above. The four nitrogen atoms are again coplanar and also close to showing a square arrangement around the metal, the bite angles for the six and five membered rings being 91.1^{o} and 88.9^{o} respectively. The ring is slightly contracted in the presence of the metal as indicated by the bite sizes of 2.95 and 2.90 Å for the six and five membered rings respectively, compared with equivalent values of 3.02 and 3.07 Å in the absence of the metal atom. The structure of the macrocyclic ligand appears largely unaffected by the axial ligand, a change in axial bond length having little or no effect upon the equatorial bond lengths. Given that the CLF parameterisation is not modified during the course of these calculations and hence the CLFSE gradient as a function of bond length is for the axial ligand is invariant, then the axial bond length may be adjusted by modifying the values of the Morse potential alpha value and the van der Waals parameters of the

chloride atom, as the minimum energy bond length is the result of a balance between these three terms. The CLFSE term favours the shortening of the metal-ligand bond lengths, the Morse potential yields a strain energy for any deviation from the defined value of b_o and the van der Waals non-bonding term generally prevents the close proximity of non-bonded atoms. Given that the CLFSE term is not modified, it is the latter van der Waals term that is initially most significant in determining the minimised axial bond length. As was described in chapter 3, the closer approach of the axial ligands as the equatorial bond lengths increase is apparently prevented by steric interactions with hydrogen atoms on the macrocyclic ligand. Such repulsive interactions will be treated by the non-bonding terms, specifically the van der Waals term in the absence of atomic charges. The van der Waals term used here takes the form shown below in equation 5.6:

$$E_{v.d.W.} = A/r^{12} - B/r^{c} \qquad \text{Eqn. 5.6}$$

where c takes a value of 9 and the values of A and B are dependant upon the interaction in question. Within the Molecular Mechanics package employed for these calculations the A and B parameters are input for each atom type and a geometric mean of these parameters is employed to calculate the interaction between two atoms. In qualitative terms, the A parameter describes the repulsive part of the interaction, whilst the B parameter describes the attractive part, as the computed values of A and B are always positive. Since the observed axial bond length is longer in the [14]ane complex than the defined value of b_o, then a lower limit for the value of the repulsive term, A, for the chloride may be determined as the value that gives rise to a minimised bond length that is just longer than b_o. Thereafter the observed bond length may be reproduced by adjusting either the Morse potential α value or by further modification of the van der Waals parameters. For this complex a value of the van der Waals A parameter for the

chloride of *ca* 450,000 is required to yield an axial bond length greater than b_o, and a value of 500,000 is employed for this parameter in the final calculations reported here. The B parameter has relatively little effect upon the axial bond length, a value of 3000 is employed for this parameter, which, along with the value of 500,000 for A, is used unchanged for the other two complexes of the series. These values compare with chlorine parameters of 154,684 and 3839.3 for A and B respectively derived for use within the Molecular Mechanics package employed for these studies. Although the difference between the two A values appears large, it is important to recognise that parameters derived for organically bonded chlorine cannot hope to model the behaviour of what is formally a negatively charged chloride ion, and hence a large difference is not unreasonable. In addition to this, one might expect electrostatic interactions to be of some significance in this complex, not in determining the qualitative structure necessarily but at least in contributing to the total non-bond energy, and so in the absence of an explicit treatment of electrostatic interactions then these effects are subsumed into the van der Waals parameterisation for the chloride atoms.

The schematic representation of this complex is shown in figure 5.7, along with relevant distances and angles which show acceptable agreement with experiment, as listed in table 5.9 along with the parameters employed. It can be seen that the chloride ligand does indeed come into relatively close contact with both the hydrogen atoms bound to the coordinating nitrogen atoms and hydrogen atoms bound to carbon atoms of the organic ring. All trans-ligand pairs show L-M-L angles of 180^o, presumably due to both the overall symmetry of the calculated structure and the implicit treatment of trans-ligand angles within the CLF term. The nickel-chloride axis is not, however, perpendicular to the plane defined by the four nitrogen atoms and the metal, but is inclined at *ca* 85^o to this plane and towards the two hydrogen atoms with which the chloride has closest contact. This apparently anomalous orientation in terms of non-bonding contacts with the hydrogen atoms is due to the conformation of the macrocyle.

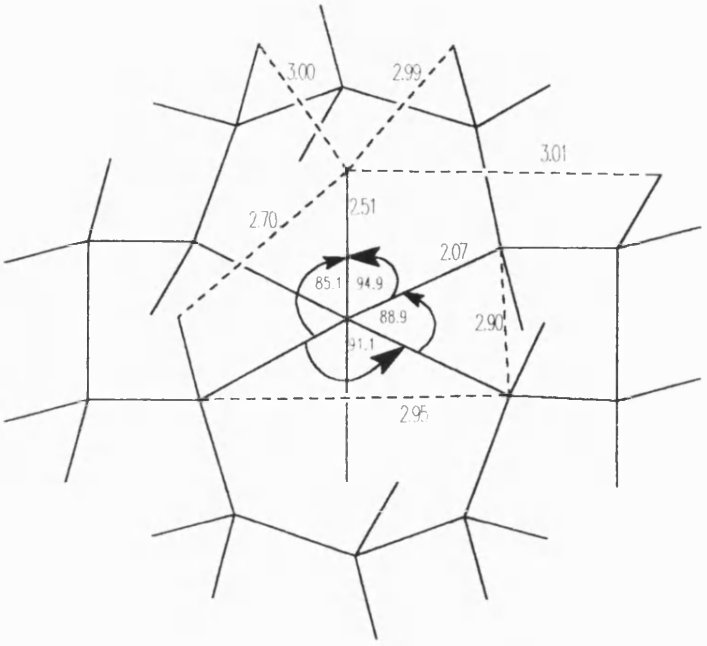

Figure 5.7: Schematic representation of the energy minimised structure of $NiCl_2$[14]ane.

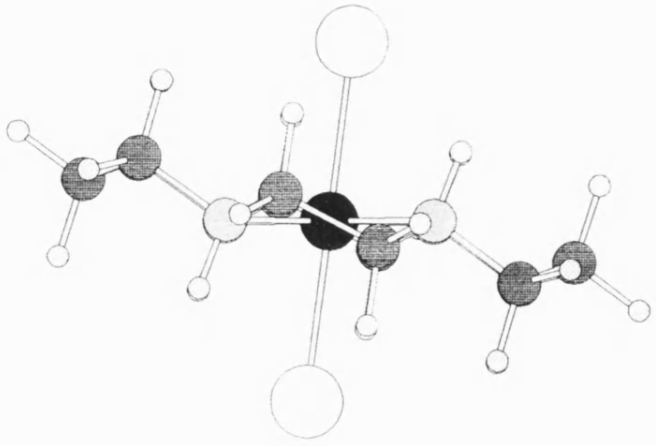

Figure 5.8: Projection of the minimised structure of $NiCl_2$[14]ane along the C_2 axis.

Figure 5.8 shows a projection of the complex along the nitrogen-metal plane. It can be seen that this deviation from the perpendicular of the nickel-chloride bond does not bring the chloride ions in significantly closer contact with the hydrogen atoms in question but does reduce the proximity of the bulk of macrocycle closest to the ligand.

5.3.2: $NiCl_2$[15]ane

The energy minimised structure of $NiCl_2$[15]ane does not show any rigourous symmetry, as predicted experimentally. Unfortunately comparison with the experimentally derived structure can only be approximate as the structure was solved under the crystallographic requirement that the nickel atom lies at a centre of symmetry, although the molecule cannot have such a symmetry element, due to a structural disorder. The calculated structure does however show the same chair-skew-chair-gauche conformation of three six and one five membered rings as indicated experimentally. The schematic representation of the complex shown in figure 5.9 shows that the chloride atom shows rather closer contact with hydrogen atoms of the macrocycle than observed for the corresponding [14]ane complex. This correlates well with the assertion made in chapter 3 that the non-bonding interactions apparently prevent any significantly closer approach of the chloride ligand on increasing the size of the macrocycle from [14]ane to [15]ane. Compared to the calculated structure of the uncoordinated [15]ane ligand, the ligand has contracted in terms of 'hole size', the four coordinating nitrogen atoms are rather closer to forming a plane with the metal, the average deviation of nitrogen atoms from the plane defined by the other three nitrogen ligands being 0.19 Å compared with 0.3 Å, and the nitrogens are considerably closer to forming a square, these effects being due to the implicit treatment of coordination geometry and bond length within the CLFSE term. The most notable difference between the [15]ane complex and the [14]ane complex is in the orientation of the axial ligands. The calculated structure of the [15]ane complex shows a Cl-Ni-Cl angle of

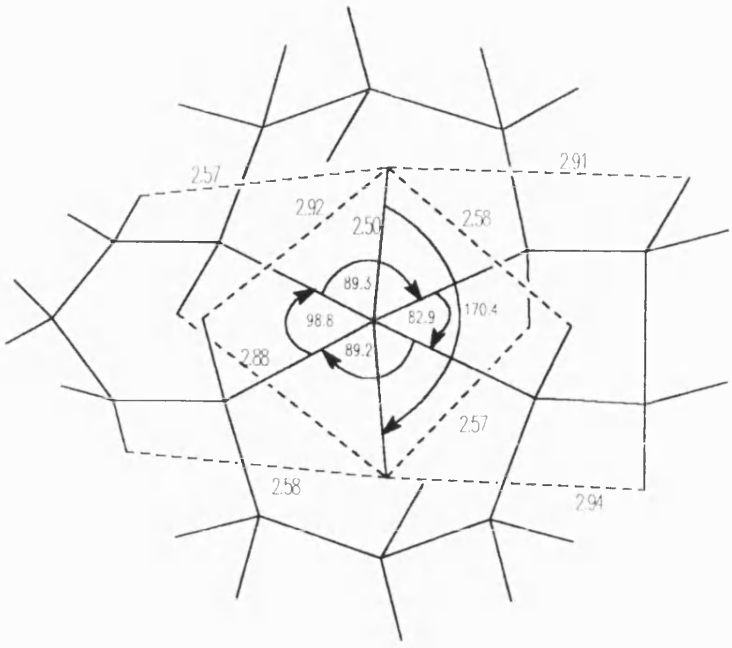

Figure 5.9: Schematic representation of the energy minimised structure of $NiCl_2$[15]ane.

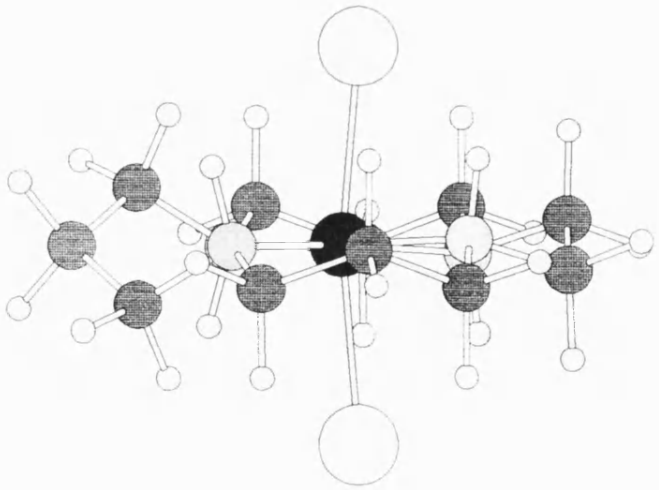

Figure 5.10: Projection of the minimised structure of $NiCl_2$[15]ane.

170.4° with both chloride atoms being oriented towards the five membered ring. This effect again appears to be due to non-bonding interactions with the bulk of the macrocyclic ligand. The asymmetry of the macrocycle prevents the axial ligands from adopting a 180° trans-angle as illustrated by the projection of the complex shown in figure 5.10, interactions with the skew six-membered ring seeming to be the main cause of the effect. The calculated bond lengths and angles around the metal are listed in table 5.9 along with the experimentally observed values and the parameter values employed to reproduce the observed structure.

5.3.3: $NiCl_2$[16]ane

The energy minimised structure of $NiCl_2$[16]ane shows the same symmetry as that shown by both the calculated and observed structures of the [14]ane complex and the calculated structure of the [16]ane ligand in the absence of the metal, as the four nitrogen atoms and the metal form a plane and the complex shows both a plane of symmetry and a C_2 rotational axis. The macrocyclic ligand shows a chair-skew-chair-skew arrangement of the four six-membered rings which gives rise to the high symmetry of the complex. This is in contrast to the experimentally observed structure, which reports a chair-chair-skew-skew conformational sequence and was used to provide starting coordinates for this calculation. Due to this conformation, the experimentally observed structure does not display any overall symmetry and differs significantly from the calculated structure in that three of the hydrogen atoms bonded to the coordinating nitrogens lie above the approximate plane defined by the metal and the nitrogen ligands and one lies below. It is therefore the asymmetry of this conformation that yields the inequivalent axial bond lengths that are observed experimentally, as the axial ligands do not share identical coordination environments. It is apparent therefore, that considerable conformational modification takes place during the course of energy minimisation of the observed structure. The chair conformation of the six-membered

rings requires the two hydrogen atoms bonded to the two coordinating nitrogen atoms of the ring to be either both above the MN_4 plane or both below the plane. Conversely the skew conformation obliges the hydrogen atoms to lie on opposite sides of this plane. The change from the chair-chair-skew-skew conformation to chair-skew-chair-skew conformation therefore requires the movement of one hydrogen atom from above the MN_4 plane to below. It is difficult to envisage such a change taking place without either considerable distortion from the defined C-N-C and H-N-C angles or significant deviation of the bonding nitrogen lone pair from the ligand-metal axis as indicated by the M-N-C and M-N-H angles. Since the latter is not explicitly parameterised within the model it is presumably the M-N-H and M-N-C angles that accommodate the change in conformation. However, if misdirected valence were to be included into the CLFSE parameterisation, as described for the nickel tris-ethylenediamine complex, then these angle terms would be treated implicitly within the CLFSE term and such deviations would not be possible. It would be likely therefore that a change in conformation would not be possible and the observed conformation would represent a local, if not global, minimum.

When the calculated structure is compared to the calculated structure of the [16]ane ligand without the central metal atom there is a notable difference in the bite sizes and angles of the notional six-membered rings. In the absence of the metal the ligand shows bite sizes of 2.93 Å and 3.69 Å for the chair and skew conformations respectively corresponding to bite angles of 76.7^{o} and 102.8^{o} respectively. However, when the metal is included, the corresponding bite sizes are 3.02 Å and 3.12 Å with angles of 88.1^{o} and 91.9^{o} respectively for chair and skew ring conformations. The bite size of the chair conformation has therefore increased due to the presence of the metal despite an overall contraction of the coordination 'hole' which might be expected to give a decrease in both bite sizes. The reason for this increase in chair conformation bite size and the large reduction in the skew conformation bite size again lies in the implicit

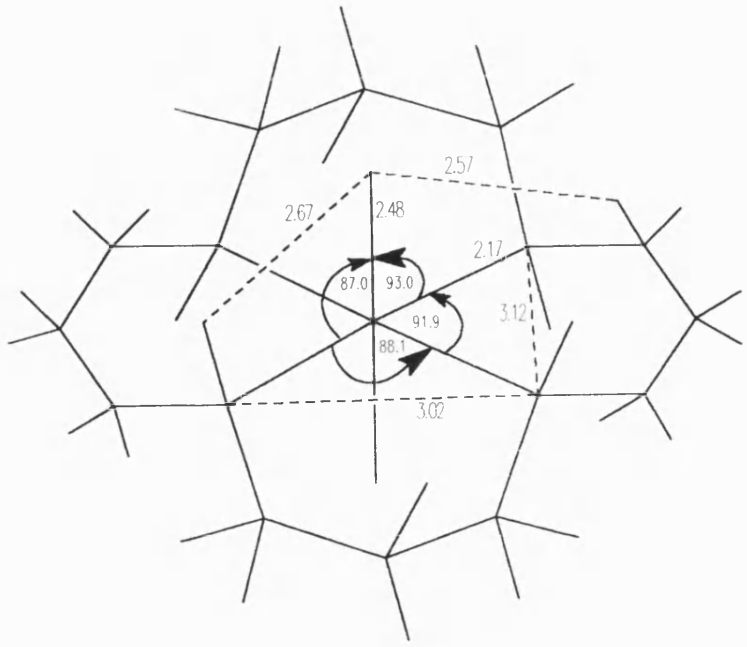

Figure 5.11: Schematic representation of the energy minimised structure of $NiCl_2$[16]ane.

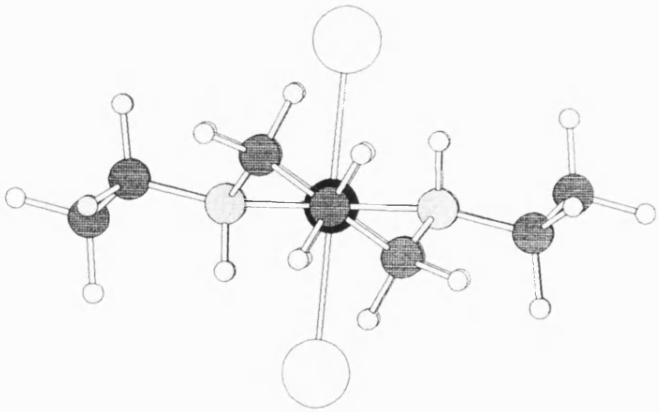

Figure 5.12: Projection of the minimised structure of $NiCl_2$[16]ane along the C_2 axis.

treatment of L-M-L angles within the CLFSE term, the CLFSE term favouring a coordination geometry as close to octahedral as possible.

The axial ligands, as observed for the [14]ane complex, are slightly distorted from an octahedral geometry, the M-Cl axis deviating some 2^{o} from the perpendicular to the MN_4 plane. Again this appears to be due to steric interactions with the bulk of the macrocyle, the orientation of the chloride ligands being analogous to that observed for the [14]ane complex. As shown schematically in figure 5.11, the chloride ligands of the [16]ane complex show the closest contact with the hydrogen atoms of the macrocyclic ring of the three complexes studied in this series, and indeed shows a closer contact with a hydrogen atom bonded to a ring carbon atom than a ring nitrogen atom. This again correlates well with the assertions of chapter 3. The final parameter set is listed in table 5.9 along with the calculated and observed bond lengths and angles, and a projection of the calculated structure is shown in figure 5.12.

5.3.4: $Ni(NCS)_2$[14]ane

The calculated structure of Ni[14]ane$(NCS)_2$ shows the same conformation of the [14]ane ligand as that for the analogous dichloro complex. The Ni-N(eq) bond lengths are essentially the same, as are the angles around the metal, and the structure again shows acceptable agreement with experiment. These bond lengths and angles are shown in table 5.9. The minimised axial bond length for the isothiocyante ligand is, as for the chloro complexes, the result of a balance between the CLFSE term favouring a decrease in bond length, the repulsive Van der Waals interactions favouring an increase in bond length and the Morse potential. All three experimentally derived structures of this series show axial bond lengths that are shorter than the defined value of b_o. Therefore, in an opposite fashion to the chloro complexes, an upper value may be determined for the repulsive van der Waals parameter as that value that yields an energy minimised axial bond length that is shorter than b_o. This may be gained by

employing a van der Waals A parameter value of less than 330,000 with a B value of 3,000. For this series of calculations van der Waals parameter values of A=250,000 and B=3,000 are employed unchanged. These values compare with 'organic' nitrogen parameters of 86,900 and 2,020 for A and B respectively.

The axial bond length in $Ni(NCS)_2$[14]ane is significantly shorter than that in $NiCl_2$[14]ane, and consequentially there is rather closer interaction between the axial nitrogen donor and the hydrogen atoms of the organic ring, as illustrated in figure 5.13. However, since the repulsive Van der Waals parameter is much smaller for the coordinating nitrogen of the isothiocyanate ligand than for the chloride ligand, as one would anticipate given the smaller size of the nitrogen atom, this closer contact with the ring hydrogen atoms does not necessarily give rise to a larger non-bonded repulsive interaction, and does not appear to cause any significant modification of the hydrogen positions compared to the analogous structure of the chloro complex. The M-N(ax) axis is, again as calculated for the chloro analogue, not perpendicular to the MN_4 plane but shows a *ca* 4.5^o deviation from the normal. This deviation is again oriented away from the chair conformation that lies on the same side of the MN_4 plane as the isothiocyanate ligand. The remainder of the ligand shows the opposite orientation however. The carbon and sulphur atoms of the ligand lie towards this chair conformation, as shown in figure 5.14, presumably due to longer range attractive van der Waals interactions with the macrocyle, and shows an M-N-C angle of 153.9^o. The four reported crystallographically independent experimental structures, that differ in the orientation of the isothiocyanate ligand only, show the M-N(ax) axis inclined by between 1.3^o and 1.9^o to the normal to the MN_4 plane and in the same sense as that shown by the calculated structure. The orientation of the rest of the isothiocyanate ligand is less clear however, and although the calculated structure does not show the same orientation as any of the four complexes there is evidently only a relatively small barrier to rotation of the isothiocyanate ligand and so this is by no means a failure of

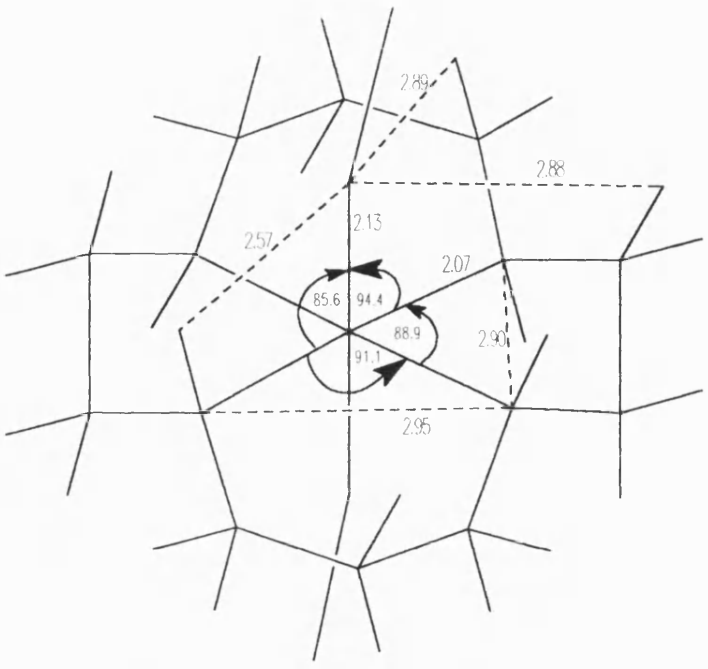

Figure 5.13: Schematic representation of the energy minimised structure of $Ni(NCS)_2$[14]ane.

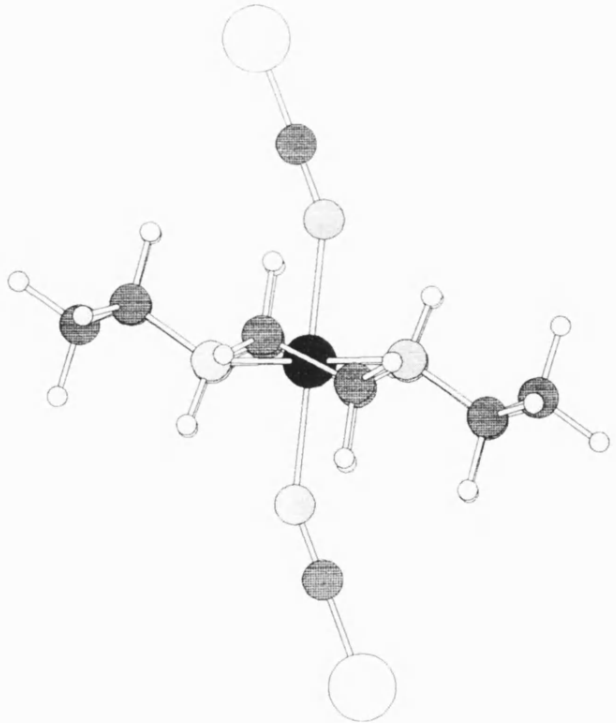

Figure 5.14: Projection of the minimised structure of $Ni(NCS)_2$[14]ane along the C_2 axis.

the model. The four complexes show M-N-C angles from 156.2° to 168.2°, compared to the calculated value of 153.9°. This angle is, however, not explicitly parameterised and, as previously discussed, would be implicitly treated by the inclusion of misdirected valence parameterisation. Such a treatment would tend to reduce this angle to a value closer to the experimentally observed value. Ito *et al*[78] suggest however, that all the isothiocyanate ligands of the three complexes in this series are involved in intermolecular hydrogen bonds and form a linear chain along the a-axis of the crystal, and that it is these hydrogen bonds that principally determine the orientations of the isothiocyante ligands. If this is indeed the case, then it is impossible to reproduce such effects within these calculations. However it would seem that from the calculations performed upon this set of complexes, all of which show significant tilting of the isothiocyanate ligand, that intramolecular non-bonding interactions may also be significant in determining the orientation of the axial ligands.

5.3.5: $Ni(NCS)_2$[15]ane

The experimentally derived structure of $Ni(NCS)_2$[15]ane shows a longer average equatorial M-N bond length than the chloro analogue, the average bond lengths being 2.131 Å and 2.114 Å respectively. This may well be due to a difference in the conformation of the macrocycle between the two compounds as the chloro species shows a chair-skew-chair-gauche conformational sequence whilst the isothiocyanate analogue is reported as showing a chair-chair-skew-gauche sequence. The energy minimised structure, however, despite employing the experimentally derived coordinates as a starting geometry, shows the same conformational sequence as that found for the chloro analogue. The course of the minimisation is presumably rather similar to that which is assumed to have occurred for $NiCl_2$[16]ane, in that one of the hydrogen atoms bonded to a coordinating nitrogen atom has moved from one side of the MN_4 plane to the other as the conformation changes. What is not clear is why a

such a difference in conformation should give rise to a noticeable difference in the average M-N bond length. It is interesting to note however, that for the chloro series the change in axial bond lengths on changing the macrocycle from [14]ane to [15]ane and [15]ane to [16]ane are 0.013 Å and 0.015 Å respectively, a very small but consistent decrease. The corresponding changes in axial bond length for the isothiocyanate series are 0.051 Å and 0.002 Å respectively. It was suggested in chapter 3 that this was due to the smaller size of the isothiocyanate donor compared with the chloride donor, so that steric interactions with the macrocycle holds the relatively large chloride ligands at about the same distance for all three ring sizes. In contrast, the smaller nitrogen donor atom of the isothiocyanate ligand initially allows for a shortening of the axial bond length from the [14]ane to [15]ane species, thereafter the isothiocyante ligand too is held at the same distance in the [16]ane. This would seem a feasible rationalisation of the observed data, but it is equally possible that the closer approach of the isothiocyanate ligand in the [15]ane species is due to the enlargement of the ligand hole size due to the difference in conformation of the macrocycle. It is worthwhile, however, to consider the difference in the parameters employed to reproduce the observed structures of $NiCl_2$[15]ane and $Ni(NCS)_2$[15]ane, as listed in table 5.9. The chloride complex requires a Morse potential α value of 0.5 for the macrocyclic nitrogen-metal bond compared with a value of 0.4 for the isothiocyanate complex to give calculated average bond lengths of 2.114 Å and 2.139 Å respectively. Given that, for the equatorial ligands, the CLFSE favours a decrease in bond length and that the bonds are shorter than the defined b_o value, one would anticipate that a smaller value of α would yield a shorter energy minimised bond length, rather than the converse as is observed. The schematic representation of the [15]ane isothiocyanate species, shown in figure 5.15, shows that this complex, although it may not display the largest total repulsive contact between the axial ligand and the ring hydrogen atoms, does show the single closest contact of 2.47 Å, of which there are four such contacts in

the minimised structure. It is possible therefore that the close approach of the isothiocyanate ligand, driven by the CLFSE derivative, actually increases the hole size of the macrocyclic ligand via strong repulsive non-bonding interactions. From the CLF parameterisation the CLF e_λ vs bond length gradient for the isothiocyanate ligand at the observed bond length is greater than that for the equatorial ring nitrogen, and consequently it is preferable for the equatorial bond lengths to increase rather than the axial bond lengths when the non-bonded contacts become close. This assertion is supported by the empirical observation that an adjustment in the Morse potential α value of the isothiocyanate ligand not only modifies the axial bond length but also the equatorial bond lengths. This effect is greater if a larger value of the Van der Waals A parameter is employed to the extent that the observed axial and equatorial bond lengths cannot be simultaneously reproduced. The suggestion is then, that even for the same conformation of the macrocyclic ligand, the isothiocyanate complex shows a longer average equatorial bond length than the corresponding chloro complex due to stronger repulsive non-bonding contacts between the nitrogen atom of the isothiocyanate ligand and the hydrogen atoms of the macrocyclic ring than in the chloro analogue.

The other interesting aspect of the calculated structure of this complex is the orientation of the isothiocyanate ligands. The N(ax)-M-N(ax) angle of 171.1^{o} is similar to that of the chloro analogue, and the deviation from the normal to the best fit $MN(eq)_4$ plane shows the same orientation away from the skew six membered ring. The notable aspect of the structure, shown in figure 5.16, is that both the isothiocyanate ligands are oriented in roughly the same direction showing a C-N-N-C torsion angle of 20^{o}, the converse of both experimental observation and chemical expectation. This appears to be due to the orientation of the coordinating nitrogen atoms of the isothiocyanate ligands, which are both oriented in the same direction. Given this initial orientation the isothiocyanate ligand is able to maximise attractive non-bonding interactions with the macrocycle, presumably via the carbon atom of the ligand as this is in closer proximity

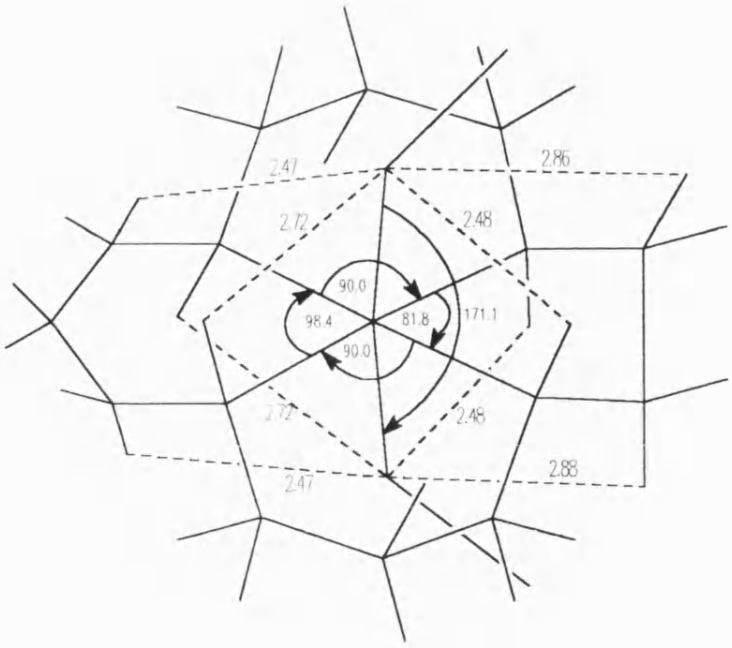

Figure 5.15: Schematic representation of the energy minimised structure of $Ni(NCS)_2$[15]ane.

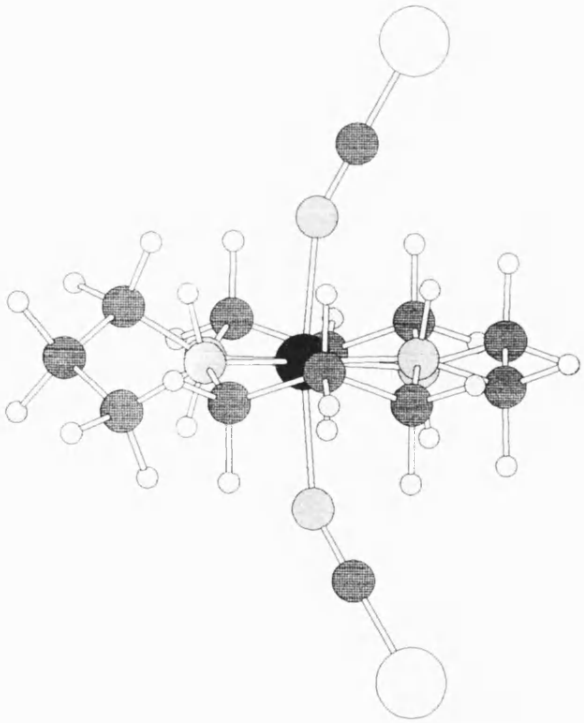

Figure 5.16: Projection of the minimised structure of $Ni(NCS)_2$[15]ane along the C_2 axis.

to the non-bonded atoms than the sulphur, by orienting itself in the same direction as the nitrogen with respect to the metal and the macrocycle. Since both nitrogen atoms are oriented in the same direction, so are the rest of the ligands, showing a M-N-C angle of 156.7^{o} compared to the experimental value of 153.8^{o}. Due to the constraints of holohedral symmetry, discussed in chapter 2, the CLFSE term is unable to differentiate between a situation in which the isothiocyanate ligands are oriented in the same direction showing a C-N-N-C torsion of 0^{o} or in opposite directions showing a torsion of 180^{o}, since in qualitative terms any misdirected valence from either sigma or pi bonding orbitals of the ligand is directed into the same pi orbital of the metal regardless of which orientation is adopted. The inclusion of misdirected valence would however provide a barrier to rotation between the two orientations and so local minima for the two opposite orientations may therefore be defined.

5.3.6: $Ni(NCS)_2$[16]ane

The calculated structure of Ni[16]ane$(NCS)_2$ is qualitatively the same as that calculated for the chloro analogue. The macrocyclic ligand shows the same chair-skew-chair-skew conformational arrangement, despite employing the experimentally observed structure as a starting point. The experimental structure displays a chair-chair-skew-skew conformation and so the course of the minimisation is evidently analogous to that of the chloro complex. The calculated structure for this complex does however show some quantitative differences from the chloro compound in the coordination of the macrocyclic ligand. The M-N(eq) bond lengths are slightly longer and the four equatorial nitrogen atoms are closer to forming a square, showing bite angles of 90.6^{o} and 89.4^{o} for the chair and skew conformations of six-membered rings respectively, as shown in figure 5.17, compared with values of 91.9^{o} and 88.1^{o} for the chloro complex. It is difficult to determine whether this effect is due to the increase in

M-N(eq) bond length upon the macrocycle or due to the presence of the isothiocyanate axial ligand rather than the chloro ligand. However, comparison with the calculated structure of the [16]ane ligand in the absence of the metal suggests that an increase in bond length is accompanied by an increasing inequivalence in the bite angles of the two conformations and so the suggestion is that the modification of the macrocycle is due to steric interactions with the isothiocyanate ligands, and this is also consistent with the increase in M-N(eq) bond length.

The M-N(ax) axis is, as for the other complexes, not normal to the $MN(eq)_4$ plane but is inclined at *ca* 4.5^{o} to the normal, slightly less than the chloro analogue. The orientation of the coordinating nitrogen is the same, however, as it is inclined away from the chair conformation on the same side of the $MN(eq)_4$ plane. The remainder of the isothiocyanate ligand shows similar behaviour to that shown by the $Ni(NCS)_2$[14]ane complex in that it is oriented towards the chair conformation on the same side of the $MN(eq)_4$ plane, the opposite direction from the coordinating nitrogen. The calculated M-N(ax)-C angle is 137.7^{o}, compared with an experimentally derived value of 160.0^{o}, but as the isothiocyanate ligands are reported as being involved in intermolecular hydrogen bonding, and that this bonding is responsible for the orientation of the ligand, this discrepancy is not of concern. It is interesting however, to compare this value with that calculated for the [14]ane analogue of 153.9^{o}. It would appear that the [16]ane complex shows more dramatic tilting of this ligand, as shown by the projections of the two complexes, figures 5.14 and 5.18 for the [14]ane and [16]ane species respectively. The [16]ane ligand is much 'flatter' than the [14]ane ligand, and so the isothiocyanate must tilt further in order to maximise attractive non-bonding contacts in the [16]ane complex. In the absence of a misdirected valence term, the ligand is able to tilt in order to maximise such interactions without incurring any strain energy as a result of changing the M-N(ax)-C angle.

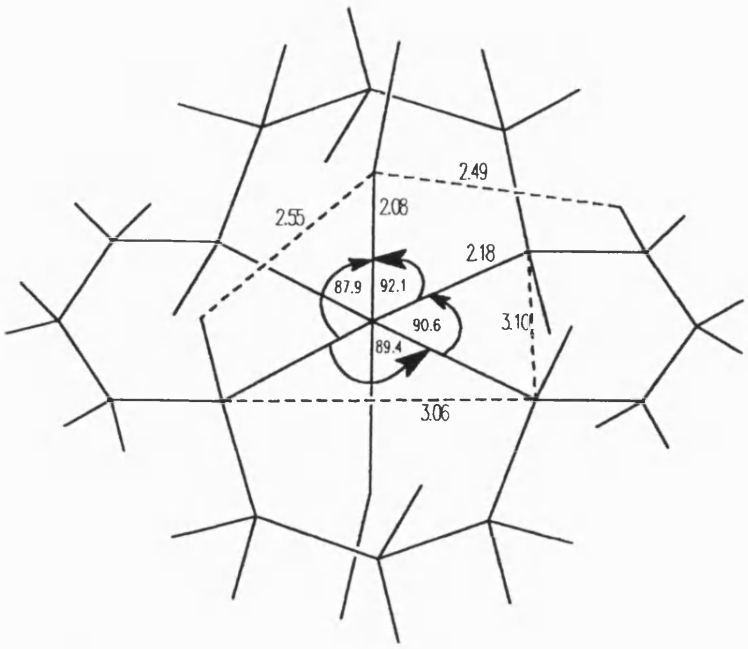

Figure 5.17: Schematic representation of the energy minimised structure of $Ni(NCS)_2$[16]ane.

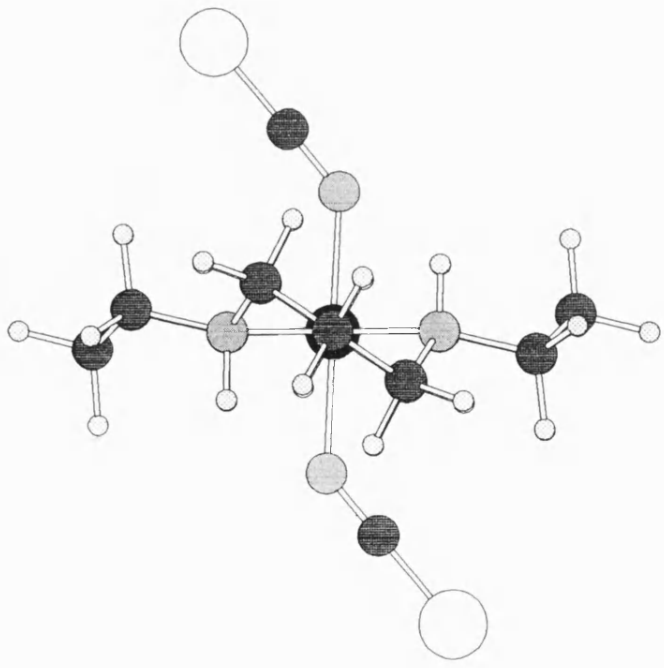

Figure 5.18: Projection of the minimised structure of $Ni(NCS)_2$[16]ane along the C_2 axis.

5.4: Discussion

It has been shown that the experimentally observed structures of all six nickel complexes of this series may be accurately reproduced in terms of bond lengths and angles around the metal. The two [14]ane complexes and the [15]ane chloro complexes also show the same conformation of the macrocyclic ligand as that observed experimentally, whilst the [15]ane isothiocyanate complex and the two [16]ane complexes show a different conformational sequence from experiment after energy minimisation. For the complexes in which the experimental conformational sequence is not reproduced, the calculated structure in each case displays a higher symmetry and may therefore represent global minima. However, it is postulated that the inclusion of misdirected valency into the CLFSE term will allow the reproduction of the observed conformations, even if these conformations do represent local rather than global minima. The largest discrepancy between the calculated and experimental structures is in the orientation and angle of the isothiocyanate ligands. This does not represent a failure of the CLFSE term though, as the orientations of the isothiocyanate ligands are reported as being due to intermolecular hydrogen bonding and such effects cannot be reproduced within a one molecule simulation.

Effective Molecular Modelling requires more than simply the reproduction of structures however, and unless some degree of parameter transferability is evident then there is little advantage in including the CLFSE term rather than employing more traditional Molecular Mechanics treatments that do not explicitly recognise the electronic term arising from the partially occupied transition metal d-orbitals. Table 5.9 shows the Morse potential α parameters employed to yield the listed calculated bond lengths, also listed are the CLFSEs and CLF sum values along with the experimentally observed values of bond lengths and CLF parameter values. Inspection of the listed parameters indicates that the Morse potential α value for the equatorial metal-nitrogen bond shows little or no correlation as the macrocyclic ring size increases for either axial ligand,

while the same α values consistently decrease on exchanging the chloride axial ligand for an isothiocyanate ligand for a given macrocycle. Similarly the α values for the axial metal-ligand bonds show little evidence of transferability. It is important, however, to study this apparent lack of transferability and to identify areas which may be modified in order to increase the possibility of parameter transfer.

Complex	α equatorial axial	Bond Lengths equatorial calc *obs*	Bond Lengths axial calc *obs*	av. e_λ equatorial calc *obs*	av. e_λ axial calc *obs*	CLFSE Σ cm^{-1}
Ni[14]ane	0.862	2.067	2.511	4975	1948,390	-13592
Cl_2	0.52	*2.067*	*2.510*	*4976*	*1580,240*	25358
Ni[15]ane	0.50	2.114	2.497	4391	2079,416	-12032
Cl_2	0.90	*2.114*	*2.497*	*4390*	*2250,575*	23399
Ni[16]ane	1.80	2.171	2.482	3778	2225,445	-10982
Cl_2	1.25	*2.171*	*2.482*	*3779*	*3100,900*	21335
Ni[14]ane	0.82	2.067	2.130	4975	2987,415	-14760
$(NCS)_2$	0.93	*2.067*	*2.130*	*4780*	*3000,100*	27508
Ni[15]ane	0.40	2.139	2.076			-13081
$(NCS)_2$	0.60	*2.131*	*2.079*	*4072*	*3600,500*	25917
Ni[16]ane	1.59	2.178	2.077	3709	3693,513	-12497
$(NCS)_2$	0.627	*2.179*	*2.077*	*3632*	*4100,750*	24273

Table 5.9: Results of energy minimisation of Ni[n]aneX_2 species.

The most obvious situation in which one would expect to observe a high degree of transferability is in the Morse potential α N(eq) parameters for a given macrocycle size for each of the two axial ligands, and indeed the agreement between the parameters employed for each pair of compounds is not unreasonable, although one might expect the values to be essentially identical. The reason that these parameters are not closer lies in the assignment of the van der Waals non-bonding parameters. As was previously described, it is only possible to define a lower limit for the value of the A parameter for a given value of B for the chloride ligand, and an upper value of A for a given value of B for the isothiocyanate ligand. Within these limits it is only possible to assign arbitrary values for the parameters and then to adjust the Morse potential alpha values until the correct minimised structure is achieved. Traditionally values for the van der Waals parameters are gained by relating these parameters to physical observables such as the van der Waals radius of an atom. This is not straight forward for formally ionic species, and as Coulombic interactions are not explicitly included for these calculations then the van der Waals term must subsume all non-bonding interactions, so such a derivation of parameter values would not be valid within this scheme. Given that the close contact and consequent repulsion between the axial ligands and the hydrogen atoms of the macrocyclic ligand appears to form such a significant role in this series of complexes, and that the van der Waals parameterisation of the axial ligand can effect both the axial and the equatorial bond lengths, then it follows that each of the three pairs of structures will only be reproduced by employing the same α value for N(eq) if the van der Waals parameterisation of the chloride and isothiocyanate ligands are correct relative to each other. It would seem that, for the calculations described here, the repulsive term for the isothiocyanate ligand is too large relative to that for the chloride. This is apparent from inspection of table 5.9. For the chloride species the value of the Morse potential α value required to reproduce the observed bond lengths is larger than that for the analogous isothiocyanate species for all three sizes of

macrocycle. For the [14]ane and [15]ane species this is easily rationalised in that while the CLFSE term favours a shortening of bond lengths, for these four complexes the Morse potential favours a lengthening of the bonds as the bond lengths are less than b_o. Therefore a reduction in the α value for N(eq) on replacing the chloride ligand with a isothiocyanate ligand would be expected to yield a reduction in bond length, however the bond lengths are seen to either remain the same for the [14]ane or increase for the [15]ane. This is due to the greater repulsive nature of the isothiocyanate ligand relative to the chloride ligand due to the assigned parameters. The behaviour of the two [16]ane complexes is less clear, as for these species the observed and calculated bond lengths are beyond b_o. A reduction in the N(eq) α value would therefore be expected to yield an increase in bond length, as is observed. The results for these complexes are not inconsistent with the above rationalisation however, as it is difficult to estimate the effect of the reduction in α upon the calculated bond length in the absence of these non-bonded interactions for purposes of comparison. It is likely then, that it is possible to assign values for the van der Waals parameters for the two axial ligands that will allow the reproduction of the observed bond lengths of the six complexes using the same N(eq) α value for each pair of complexes with the same size macrocycle.

The behaviour of the Morse potential parameters as the macrocyclic ring size increases for each axial ligand are rather more complex. The three chloride species show an increase in the chloride α value as the ring size increases. It is apparent therefore that as the ring size increases the axial ligands are subject to an increasing net repulsive interaction as a significantly larger value of α is required to bring the ligand only slightly closer to the value of b_o, which is shorter than the observed bond length in all three complexes. It is shown in figures 5.7, 5.9 and 5.11 and figures 5.13, 5.15 and 5.17 that the contacts between the axial ligands and the hydrogen atoms of the ring become closer as the ring size increases, and so it is obvious therefore that the repulsive interactions increase more rapidly as a function of decreasing axial bond length than the

CLFSE. Transferability of the chloride α value will only occur if the parameterisation of the non-bonding term and the CLFSE term for the axial ligand yield appropriately balanced energy gradients. The same is true of the isothiocyanate ligands which display similar behaviour. The N(ax) α value decreases as the ring size increases, and as the observed bond lengths are shorter than b_o it is again apparent that the net repulsive forces increase as the ring size increases. The behaviour of the α value of the axial ligands is therefore dependant upon the relative gradients produced by the repulsive non-bonding term and the attractive CLFSE term and hence it may well be possible to solve the problem of parameter transferability by adjustment of the parameterisation of these two terms.

The non-bonding term apparently yields an energy gradient that is too steep with respect to the distance between the axial ligand and the hydrogen atoms of the ring, at least at the contact distances observed here. This gradient may be modified in one of two ways. The transferability of the N(eq) α value on changing the axial ligand appears to be dependant upon assigning van der Waals parameters for Cl^- and NCS^- that are correct relative to each other, but the magnitude of the parameter values is unimportant. The transferability of the axial α values as the ring size increases is dependant upon the magnitude of these values, however, as it is these values that determine the non-bond energy gradient for a given interaction. It is, therefore, entirely feasible that via some appropriate fitting process both the magnitude and relative magnitudes of the van der Waals parameters for the axial ligands may be determined so as to satisfy the conditions for parameter transferability. It is also possible, however, that such a fit cannot be gained and that the form of the van der Waals non-bonding term is unable to produce appropriate energy gradients to give such parameter transferability. Such a scenario would demand a more chemically complete treatment in that the role of atomic charges may demand consideration. For these complexes the inclusion of an atomic charge energy term would not be expected to modify the

calculated structures in a qualitative sense, although some stiffening of the angular potentials would result, but would inevitably have an effect upon the parameter values required to reproduce the observed structure. Given that the Coulombic term usually employed to compute charge interactions shows a r^{-1} dependence, where r is the distance between the interacting atoms, then it is likely that the combination of this term with the van der Waals term, when suitably parameterised, will yield energy gradients that will allow parameter transferability.

The CLFSE parameterisation for the axial ligand may also be modified to yield a steeper e_λ vs bond length gradient at the observed bond lengths, which would provide an increasing CLFSE gradient as the bond lengths shorten. However, this would be inconsistent with the use of the database values to provide CLF e_λ vs bond length curves for the general case. It is feasible, though, that the sum rule has a role to play here, if modification of the CLFSE gradients is deemed necessary. Inspection of table 5.9 shows that as the macrocyclic ring size increases the axial e_λ and consequently the sum deviate increasingly from the values determined in the CLF analyses of chapter 3. The problem here is that, as shown in chapter 3, the axial e_λ are not necessarily related to the axial bond length where steric interactions inhibit the movement of ligands, the e_λ(ax) being capable of increasing significantly without a corresponding change in axial bond length. It is therefore possible to rectify these discrepancies via a sum rule algorithm that will increase the CLFSE energy derivatives for the appropriate ligands.

The choice of van der Waals parameters for the axial ligands also has an effect upon the transferability of the N(eq) Morse potential α parameter as the macrocyclic ring size increases. As the ring size increases the non-bonding contacts between the axial ligands and the ring hydrogen atoms become closer and hence a larger non-bonding energy results and this manifests itself in both the axial and equatorial ligand parameter values. In the same fashion as for the axial α parameters along a series, if the non-bond energy gradient is too large, as it appears to be, then this will prevent parameter

transferability. Again, modification of the non-bond energy parameterisation via either of the two methods described above will improve the possibility of parameter transferability for the equatorial ligands.

The non-bonding terms may not, however, account entirely for the lack of transferability as the role of the 'organic' force field must not be neglected. No attempt is made to optimise the conventional Molecular Mechanics parameters and the default values listed for the programme are employed. This is not necessarily an appropriate force field for the species studied here, however, and so may well yield energy gradients that do not balance well with the description of the metal centre. This is illustrated by comparison of the calculated ligand structures with and without the metal centre. All three ligands, despite identical 'organic' parameterisation, show different magnitudes of difference between the calculated hole sizes with and without the metal atom. For example, the [16]ane complexes show the largest hole size difference with and without the metal, and so in the presence of the metal the macrocycle ring shows the largest deviation from the least strained geometry. At the observed metal-ligand bond lengths these complexes therefore show the largest strain energy resulting from the conformation of the macrocycle and consequently the total energy gradients favouring contraction of the ring must be the largest for all three ring sizes. Conversely, the [14]ane complexes show the smallest difference between the hole sizes with and without the metal and so at the observed metal-ligand bond lengths these complexes show the least strain energy resulting from the macrocycle and hence require a much smaller net energy gradient favouring contraction of the ring size. Both the uncoordinated [16]ane ligand and the [16]ane complexes show notional metal-ligand bond lengths greater than the defined value of b_o and so both the CLFSE and the Morse potential act so as to contract the ring, whilst for the [14]ane species the Morse potential prevents further contraction of the ring as favoured by the CLFSE as the calculated bond lengths are shorter than b_o. The suggestion is then that in the absence

of the Morse potential the [14]ane complexes would show further ring contraction whilst the [16]ane complexes would favour ring expansion. Even given that the [14]ane complexes have a larger CLFSE gradient than the [16]ane complexes at the observed bond lengths due to the parametric form of CLF e_λ vs bond length expression, and hence may give a net energy gradient favouring contraction of the ring that would compensate for the larger ring strain energy favouring expansion of the ring in the [16]ane complexes, it is unlikely that the Morse potential energy derivative will be able to yield gradients that are appropriate for both ring sizes by employing the same Morse potential b_0 and α parameter values. If the structures of the [14]ane and [16]ane complexes are to be reproduced employing the same parameter values, then these values must be chosen such that the Morse potential yields gradients that are equal and opposite to the net energy gradients favouring contraction in the [14]ane complexes and expansion in the [16]ane complexes. Such a choice of parameter values is possible, but is unlikely to simultaneously yield the observed structure for the [15]ane complex unless some modification of the organic force field is also effected.

5.5: Conclusions

The calculations reported in this chapter illustrate that, for the complexes showing octahedral based geometries studied here, the CLFSE term is capable of modelling the structures of such species as well, if not better, than any conventional Molecular Mechanics approach. The advantage that the CLFSE brings to the modelling of such species is the recognition of the effects of the LFSE. This includes, for example, the reproduction of the behaviour of the heats of formation of the first row hexamine complexes, in which the "double hump" behaviour is reproduced as a consequence of the additional energy arising from the CLFSE term, rather than as the consequence of fitting the Morse potential D_0 values to the observed data, and so both the results and the methodology are in accordance with basic coordination chemistry rationale. The

most significant result of the hexamine series is, of course, the calculated structure of the $Cu(NH_3)_6^{2+}$ complex, which shows inequivalent axial and equatorial bond lengths from identical parameterisation. This is as a consequence of the Jahn-Teller effect as modelled by the CLFSE term, and, although the extent of axial elongation is initially underestimated, this is a unique result for the molecular modelling of coordination compounds. Although an additional energy term, the sum rule, is required to reproduce the observed bond lengths for this complex, the use of such a term is entirely justified within the CLF formalism and the sum rule is likely to provide a useful tool for future studies.

The series of calculations for the trisethylenediamine species illustrates that the CLFSE is as effective for modelling more complex species as for the simple hexamines. The implicit treatment of L-M-L angles within the CLFSE term simplifies the parameterisation of the force field considerably and the structural results are again as good as those gained by traditional molecular mechanics treatments[26]. Unfortunately the experimental data is not sufficient to draw any definite conclusions as regards the copper complex, but again the Jahn-Teller activity of the d^9 species is highlighted. The nickel tetraazamacrocyle series of complexes shows that the CLFSE term not only reproduces the experimental structures but is also capable of providing a chemical insight into the behaviour of these complexes despite the simplistic treatment. The CLFSE term provides particular insight as regards the nature of the metal-ligand bonding, and the interaction between the axial and equatorial ligands. It is the chemical transparency of the CLF parameter formalism that allows the metal-ligand bonding to be interpreted, the CLF parameters yielding information that would not be apparent from traditional bonding descriptions.

The calculations reported in this chapter have also served to highlight areas in which this method of modelling transition metals may be improved. The ethylenediamine and the tetraazamacrocyclic series of complexes both illustrate the potential utility of

including missdirected valence into the CLFSE parameterisation so as to treat M-L-N angles, where N represents the next atom bonded to the ligand. As for the treatment of L-M-L angles, it is preferable to model such effects implicitly within the CLFSE term both to reduce the degree of parameterisation and to avoid problems resulting from the choice of an inappropriate angular deformation term, a problem encountered in traditional Molecular Mechanics force fields.

The one failing of the CLFSE term that is apparent is the lack of parameter transferability between species within a series of related complexes. Almost any parametric model is capable of reproducing observed structures, and, although the CLFSE term provides an intuitively appealing means of reproducing structures from a coordination chemists' point of view, the model will not find widespread use unless this problem can be overcome. The reasons for the lack of parameter transferability have been discussed extensively for the tetraazamacrocycles, the series in which one would anticipate the largest degree of transferability, and it would seem that this problem may potentially be overcome by a number of means, all of which appear reasonable. It is likely, therefore, that the problem of parameter transferability will not impair the progress of the CLFSE term, once appropriate parameterisation is achieved.

Chapter 6

Results of Molecular Mechanics: 2

6.1: Introduction

It was shown in the previous chapter that the structures of six coordinate complexes showing octahedral based geometries may be reproduced by employing the CLFSE to treat the metal centre and immediate coordination sphere within a Molecular Mechanics scheme. The treatment was, however, chemically incomplete as no account was made of atomic charges, and so is only applicable to systems in which the structural effect of such charges is insignificant. This is indeed the case for octahedral based geometries, as both the CLFSE and the electrostatic interactions will favour an octahedral arrangement of the ligands around the metal, as predicted by simple VSEPR theory. The inclusion of an energy term to account for these electrostatic interactions will not therefore yield minimised structures that are significantly different in a qualitative sense, although some modification to the value of the variable parameters would be anticipated to reproduce the experimentally observed structures.

This is not true however, of other coordination numbers. For example, $[CuCl_4]^{2-}$ would be expected to adopt a tetrahedral geometry from simple electrostatic considerations, whilst it was shown in chapter 4 that the CLFSE term would favour a square planar geometry due to the strong Jahn-Teller effect for such a Cu(II) species. Experimental determinations of the structures of $[CuCl_4]^{2-}$ with a range of counterions show that the complex in fact displays a severely flattened tetrahedral or even a square planar geometry[36] depending upon the counterion in question. It is apparent therefore that the observed geometry is the result of a balance between the electrostatic interactions favouring a tetrahedral geometry and the Jahn-Teller effect favouring a square planar geometry. The latter is treated within the CLFSE term, whilst the former must be treated explicitly by means of a Coulombic energy term of the form:

$$E_{Coulomb} = q_i q_j / r \qquad \text{Eqn. 6.1}$$

where q_i and q_j are the atomic charges of the two interacting atoms and r is the separation between them. Traditional molecular mechanics force fields generally do not compute 1-3 or 1-2 interactions as defined in figure 6.1 as these are assumed to be implicitly parameterised within the angle and torsion terms, especially for 'organic' systems. However, in the absence of any explicit parameterisation of such angle and torsion energies around the metal centre when employing the CLFSE term, these L-L and M-L interactions must be included by means of a Coulombic term, as is appropriate for coordination compounds which are likely to show rather larger atomic charges than organic molecules and often carry a formal overall charge.

The results of three sets of calculations including parameterisation of atomic charges are now described in detail.

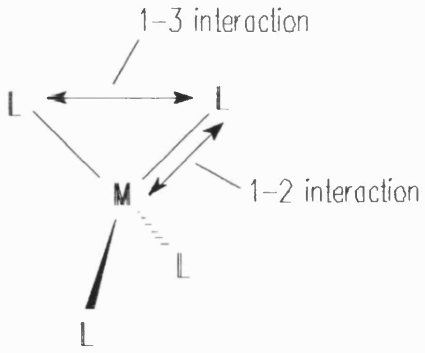

Figure 6.1: Illustration of 1-2 and 1-3 interactions.

6.2: $M(NH_3)_6^{2+}$

Analyses of three of the complexes studied in the previous chapter are repeated here with the inclusion of atomic charges, these being $Ni(NH_3)_6^{2+}$, $Cu(NH_3)_6^{2+}$ and $Zn(NH_3)^{2+}$. The nickel and zinc complexes are included to illustrate that the inclusion of atomic charges does not cause any qualitative change in the calculated structures both with and without CLFSE contributions, and while the copper complex also shows no qualitative differences, the quantitative differences are most significant.

The input parameters for these calculations are identical to those listed in table 5.1, with the exception of the charge parameters and the Morse potential α value as indicated in table 6.1. Table 6.1 also shows the structural results of energetic minimisation for the three complexes along with relevant minimised energies for varying values of the charge parameters in atomic units and α values.

The structural results listed in table 6.1 illustrate that for the copper species the observed structure may be reproduced without recourse to the sum rule as in chapter 5, while the nickel and zinc complexes are qualitatively unchanged by the inclusion of the Coulombic term, both species showing a regular octahedral geometry. It is apparent for the copper complex that once a distortion from octahedral symmetry is created via the CLFSE term, as was observed without atomic charges, then the Coulombic term contributes to the energy derivatives favouring axial elongation while the equatorial bonds shorten. A regular octahedral geometry once again represents a global energetic maximum, as anticipated from Jahn-Teller theory, and hence the energy minimised structure displays either an axially elongated or an axially compressed geometry depending upon whether the starting coordinates showed an elongation or compression respectively. The results for the copper species also indicate that if one of the three variable parameters is fixed then there is a unique pair of values of the other two parameters that will reproduce the observed structure. For example, as shown in table 6.1, for a given value of α there is a single pair of values of the metal and ligand

charge that will yield the observed bond lengths, although the charge parameters do not show any obvious relationship to each other such as a constant ratio or a given increase in each parameter on changing from one α value to another. It is apparent therefore that if one variable can be fixed, or if the ratio of the metal and ligand charges can be determined from some other source, then a unique set of parameters that reproduce the observed structure may be gained.

Metal	α	Charge M a.u.	Charge N a.u.	Bond Length Å	CLFSE cm^{-1}	Σ cm^{-1}	E_{char} kcal	E_{min} kcal
Ni	0.58	0.072	-0.049	2.0323	12542	20907	160.2	128.2
Cu	0.845	0.072	-0.049	2.0824 2.5460	12626	21825	136.9	122.1
	0.845	0.075	-0.052	2.0806 2.6331	12976	20776	170.3	160.6
	0.800	0.064	-0.047	2.0822 2.6262	12871	20723	187.2	174.4
	0.900	0.086	-0.057	2.0804 2.6237	12941	20912	141.7	134.8
Zn	4.0	0.075	-0.052	2.0846	----	----	198.7	198.9
	3.0	0.075	-0.052	2.0883	----	----	198.4	198.8

Table 6.1: Results of energy minimisations for three $M(NH_3)_6^{2+}$ species.

The nickel and zinc complexes, although remaining qualitatively unchanged, do require modification of the α parameter when atomic charges are included, at least for the values of the charge parameters employed here. As indicated by the total Coulombic

energy, E_{char}, the Coulombic term yields energy gradients that are essentially repulsive as indicated by the positive value of E_{char}, and so favours an increase in bond length. The nickel complex therefore requires a value of α that is less than that in the absence of charges in order to compensate for the introduction of the repulsive charge term. Similarly the zinc complex shows minimised bond lengths that are slightly longer than b_o, the magnitude of the deviation from b_o being dependant upon the value of α.

It is apparent then that the inclusion of an atomic charge energy term does not significantly alter the calculated geometries of octahedral transition metal species for high-spin electronic configurations other than d^9, although some modification of parameter values may be required to yield the observed bond lengths. For the Cu(II) species studied here the inclusion of atomic charges allows the reproduction of the observed structure without recourse to any additional energy terms such as the sum rule, while the magnitude of the Morse potential α value and, more importantly, the magnitude of the atomic charges appear entirely reasonable and compatible with traditional Molecular Mechanics values. It may initially appear anomalous that the sum of the atomic charges suggests that these species carry a formal overall negative rather than positive charge, but it must be recognised that if a negative charge is assigned to the nitrogen atoms then a positive charge should, in principle, be assigned to the hydrogen atoms bonded to the nitrogen atom such that the ammonia ligand remains a formally neutral species.

6.3: MCl_4^{2-}

The crystal structures of the tetrachloro complexes have been reported for Mn to Zn[100-103]. The input values for the Morse potential b_o parameters are gained from a linear interpolation of the Mn and Zn bond lengths, whilst the D_o values are gained from a similar interpolation of heats of formation from literature sources[96]. The CLF e_λ vs bond length parameterisation is gained from the database values with e_π parameters fixed at 1/5 e_σ, while the value of δ is adjusted to ensure a CLF sum of 23000 cm^{-1} at the observed bond lengths. The input parameters are summarised in table 6.2.

Metal	D_o, kcal	b_o, Å	CLF A	CLF B	δ
Mn	100	2.343	----	----	----
Fe	101.6	2.332	450000	950	-0.053
Co	103.2	2.321	450000	950	-0.066
Ni	104.8	2.309	450000	950	-0.073
Cu	106.4	2.298	450000	950	-0.121
Zn	108	2.287	----	----	----

Table 6.2: Input parameters for Morse potential and CLFSE terms used in the structural calculations of the MCl_4^{2-} species.

The key complex of this series is the copper species. It is through reproduction of the structure of this complex that one may gain an estimate of the non-bonding parameter values. These calculations seek to reproduce the structure of Cs_2CuCl_4, which shows a flattened tetrahedral geometry as indicated by a Cl-Cu-Cl angle of 129° as defined in figure 4.10. Given that the Morse potential term and any metal-ligand non-bonding

interaction term can only influence the radial properties of the metal-ligand bonds, then it is clear that the angular orientation of the ligands is the result of a balance between the CLFSE term and the ligand-ligand non-bonding interactions. Reproduction of the observed geometry therefore allows a measure of the ligand-ligand repulsion relative to the CLFSE and hence it is possible to refine the non-bonding parameters.

Preliminary calculations illustrate that the non-bonding interactions must be treated by employing a Coulombic term rather than a van der Waals term. Treatment of the ligand-ligand interaction within a van der Waals term leads to unacceptably large parameter values if the observed structure is to be reproduced, typically the repulsive chloride parameter must be some 16 times that employed for the nickel macrocycle species studied in the previous chapter. Parameter values that are more consistent with those employed in chapter 5 yield energy minimised structures that show geometries that are only a few degrees away from square planar. However, if the ligand-ligand interaction is treated within a Coulombic term, then appropriate minimised geometries may be gained by use of charge parameters that are consistent with those employed for the hexamine species reported above.

The parameterisation of the ligand-ligand non-bonded interaction may then be refined so as to reproduce the observed angular geometry at the observed bond lengths, for a given parameterisation of the CLFSE. The radial properties of the structure are more complex however. The ligand-ligand non-bonding interaction will favour an increase in metal-ligand bond length, while the metal-ligand charge interaction and the CLFSE both favour a decrease in bond length. However, if the CLFSE parameterisation is invariant and the ligand charges are fixed so as to yield the observed angular geometry, then if either the metal charge or the value of the Morse potential α value is defined then the value of the other parameter may be determined. Deeth has reported[104] discrete variational X_α calculations upon the $CuCl_4^{2-}$ anion restricted to a D_{2d} symmetry, and lists net charges for both the metal and ligand atoms. These charges are

not directly transferable to a molecular mechanics calculation of course, but it is not unreasonable that the ratio of the charges may be employed here. This provides a mechanism by which the metal charge may be assigned relative to the derived value of the ligand charge and hence a unique value of α may be gained so as to reproduce the observed bond lengths. The charge parameters that are derived for the copper species in this way are employed unchanged for all the complexes of the series, whilst Van der Waals interactions are also included using default parameter values for all complexes, although the effect of this term is small.

Table 6.3 describes the energy minimised structures of the six complexes in terms of metal-ligand bond lengths and L-M-L angles as defined in figure 4.10, along with the appropriate parameter values and the minimised energies.

It is shown in table 6.3 that both the manganese and zinc tetrachloride complexes show regular tetrahedral geometries, as would be predicted by VSEPR theory and as is experimentally observed. Both complexes show energy minimised bond-lengths that are essentially equal to the defined value of b_o, as anticipated in the absence of a CLFSE contribution. The cobalt complex also shows a regular tetrahedral geometry as a high-spin d^7 configuration is Jahn-Teller inactive in a tetrahedral environment, while the calculated bond lengths are shorter than b_o due to the effect of the CLFSE, as is the case for all four complexes studied here that show a non-zero CLFSE. The contraction of the bond lengths relative to b_o is, however, smaller than the for the octahedral species already discussed since the overall CLFSE is smaller in tetrahedral symmetry. All species show calculated bond lengths that are essentially identical to those observed experimentally. In contrast to the cobalt complex, the iron and nickel complexes do display a formally degenerate ground state and hence are Jahn-Teller active. Due to this Jahn-Teller activity a tetrahedral geometry represents an energetic maximum for these species, and so calculations are reported for starting coordinates that show both a slight tetrahedral flattening and elongation. The nickel complex shows a clear energetic

preference for tetrahedral elongation, while the iron complex shows very similar minimised energies for the flattened and elongated geometries, which in turn show a relatively small deviation from the calculated energy of the parent regular tetrahedral geometry. The copper complex shows the most severely distorted structure of the series, as anticipated from the strong Jahn-Teller effect for a d^9 species, the calculated L-M-L angle of 129.5^o agreeing closely with experiment.

Metal	α	Charge M, a.u.	Charge Cl, a.u.	Bond length	Cl-M-Cl angle	CLFSE Σ	E_{char} E_{min}
Mn	3.00	0.0486	-0.0497	2.3413	109.5	---- ----	-28.014 -28.041
Fe flat.	1.05	0.0486	-0.0497	2.293	111.7	-2459 22983	-28.544 -34.899
elong.	1.05	0.0486	-0.0497	2.293	106.5	-2492 23006	-28.492 -34.931
Co	1.30	0.0486	-0.0497	2.281	109.5	-4806 22930	-28.760 -41.334
Ni flat.	1.29	0.0486	-0.0497	2.276	114.7	-3847 22727	-28.317 -38.452
elong.	1.29	0.0486	-0.0497	2.273	101.0	-4119 22976	-27.855 -38.724
Cu	0.88	0.0486	-0.0497	2.225	129.5	-4122 22944	-25.441 -35.385
Zn	3.00	0.0486	-0.0497	2.285	109.5	---- ----	-28.699 -28.726

Table 6.3: Results of energy minimisations for the MCl_4^{2-} species.

There is, however, an obvious omission from the CLFSE parameterisation in that no account is made of void cell contributions, which may be of significance for the calculated structure of the copper complex. Unfortunately the inclusion of void cell contributions is, as discussed in chapter 4, a complex problem. It was concluded that a linear relationship between void cell parameter values and the angle of tetrahedral flattening is not appropriate in a general sense, while some mechanism by which the CLF sum can be maintained is required as the distortion proceeds and the magnitude of the void cell contribution increases. It was also suggested that a void cell contribution is neither desirable nor necessary on the basis of previous CLF studies until a flattening angle of 130-135^{o} is reached. This is illustrated by a CLF analysis[54] of Cs_2CuCl_4 that reports a void cell contribution of only -850 cm^{-1} for a L-M-L angle of 129.2^{0}, and so the inclusion of a void cell appears to be of relatively little importance for the reproduction of the structure of $CuCl_4^{2-}$ as such a small void cell parameter would have a very small effect upon the CLFSE. However, for the purposes of comparison, figure 6.2 shows the results of 'hand' calculations upon $CuCl_4^{2-}$ which include the CLFSE, atomic charges and the effect of void cell contributions. The graph shows the change of total energy as a function of flattening angle for three different methods of treating the complex. Firstly the total energy is calculated in the absence of void cell contributions and so shows a minimum as reported in table 6.2. Secondly the energy is calculated with a linear increase in magnitude of the void cell as the flattening angle increases without any modification of the other CLF parameters, and hence the CLF sum is not constant. Finally the energy is calculated for the same method of void cell parameterisation but the CLF sum is maintained by increasing the other CLF parameters as the magnitude of the void increases.

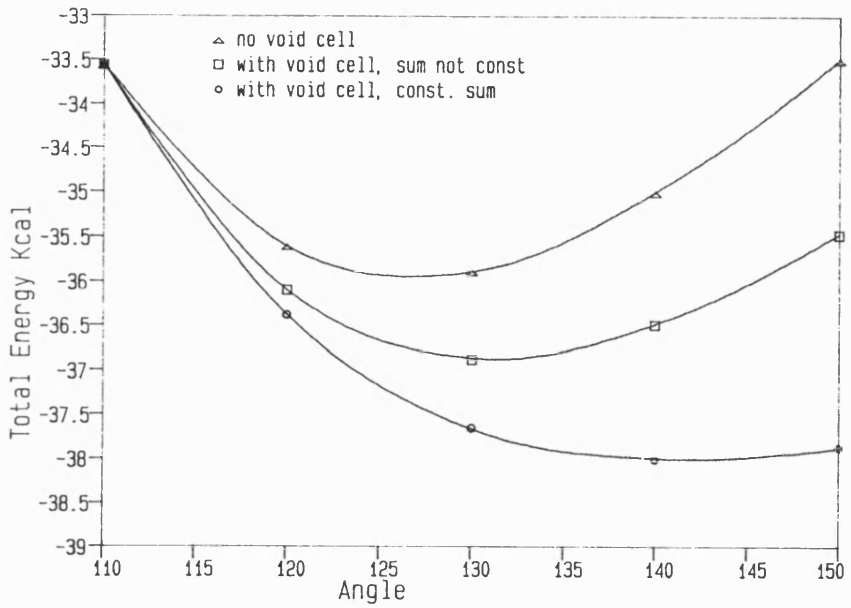

Figure 6.2: Change of the total energy as a function of angle for $CuCl_4^{2-}$, i) in the absence of a void cell, ii) with a linear void cell contribution and iii) with a void cell and a constant CLF sum value.

In the absence of void cells the minimum energy occurs at an energy of *ca* 130°, compared with an angle of *ca* 135° when a void cell is included without maintaining the sum. This relatively small difference does not warrant the inclusion of a void cells by this means, and the small difference in total energies also suggests that the effect of the void is negligible. A larger difference is observed if the sum is maintained as the magnitude of the void cell increases, both in that energetic minimum occurs at *ca* 140° and that the energetic difference of the minimum compared with the minimum without void cells is considerable. It must be recognised, however, that a linear interpolation method of calculating the void cell contribution is likely to yield a maximum value for the void cell at these angles, as a more sophisticated method of computing the void cell

would be likely to take a non-linear form with the rate of change of void cell contribution increasing as the angle of flattening increases, and hence the computed value of the CLFSE also takes a maximum value. If the position of the calculated energetic minimum in terms of both flattening angle and energy is therefore regarded as the maximum possible deviation from the results listed in table 6.3 as a consequence of including void cells, then it is apparent that void cell contributions are not as important as may have been initially anticipated. Although the energetic minimum that is calculated for the inclusion of void cells with a constant sum shows a difference of *ca* 10^{o} in the minimised structure and a minimum energy that is some 10 % lower, these differences would be easily accommodated by modification of the ligand charges. As the inclusion of void cells does not alter the form of the CLFSE energy as a function of tetrahedral flattening and only yields a small modification in the energy gradient, then it would seem reasonable not to include void cell contributions, at least for species that show the degree of flattening considered here.

6.4: $[M(Me_6tren)Br]^+$

The series of complexes from Mn to Zn of the form $[M(Me_6tren)Br]^+$ where Me_6tren represents tris(2-dimethylaminoethyl)amine, a 'tripod' ligand shown schematically in figure 6.3, is the most chemically and computationally complex of the sets of species studied in this work. The most significant feature of the series is the coordination of the tripod ligand, which forms both the equatorial bonds and one of the axial bonds of the trigonal bipyramidal structure via the four saturated nitrogen donors, and hence the organic backbone of the ligand provides a link between the axial and equatorial bond lengths. It is the relationship between the axial and equatorial nitrogen bond lengths that provides the main chemical feature of the series, which may be summarised in terms of the Fe, Co and Zn complexes showing axial nitrogen bond lengths that are longer than the equatorial bond lengths, while the Mn, Ni and Cu complexes show the

converse behaviour as the axial bonds are shorter than the equatorial bonds, according to the structural determinations reported by Di Vaira and Orioli[105-107] and summarised in table 6.4.

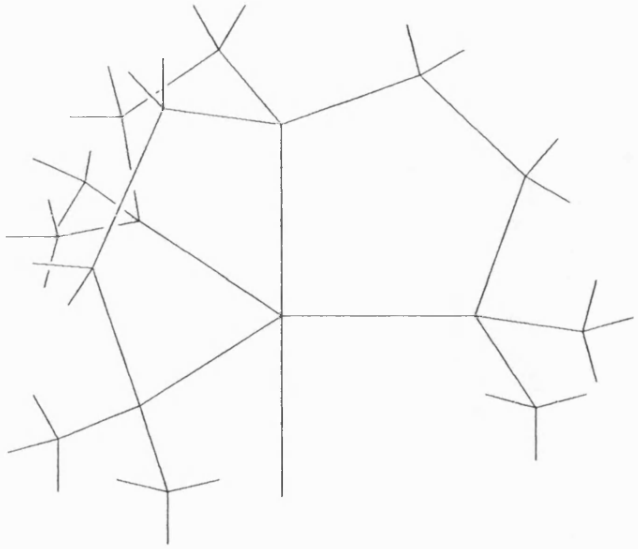

Figure 6.3: Schematic representation of $[M(Me_6tren)Br]^+$ species.

Metal	M-N(eq) Å	e_σ(eq)	M-N(ax) Å	M-Br Å	e_σ,e_π(ax)
Mn	2.27	---	2.19	2.491	---
Fe	2.15	4000	2.21	2.482	4000,1000
Co	2.08	4000	2.151	2.431	4000,1000
Ni	2.13	3900	2.10	2.467	5000,1000
Cu	2.14	3300	2.07	2.393	5800,1000
Zn	2.11	---	2.19	2.449	---

Table 6.4: Summary of structural details and CLF parameter values for $[M(Me_6tren)Br]^+$ species.

This series of complexes have been the subject of a ligand field analysis by Deeth and Gerloch[51] within the CLF formalism, and the conclusions of that work are most relevant here. The ligand field analyses yield best fit CLF e_λ values, listed in table 6.4, that correlate well with the observed bond lengths in that the mean axial donation is indicated to be less than the equatorial donation for the iron and cobalt complexes, a mean value only for the axial donation is possible due to the constraints of holohedral symmetry, while for the nickel and copper complexes the axial donation is significantly larger than the equatorial donation. The behaviour of both the observed bond lengths and CLF e_λ parameters for the series is rationalised in terms of the stereochemical activity of the incomplete d-shell. In the threefold symmetry of these complexes the d-orbitals are split into three sets which are, in order of decreasing energy, $d_z2 > d_{xy}$, $d_x2-y2 > d_{xz}, d_{yz}$. This splitting pattern along with the approximately trigonal bipyramidal geometry and the purely σ-bonding role of the Me_6tren ligand allows a ready separation of σ and π−bonding effects. The d_z2 orbital is principally involved with axial σ interactions and the d_{xy}, d_x2-y2 orbital pair are predominantly involved with equatorial σ interactions while the d_{xz} and d_{yz} orbitals are involved with the π interaction with the axial bromide ligand. In both the iron and cobalt complexes there is a symmetrical distribution of holes in the σ type orbitals, the extra electron being accommodated by the π set. As the π bonding influences upon stereochemistry are likely to be small, the effect of including an extra electron in the π orbital set has little geometric effect. Both complexes have similarly elongated geometries, as observed for the closed shell zinc complex, together with identical CLF parameter sets. The nickel complex however, shows an asymmetry in the σ configuration with only one hole in the equatorial plane, and so this complex represents an intermediate between the cobalt and copper complexes in terms of d-electron distribution and consequently the resultant geometry. The copper complex shows a single hole in the d_z2 orbital and a double occupancy of the equatorial σ−bonding orbitals. This equatorial repulsion along with

the axial hole leads to an axially compressed geometry, contrary to the predictions of the closed shell theory of Gillespie and Nyholm[28,108] in which an elongated geometry would be anticipated like that of the zinc analogue. The apparently anomalous complex of the series is the manganese compound, which shows an axially compressed structure. Di Vaira and Orioli rationalise this in terms of the large size of the metal ion and the geometrical constraints of the ligand which apparently prevent the attainment of the expected elongated structure for the symmetric d^5 configuration.

The observed trends in the geometries of this series of complexes, with the exception of the manganese compound, are clearly due to the stereochemical activity of the incomplete d-shell. These trends can therefore only be reproduced in a consistent fashion if they are recognised as being due to ligand field effects and are treated accordingly. A traditional Molecular Mechanics force field would not account for the significant electronic difference between nickel and copper and the other metals ions of the series. The consequence this would be that the computed structures would all show an elongated geometry unless the nickel and copper species were treated in a different fashion from the other compounds, thereby introducing an inherent inconsistency. The calculations reported here explicitly recognise the importance of the electronic configuration of the transition metal in question via the CLFSE, and therefore the computational procedure is free of any artificial means of reproducing the structural trends.

Before attempting to model this series of complexes in full, it is useful first to simplify the problem in order to study the nature of the CLFSE term in a trigonal bipyramidal five coordinate geometry. This is achieved in two ways, firstly the species are treated simply as five identical coordinating charged atoms around the metal centre displaying σ only bonding capabilities, and secondly as four σ only donors occupying the equatorial and one axial site and one σ and π donating ligand occupying the other axial site.

The invariant input parameters for these calculations are listed in table 6.5, these parameters being derived from the usual interpolations, and are used unchanged for both sets of simplified calculations and for the full calculations reported later. It is of particular note that identical Morse potential parameters are employed for both the axial and equatorial metal-nitrogen bonds. The CLFSE parameterisation employs the same A and B parameters for the nitrogen atoms as were used for the hexamine species with δ values adjusted to yield the CLF parameter values derived by Deeth and Gerloch at the observed bonds lengths. The bromide parameters are assigned in a similar fashion.

Metal	N D_o kcal	N b_o Å	Br D_o kcal	Br b_o Å	N CLF A	N CLF B	δ	Br CLF A	Br CLF B
Fe	102	2.24	98.7	2.483	225800	900	0.075	580000	900
Co	104	2.20	100.4	2.474	225800	900	0.005	530000	900
Ni	106	2.16	102.0	2.466	225800	900	0.048	595000	900
Cu	108	2.12	103.7	2.457	225800	900	0.015	55000	900
Zn	110	2.13	103.7	2.449	----	----	----	----	----

Table 6.5: Input parameters for Morse potential and CLFSE terms used in the structural calculations of the $[M(Me_6tren)Br]^+$ species.

Tables 6.6 and 6.7 show the results of the simplified calculations for MN_5 and MN_4Br species respectively. The MN_5 species all behave as one would anticipate. The zinc species shows an elongated geometry for ligating atoms that carry a charge, a result that is consistent with conventional closed shell theory, and the same result would be found for the manganese analogue. In the absence of charges the zinc and manganese species will both show five equivalent bond lengths with the bond lengths being equal

to the defined values of b_0. The iron and cobalt species also show an elongated geometry which is consistent with the d-orbital occupation argument of Deeth and Gerloch, as is the axially compressed geometry displayed by both the nickel and copper species. Interestingly the nickel complex shows inequivalent equatorial bond lengths, one bond being slightly longer than the other two. This is due to the d^8 configuration displaying a formally degenerate ground state in an exact trigonal bipyramidal geometry, the orbital pair showing the degeneracy being the predominantly equatorially σ bonding d_{xy}, $d_{x^2-y^2}$ pair. This degeneracy may therefore be raised by the modification of one of the equatorial bonds. The iron species also shows a similarly degenerate ground state, but the orbital pair giving rise to the degeneracy of the d^6

Metal	α	Charge	Charge	Bond	Length	CLFSE	E_{char}
		M a.u.	N a.u.	ax Å	eq Å	Σ	E_{min}
Fe	0.65	0.0565	-0.0452	2.213	2.151	-3644	23.020
						18222	13.744
Co	0.93	0.0858	-0.0663	2.150	2.081	-9094	-1.215
						22734	-22.419
Ni	1.30	0.0489	-0.0392	2.096	2.130	-8611	18.660
					2.149	20286	-3.987
Cu	1.51	0.0504	-0.0459	2.067	2.140	-7397	108.187
						18529	88.657
Zn	0.50	0.0489	-0.0384	2.194	2.110	----	7.475
						----	7.725

Table 6.6: Results of energy minimisations for the MN_5 species.

configuration are the predominantly axial π-bonding d_{xz}, d_{yz} orbital pair. The axial ligands, do not show any π-bonding capability in the MN_5 species and so there is no mechanism by which this degeneracy may be lifted, hence no asymmetry of bond lengths is observed. It is noteworthy that the resultant structures are, for all the species studied, essentially independent of the starting coordinates with respect to axial elongation or compression. The Morse potential α and charge parameters that are employed to yield the metal-nitrogen bond lengths that are observed for the $[M(Me_6tren)Br]^+$ species do not show any consistency along the series, but this is not of any surprise as these simplified species can take no account of the effect of the asymmetry of the axial coordination and the consequences that this may have for the metal-ligand bond lengths.

The results of calculations for MN_4Br species are shown in table 6.7. These results show little qualitative difference as a result of the inclusion of the bromide ion in terms of axial elongation and compression but it does introduce an asymmetry of axial coordination. The effect of this asymmetry is that the metal no longer lies in the plane of the equatorial nitrogen atoms as observed for all the MN_5 species, but lies out of the equatorial plane by some 0.04 Å towards the bromide ion due to the larger charge assigned to this ligand. The nickel complex again shows inequivalent equatorial bond lengths, while the iron complex again has no mechanism by which the π orbital degeneracy may be raised due to the cylindrically symmetric π-bonding capability of the bromide ligand. The most significant effect of the bromide ligand is that the observed bond lengths may now be reproduced to a reasonable degree of accuracy by using the same metal charge for all species and similar ligand charges, the values of the charge parameters being consistent with those derived for the hexamine and tetrachloro species already discussed. The Morse potential α values again show no correlation, but this is to be expected if the role of the organic backbone and the consequent effects upon the bond lengths is not included.

Metal	α(N)	α(Br)	Charge a.u.			Bond length		CLFSE	E_{char}
			M	N	Br	ax	eq	Σ	E_{min}
Fe	0.66	5.00	0.0489	-0.0378	-0.0388	2.212	2.149	-3438	1.643
						2.483		22168	-6.984
Co	0.75	0.55	0.0489	-0.0384	-0.0459	2.154	2.074	-6785	25.97
						2.430		21055	9.829
Ni	1.10	5.50	0.0489	-0.0422	-0.0437	2.102	2.125	-8079	63.49
						2.465	2.115	23028	41.31
							2.153		
Cu	1.34	1.05	0.0489	-0.0452	-0.0485	2.071	2.138	-7618	119.9
						2.393		21409	99.32
Zn	0.5	2.05	0.0489	-0.0384	-0.0414	2.191	2.112	----	13.88
						2.456		----	14.03

Table 6.7: Results of energy minimisations for the MN_4Br species.

It is clear then that the CLFSE term is capable of reproducing the ligand field effects that determine the geometries adopted by this series of trigonal bipyramidal complexes, and of reproducing those geometries to a reasonable degree of accuracy in the absence of the organic backbone of the Me_6tren ligand. The modelling of these complexes is, however, inevitably more complex when the organic framework is included, as this structure provides a link between the axial and equatorial nitrogen bond lengths as well as imposing steric constraints upon the structures due to its own conformational preferences.

The results of full treatments of these species are now presented, with the organic backbone modelled using appropriate conventional Molecular Mechanics force field

terms and parameter values as listed in the appendix. No attempt is made to optimise these parameters, and the invariant input parameters for the metal centre are used as per table 6.5. The only parameters that are varied are the atomic charges for the metal and the ligands of the zinc species, thereafter these parameters remain constant, and the Morse potential α parameters describing the M-N and M-Br bonds are adjusted for all species of the series to gain the best agreement with experiment. As for the simplified species, both the axial and the equatorial metal-nitrogen bonds are treated as being equivalent in terms of parameter values.

The zinc species provides the basis for the assignment of atomic charges for the series. The structure of the zinc complex may be considered as a result of a balance between the preferred orientation of the Me_6tren ligand and the stereochemical effect of the metal and ligand charges. Given that the parameterisation of the organic backbone of the Me_6tren ligand is not modified, then charges may be derived so as to reproduce the observed structure along with the values for the Morse potential α values for the metal-ligand bonds. Table 6.8 shows the results of energy minimisations for three choices of charge parameterisation for the zinc complex.

α(N)	α(Br)	Charges a.u.			Bond Lengths		E_{char}
		M	N	Br	ax.	eq.	E_{min}
0.70	5.00	0.00	0.00	0.00	2.1318	2.1932	0.00
					2.4494		7.786
0.80	1.15	0.0489	-0.0384	-0.0414	2.1630	2.1861	15.748
					2.4763		23.931
0.70	5.00	0.0964	-0.0632	-0.0662	2.1922	2.1113	-217.11
					2.4533		- 197.42

Table 6.8: Results of energy minimisations for the $[Zn(Me_6tren)Br]^+$ complex.

It is shown that if atomic charges are not included, then the complex adopts an axially compressed geometry. This then, is the preferred geometric conformation of the Me_6tren ligand, at least for the Molecular Mechanics parameter values employed here. In the absence of the organic backbone the metal-ligand bond lengths would, of course, minimise to give the b_o values and so the four metal-nitrogen bond lengths would be equivalent. The organic backbone therefore acts against the preference for axial elongation caused by the introduction of atomic charges. This is supported by the results of minimisation using the charge parameters of table 6.7. This structure again shows an axially compressed geometry, albeit to a lesser extent. It is apparent therefore that rather larger values for the atomic charges are required to reproduce the observed structure. The third set of results shown in table 6.8 show the magnitude of charges required to produce the desired degree of elongation for a M-N α value of 0.7. This by no means represents a unique parameter set that will reproduce the observed geometry, but the three charge parameters are essentially unique for a given pair of Morse potential α values for the M-N and M-Br bonds. The charge parameters derived for the zinc complex are used unchanged for the remainder of the series, and the results of energy minimisation are shown in table 6.9.

The minimised structures summarised in table 6.9 show the same qualitative behaviour as is experimentally observed. The quantitative agreement with experiment is, however, not as close as one would hope, but given that the structures are reproduced by means of adjustment of only the two metal ligand Morse potential α values then the general agreement between the calculated and experimental structures is remarkable. In general terms the structures show excellent agreement with experiment, in that the computed structures show an overall symmetry that is close to C_3 with colinear bromide, metal and axial nitrogen atoms, as observed experimentally, including the nickel complex which shows a much smaller asymmetry of equatorial bond lengths in

the presence of the organic backbone. This is illustrated by the projection along the C_3 axis of the copper complex shown in figure 6.4.

Metal	α(N)	α(Br)	Bond Lengths		CLFSE	E_{char}
			ax.	eq.	Σ	E_{min}
Fe	1.05	4.00	2.212	2.136	-3631	-213.6
			2.482		22804	-201.6
Co	0.65	2.45	2.179	2.081	-6505	-220.9
			2.473		19639	-216.5
Ni	2.35	5.00	2.137	2.169	-6802	-212.7
			2.468		20811	-211.6
Cu	1.956	1.45	2.067	2.141	-7467	-219.7
			2.399		21209	-217.5
Zn	0.70	5.00	2.192	2.111	----	-217.1
			2.453		----	-197.4

Table 6.9: Results of energy minimisations for the $[M(Me_6tren)Br]^+$ species.

The angles at the metal also show excellent agreement with experiment. Di Vaira and Orioli report N(ax)-M-N(eq) angles of 81.3, 81.1, 84.2, 84.7 and 82.6° for the Fe, Co, Ni, Cu and Zn complexes respectively which compare with computed values of 83.1, 83.9, 83.4, 84.9 and 83.5°. This corresponds to the metal lying 0.2 - 0.36 Å out of the equatorial plane towards the bromide ion as experimentally determined, compared with computed deviations from the plane of 0.19 - 0.26 Å. Di Vaira and Orioli report that these angles and deviations from the plane are principally imposed by the Me_6tren ligand, however the results of the calculations carried out for the zinc

complex indicate that the asymmetry of axial atomic charge may also play a role, as the computed N(ax)-M-N(eq) angle varies from 85.1° in the absence of charges to 83.5° when the final charges are assigned.

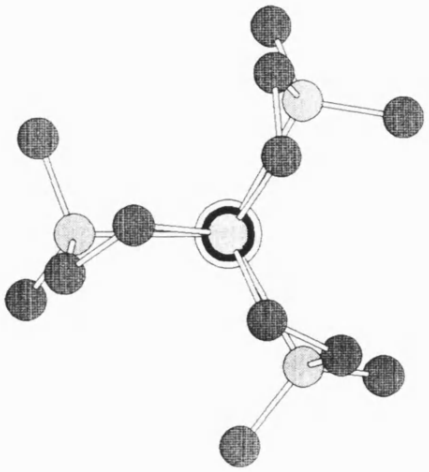

Figure 6.4: Projection of $[Cu(Me_6tren)Br]^+$ along the C_3 axis. Hydrogen atoms are omitted for clarity.

The agreement between experimental and calculated bond lengths may be improved by several means. Firstly, one could make a case for assigning different Morse potential α values to the axial and equatorial metal-nitrogen bonds, as although both types of coordinating nitrogen atom are formally tertiary amines they do occupy different coordination environments. This is however an rather unsatisfactory solution to a problem that is more likely to find its source in the parameterisation of the organic force field. The parameters used here are not necessarily suited to the aliphatic structure of the Me_6tren ligand and this may have most important implications for the possibility of reproducing the observed bond lengths by simply adjusting the two different metal-ligand Morse potential α parameters for a given set of charges, in the

same way as the parameterisation of the organic force field may well have prevented parameter transferability for the nickel macrocyclic species studied in the previous chapter. The unsuitability of the organic force-field parameterisation is also indicated by the magnitude of the charges required to produce the desired degree of elongation for the zinc complex. When compared to the charges employed for the hexamine and tetrachloro complexes they appear rather large, and although the charges derived for the hexamine complex are dependant upon the value of the Morse potential α parameter that is employed, the charges for $CuCl_4^{2-}$ are more clearly defined.

The final means by which the agreement between calculated and experimental structures may be improved along with the possibility of parameter transferability lies in the way in which the charges are assigned. It is reasonable to employ the same charge parameters across the series for a 'first pass' calculation, but to use consistent metal charge parameters is surely contrary to the increasing effective nuclear charge, Z_{eff}, of the metals from Mn to Zn as a consequence of increasing nuclear charge coupled with the poor shielding afforded by d- electrons. Deeth and Gerloch[51] stress the importance of this effect in determining the observed bond lengths as the increasing effective nuclear charge would be expected to cause a general decrease in metal-ligand bond lengths upon which would be superimposed the asymmetric influences of the d-electrons. The transition from iron to cobalt involves no change in the σ type orbital configuration and so the general decrease in bond lengths of about 0.06 Å is mainly associated with the increase in Z_{eff}. Figure 6.5 shows this difference extrapolated in a linear fashion for the sake of discussion along with the observed bond lengths. From cobalt to copper, electrons are added progressively to the d-orbitals lying in the equatorial plane, and this results in a general increase in the equatorial bond lengths. The population of the d_z^2 orbital remains unchanged however, and hence a general decrease in axial metal-nitrogen bond lengths is observed. At zinc the doubly occupied d_z2 orbital results in a sharp increase in the axial M-N bond length. The metal-bromine

distances follow a similar trend to that of the M-N(ax) bonds, except for the nickel complex in which steric interactions are suggested to prevent a closer approach.

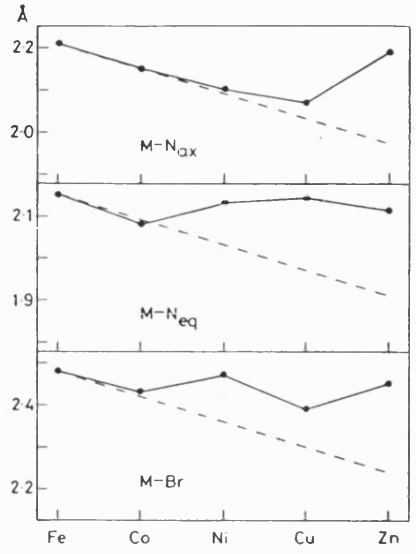

Figure 6.5: Variation in metal-ligand bond lengths for the Me_6tren complexes (solid lines). The broken lines represent estimated bond length decrease arising from variations in Z_{eff} alone. Reproduced from reference 51 by permission of Dr.R.J.Deeth.

It is apparent then that if the observed structures are the result of a combination of ligand field and effective nuclear charge effects, then the calculated structures would be closer to experiment if both effects were included in the treatment. This is especially relevant for the manganese complex which is reported as showing an axially compressed geometry, contrary to what would be predicted from simple closed shell theory and in contrast to the elongated geometry shown by the zinc analogue. This is rationalised by Di Vaira and Orioli in terms of the large size of the metal ion and the geometrical constraints of the ligand, arguments that find some support here. Table 6.10 shows the results of energy minimisations for the manganese complex.

α(Br)	α(Br)	Charges a.u.			Bond Lengths		E_{char}
		M	N	Br	ax.	eq.	E_{min}
1.60	2.30	0.00	0.00	0.00	2.2494	2.2558	0.00
					2.4923		6.287
1.60	2.30	0.0964	-0.0632	-0.0663	2.2249	2.2515	-201.17
					2.4946		-185.84
1.60	2.30	0.0751	-0.0590	-0.0618	2.2562	2.2723	32.025
					2.5080		50.164

Table 6.10: Results of energy minimisation for the $[Mn(Me_6tren)Br]^+$ species.

In the absence of charges the manganese complex shows a rather smaller degree of compression than was observed for the equivalent calculation for the zinc complex. However, when the same charge parameters are employed as were used to gain the observed structure for the zinc complex, the energy minimised structure still shows a slightly compressed geometry, the axial metal-nitrogen bond being some 0.027 Å shorter than the equatorial bonds, although it should be stressed that the minimised bond lengths are extremely sensitive to variations in the Morse potential α values for both the M-N and M-Br bonds. This compression is the consequence of modifying the Morse potential D_o and b_o parameters for the M-N and M-Br bonds only, the values of b_o are both increased while the values of D_o are decreased relative to zinc. This increase in b_o may be considered as some measure of the increase in size of the metal, while reproduction of the longer M-N bond lengths may also impose steric constraints upon the organic backbone that give rise to a preference for a compressed geometry. The third set of calculations employ the same values for the α values, but the manganese charge parameter is calculated so as to show the same ratio to the zinc

parameter as is found from the effective nuclear charges of the two ions derived from the formula of Clementi and Raimondi[109]. The nitrogen and bromine charges are then assigned such that the total charge of the complex remains unchanged and the ratio of the nitrogen to bromine charge is also unchanged. This reduction in charge does not increase the degree of compression however, as one might expect, indeed it serves to reduce the difference in axial and equatorial nitrogen bonds to 0.016 Å. The main effect of this change in charge parameterisation is to yield a net repulsive rather than attractive effect, as is indicated by the positive value of the total charge energy for the smaller charges compared with a negative value for the zinc charges and by the general increase in the metal-ligand bond lengths.

6.5: Discussion

The assignment of charges to a species under investigation is a complex issue. Particular care must be taken if a modification is to be made to the charge parameters in order to account for increasing nuclear charge along a series such as the $[M(Me_6tren)Br]^+$ species studied in this chapter, as there is a danger of "double counting" the effects of the increase in Z_{eff}. These effects are already treated implicitly, at least in part, by the decrease in the Morse potential b_o parameters and the increase in the D_o parameters. The CLFSE term will also account for these effects as the value of δ used in the CLF e_λ vs bond length dependence is altered so as to yield the e_λ derived by Gerloch and Deeth[51] at the observed bond length for the $[M(Me_6tren)Br]^+$ complexes.

Even if the possibility of double counting is ignored, it is still difficult to derive a chemically consistent formula by which the effect of a change in Z_{eff} may be accounted for. One system of modifying the charges assigned to the metal and ligands is described for the $[Mn(Me_6tren)Br]^+$ species. The charge of the metal is assigned so that the ratio of the Mn and Zn charges is equal to that of the estimated values of Z_{eff}

for the two metals, Z_{eff} being estimated according to the formula of Clementi and Raimondi[109]. The ligand charges are then adjusted so that the overall charge of the complex is unaltered with respect to the zinc analogue, and so that the ratio of the nitrogen and bromide charges are unchanged. This means of adjusting the ligand charges is problematic, however. If one were to consider the ligands as discrete units before complex formation then one would expect the ligands to carry consistent charges, as it is not the ligand that is modified along the series of complexes. The metals however may be expected to increase in effective nuclear charge, but in terms of formal charge they too must show a consistent charge parameterisation, if considered as discrete units in the same way. It must be remembered, however, that when assigning charges to a species within a molecular mechanics scheme that one is assigning net charges, after complex formation, and that these charges do not necessarily show the same trends as the discrete units before the complex is formed.

If then, within a series of complexes, the Z_{eff} of the metal atom increases, this may be accounted for by increasing the charge assigned to the metal. However, as Z_{eff} increases there is expected to be an associated increase in the degree of covalent bonding between metal and ligand. The effect of this increasing covalency is to increase the amount of charge donation from ligand to metal, and hence the positive charge carried by the metal is reduced. Unfortunately it is difficult to estimate the effect that this increased donation from ligand to metal has in a quantitative sense. If the CLF sum is a measure of charge donation from the ligand set to the coordinated metal then one might expect the sum that is derived from a series of analyses to reflect this increase in charge donation as the Z_{eff} of the metal increases. However, there is no evidence to suggest that such behaviour of the sum is observed for such series of complexes, the sum for the analyses of the $[M(Me_6tren)Br]^+$ series shows an increase from 22000 cm^{-1} for the iron complex to 23500 cm^{-1} for the copper complex, an increase that is insignificant relative to the inherent errors in the parameter values. It would seem that

it is impossible, therefore, to evaluate the trend in the net charges of the metals, and consequently the ligands, *a priori.*

6.6: Conclusions

The results presented in this chapter illustrate that atomic charges have a significant role to play in the modelling of transition metals by this means. The structure of the $Cu(NH_3)_6^{2+}$ complex may be reproduced without recourse to the CLF sum-rule as was necessary in the absence of charges, whilst it would be impossible to reproduce the observed flattened tetrahedral structure of $CuCl_4^{2-}$ without some form of ligand-ligand repulsive interaction, this 1-3 interaction seeming to be modelled more appropriately by a Coulombic term rather than by a van der Waals term. The $[M(Me_6tren)Br]^+$ series of complexes also illustrate the importance of including atomic charges, and these complexes represent a significant success for the CLFSE term as the qualitative behaviour of the axial and equatorial bonds with respect to axial elongation and compression is reproduced. Although the quantitative reproduction of the observed bond lengths is not as good as one might hope, the agreement between calculated and experimental structures is remarkable considering that only the Morse potential α values for the M-N and M-Br bonds are freely adjusted.

It is clear from the results and discussion in this chapter that the assignment of charges to the metal and ligands of a complex is a complex issue. Due to the nature of the terms that are used to model transition metals in this way, it is impossible to separate the effects of each term in order that comparison with experiment can be made to facilitate parameterisation. For example, the radial nature of the metal-ligand bond is treated by the Morse potential, the CLFSE term and the 1-2 and 1-3 non-bonding interactions, while the angular nature of the coordination sphere is treated by the CLFSE and the 1-3 non-bonded interactions. One cannot, therefore, treat the general decrease in bond lengths along the series of $[M(Me_6tren)Br]^+$ complexes simply by

altering the metal charge parameters according to the increase in Z_{eff} of the metal, as this would ignore the radial aspects of the CLFSE and Morse potential terms that also account for this effect in part, while there is no obvious way to determine the change in net metal charge in order to implement such a scheme.

It is apparent, however, that if the parameterisation of two of the three terms describing the metal centre can be fixed for the $[M(Me_6tren)Br]^+$ species, for the calculations reported here the CLFSE and the Coulombic terms, then the parameters for the remaining term, in this case the Morse potential, may be varied so as to gain the best agreement of the minimised structure with experiment. For the studies reported here, it appears that the Morse potential parameters that yield the best agreement with experiment are unique, and so it is likely that if the parameterisation of the CLFSE and Morse potential terms are kept constant then the experimental structures may be reproduced by a unique set of charge parameters. The advantage of such a scheme is that the Morse potential parameters, after an extensive study of parameter transferability, may be derived from studies of related species and are less likely to vary from species to species than the charge parameters. Since the charge parameters model the net charges shown by the atoms of a particular species after complex formation, and thereby monitor the charge distribution within the complex, they are likely to be the most sensitive to a change in the metal or ligand set in terms of the parameter values required to reproduce the observed structure. It is also likely, given the relationship between the charge parameters and the electron distribution within the complex, that these parameters will contain a good deal of chemical information, although care must again be taken to ensure that a "double counting" of such effects is avoided, as the charge distribution in a complex is also monitored by the CLF parameters.

It is also feasible, however, that as a result of a full parameter transferability study the charge parameters may prove to be less sensitive than anticipated, and so it may be

possible to reproduce experimental structures with a single set of refined parameters, at least for related complexes of a specific metal. These issues are considered further in the next chapter, which discusses proposals for future work.

Chapter 7

General Conclusions and Future Work

The results presented in this work have clearly shown that the CLFSE term is of the correct form for modelling open-shell transition metal species within a molecular mechanics scheme. The CLFSE has reproduced the general properties of LFSEs in terms of the reproduction of the "double hump" behaviour that is displayed by many of the thermodynamic properties of the first row transition series, the reproduction of the stereochemical activity of d-orbital "holes" displayed by the five coordinate $[M(Me_6tren)Br]^+$ species, and the distortions from regular geometry that are observed for $Cu(NH_3)_6^{2+}$ and $CuCl_4^{2-}$ as a result of the Jahn-Teller activity of the d^9 configuration in octahedral and tetrahedral environments. The CLFSE term also correctly indicates the Jahn-Teller instability of regular geometries for configurations other than d^9, for example the d^1 and d^3 configurations in tetrahedral and trigonal bipyramidal symmetry.

The CLFSE term brings two main improvements to the Molecular Mechanics treatment of transition metals. Firstly, the CLFSE treats the effects of LFSEs as they are. For example, the behaviour of the $[M(Me_6tren)Br]^+$ species for M = Ni and Cu may be considered as the result of maximising the LFSE, and this is modelled directly by the CLFSE term. The Jahn-Teller effect may be considered in the same fashion, as the driving force for a Jahn-Teller distortion is the increase in LFSE. This too is modelled directly by the CLFSE. Traditional Molecular Mechanics methods would be unable to treat such systems in such a chemically consistent fashion. For example, the structure of $Cu(NH_3)_6^{2+}$ has been reproduced[26] by assigning a much larger value of b_o to the axial bonds than to the equatorial bonds, thereby enforcing a tetragonally elongated energy minimised structure. The observed structure is reproduced, but the result is chemically meaningless. The ligands of the complex cannot be distinguished *a priori*, and to discriminate between the axial and equatorial ligands in the initial

parameterisation is inconsistent from a coordination chemists' point of view. The treatment of this complex using the CLFSE term does not suffer these restrictions, however, and the experimentally observed difference in the axial and equatorial bond lengths is reproduced from identical parameterisation of the six ligands.

The implicit treatment of L-M-L angle terms and, in principle, the treatment of M-L-N angles, where N is the next atom bonded to the ligand, are also a significant benefit of the CLFSE term. Molecular Mechanics force fields encounter special problems concerning the treatment of angle around the metal due to the form of the angular potential employed in popular force fields. The common harmonic angle bend potential function is unsuitable for describing the deformation of angles around the metal centre both in terms of the behaviour of the function at large deviations from the ideal value which predicts inappropriately large energy gradients, and in the behaviour of the term at the angular limit. Harmonic potentials show cusps at this limit where the slope of the curve should be zero. An additional problem of using explicit angle terms for the metal centre is the definition of unique angles and corresponding equilibrium values, referred to as the unique labelling problem. For example, *cis*- diaminodichloroplatinum(II) requires two N-Pt-Cl values (90^{o} and 180^{o}). This problem arises for any molecular geometry that shows the possibility of cis and trans orientations, which includes T-shaped, square planar, trigonal bipyramidal, square pyramidal and octahedral idealised geometries, some of the most common geometries shown by transition metal species. This problem may be overcome by the incorporation of multiple equilibrium positions and redundant atom labelling schemes, but a more common strategy is to circumvent the problems associated with harmonic angle terms by setting the angle bend force constants to zero, and to allow ligand-ligand 1-3 nonbonded interactions to determine the angular geometry of the complex. This is analogous to a VSEPR treatment of such species. This stategy prevents the effective modelling of species such as $CuCl_4^{2+}$, however, which shows a flattened tetrahedral structure rather than a regular tetrahedral

structure as would be predicted from VSEPR theory. Within a Molecular Mechanics scheme that does not parameterise the angles around the metal, the structure of $CuCl_4^{2-}$ cannot be reproduced. The CLFSE term treats the L-M-L angles implicitly, and, as described in chapter 4, will favour a square planar geometry for such a species due to the strong Jahn-Teller activity of the d^9 configuration, and so the observed flattened tetrahedral geometry may be reproduced as the result of a balance between the CLFSE term and a suitable ligand-ligand 1-3 nonbonding term. The only Molecular Mechanics force field that appears to be able to model $CuCl_4^{2-}$ is the SHAPES force field of Allured *et al*[31] which, by the use of Fourier terms to describe the metal centre by means of a spherical coordinate system, is able to define a idealised square planar geometry from which 1-3 nonbonded interactions will cause distortions. Although such a scheme is capable of reproducing the observed structure, the result is again chemically meaningless as no account is made of the Jahn-Teller effect which is indisputably responsible for the observed distortion from the regular tetrahedral geometry.

The second benefit that the CLFSE term brings to the modelling of transition metal species is the prediction of the ligand field properties of an energy minimised structure. The final CLF e_λ values may be used to generate d-d spectra, esr g-values and magnetic moments if an appropriate basis set and parameters to describe spin orbit coupling and interelectron repulsion are provided. The CLFSE term can then provide valuable additional information for comparison with experiment. This is a particularly valuable asset of the CLFSE term as it may be anticipated that in Molecular Mechanics calculations of transition metal species it will be the metal centre that is of prime interest, in terms of the coordination environment of the metal and the resultant ligand field properties.

It is apparent then that the CLFSE term provides a superior method for treating the general effects of the LFSEs that dominate the chemistry of open-shell transition metal

species. However, as was mentioned in chapter 5, a successful Molecular Mechanics scheme requires more than the reproduction of the structures and energetics of individual species. Unless some degree of parameter transferability is possible between related species then there is little advantage in including the CLFSE term in Molecular Mechanics treatments. The problem of parameter transferability, and the means by which the possibility of transferability may be increased were discussed extensively for the [NiX_2[n]ane] species in chapter 5 and a number of strategies were suggested. However, the principle aim of the work reported here is to illustrate that the CLFSE term is of the correct form to model the effects of LFSEs in a general sense, rather than to produce a comprehensive force field for modelling transition metals. In order to maximise the possibility of parameter transferability between species it is important to review the base assumptions that were made for the modelling of the complexes reported here.

It would seem that, for general circumstances, that the CLFSE term is suitably parameterised by the e_λ vs bond length description that were gained from the CLF database described in chapter 2. There are, however, areas in which the parameterisation of the CLFSE term may be improved. Firstly, although it may not be of particular benefit to the possibility of improving parameter transferability, it was shown in chapter 5 that the effect of misdirected valence must be included in the CLFSE term. This term provides an implicit treatment of the M-L-N angles. It was these angles that showed the largest deviation from experiment for the $M(en)_3^{2+}$ species when no treatment, either explicit or implicit, of these angles was included, and it was suggested that the inclusion of a description of these angles would improve the calculated structures of these species. The inclusion of misdirected valency would also prevent the change in conformation of the macrocyclic ring that is calculated for the $Ni(NCS)_2$[15]ane and both NiX_2[16]ane complexes. The M-L-N angle could be treated by means of a traditional harmonic term, as these angles are unlikely to show the large

deviations from ideal angle that occur for L-M-L angles, but for internal consistency it would be preferable to treat these angles implicitly within the CLFSE term. This implicit treatment is particularly important if the CLFSE term is to be used to predict the ligand field properties of the metal as misdirected valence has been show to exert a significant effect upon these properties[55,63,74].

The effect of void cell contributions has also been discussed in this work, and while it was concluded that the effect of the inclusion of these contributions was not of any great significance for reproducing the structure of Cs_2CuCl_4 which shows a flattening angle of 129.2°, this is will not be the case generally. It is evidently important that an algorithm be developed such that the presence of a void cell may be detected and then suitably parameterised, both in terms of the dependence of the value of the void cell contribution upon the size of the angle that the void occupies, and possibly in the modification of the parameters for the remainder of the ligands, as it has been show that the introduction of a void cell has little effect upon the CLFSE if the CLF sum is not maintained, at least for the d^4 configuration that is most likely to undergo such large distortions.

A related feature of the CLF parameterisation is the behaviour of the CLF e_λ vs bond length function at long bond lengths. It would seem that the r^{-5} dependency upon bond length is suitable for bond lengths less than *ca* 2.3 Å, and also when large negative values (*ca* -1000 cm^{-1}) are reached for bond lengths of *ca* 2.6 Å for the data collected for Cu(II) complexes, but due to the nature of the d^9 configuration the observed bond lengths tend to be either long or short. It is difficult, therefore, to predict the behaviour of e_λ for intermediate bond lengths with any great degree of confidence, and the form of the e_λ vs bond length function in this range is likely to be of significance in determining the course of a minimisation. It is conceivable, for example, that the function should show in inflexion when the e_λ become negative, and thereafter decrease in at least a linear fashion until an e_λ of -3000cm^{-1} is reached. To investigate

the behaviour of the e_λ vs bond length function in this intermediate region it would be useful to carry CLF analyses on structures that show such bond lengths, which are likely to occur as the result of steric constraints upon the ligands. The initial aim of the analyses reported in chapter 3 was to investigate this region of bond length for Ni(II), but as was seen from the analyses of the NiX_2[n]ane species, the large increase in axial donation on increasing the macrocyclic ring size is not necessarily associated with a significant decrease in axial bond length. It is possible, therefore, that data for the region of bond lengths of interest will remain elusive.

The most important factor influencing the possibility of parameter transferability is the parameterisation of the organic force field. The force field used in this work is not necessarily suited to the aliphatic structures that were modelled, and is almost certainly not optimally defined for such species. Parameter transferability will only be achieved if an appropriate balance is achieved between the organic force field terms and the terms that are used to treat the metal centre. The parameterisation of the organic terms must, therefore, come under close scrutiny. It may, however, also be necessary to review the form of the organic terms where these terms come into contact with the metal, specifically the metal-ligand bond term. It is entirely possible that a Morse potential does not adequately represent the energy change that occurs on modifying a metal-ligand bond from the equilibrium position, especially in terms of the asymmetry of energy gradients for stretching and compressing a bond. A Morse potential may be adequate if it provides the only description of the metal-ligand interaction, but if the CLFSE term is included then this term also implicitly treats the metal-ligand 1-2 interaction, as will a Coulombic potential if atomic charges are included for the ligand and metal atoms, and so the net description of the 1-2 potential is more complex. The problem that exists with the Morse potential function is that there is only one parameter that may be adjusted to alter the gradient of the curve, which alters the energy derivatives for both compression and elongation of the bond. If, however, a Lennard-

Jones type potential was employed, as suggested by Vedani and Huhta[30], then the form of this function, although qualitatively similar to a Morse function, allows for more control of the asymmetry of the energy gradients with respect to compression or elongation of the bond. Suitable parameterisation of this term could therefore be achieved such that the net 1-2 metal-ligand interaction, when the CLFSE and Coulombic terms are included, is appropriate. This parameterisation may be achieved by comparison of the data derived from the Molecular Mechanics approach with that gained from a higher level ab initio computational scheme, such as Xα. The assumptions that are made within the parameterisation of the Morse potential for the work reported here should also be examined, specifically the assumption that a linear interpolation of b_0 and D_0 values from Mn to Zn will reproduce the effect of modification of the metal in the absence of a LFSE.

The method by which charges are assigned should also be investigated. As was mentioned in the previous chapter, it is likely that the derived net charges that result from fitting the experimental structure of a complex, with consistent metal-ligand bond and CLFSE parameters, will reflect the charge distribution in a complex, and as such are likely to be the most sensitive parameter set in terms of a change in metal or ligand set. If the charges do reflect the charge distribution then it is not unfeasible that the charges should therefore be linked to the CLF e_λ in some way. For example, although it would be difficult to justify the use of separate Morse potential parameters for the axial and equatorial metal-nitrogen bonds for the $[M(Me_6tren)Br]^+$ species, it would seem reasonable to assign different charge parameters to the nitrogen atoms as the e_λ for the axial and equatorial nitrogen atoms are different. If the nitrogen atoms are assumed to all carry the same charge before complex formation, and given that the CLF e_λ are a measure of charge donation from ligand to metal, then it would seem reasonable to assign smaller charge parameters to the axial nitrogen atoms for the Ni and Cu to reflect the increased degree of axial donation relative to the other complexes

of the series. However, as was mentioned in the previous chapter, care must be taken to avoid double counting, while it may be possible to reproduce the structures of complexes of a given metal without modifying the charge parameters.

Once the correct form of the potential functions, and suitable parameterisation of these functions is achieved, then the process of deriving transferable parameters may be carried out. Such a process should involve the reproduction of as large a set of related complexes as possible, and the use of some fitting routine so that an optimum parameter set may be gained so as to adequately reproduce the experimental data. It would, perhaps, be over-ambitious to expect a parameter set to emerge that is transferable from metal to metal, or indeed to show any trends in the parameters used to treat a series of metal complexes, but one could reasonably expect to derive a set of parameters that are capable of consistently reproducing the structures of complexes of a given metal.

In order to extend the potential utility of the CLFSE term within Molecular Mechanics it is important to perform CLF analyses so as to extend the range of ligand and metal types within the CLF database so as to facilitate the parameterisation of new ligand and metal types for the CLFSE term. Such analyses should include complexes containing metal-oxygen and metal sulphur bonds, and there is extensive structural, spectroscopic and magnetic data for such species available in the literature. In particular, data for the complexes $M(H_2O)_6^{n+}$, M = Ti to Cu, n = 2,3 found in Tutton salts and alums are readily available[110]. Several neutron diffraction studies[111] have located the exact positions of the water hydrogen atoms, and although preliminary studies carried out for these systems suggest that the analyses are both complex and under-determined, there is valuable information to be gained concerning the nature of water coordination. A wealth of data also exists for macrocyclic complexes, both with saturated and unsaturated ligands and a variety of transition metals. Donor sets include N_4, S_4, O_4,

N_2S_2, N_2O_2, S_2O_2 etc., and these species should form the subject of both CLF and CLFSE studies.

The extension of the CLFSE data set is most important if the CLFSE term is to fulfil its potential as a means of investigating transition metal complexes. Transition metals play vitally important roles in a wide variety of biological processes with one or more metal ions located at the active sites of many important proteins and enzymes[112]. For example, plastocyanin, an important "blue" copper protein vital in photosynthesis, is a Cu(II) ion in a highly-distorted tetrahedral N_2S_2 environment[113]. The CLFSE term may also be applied to the investigation catalytic systems involving open-shell transition metals, in which the coordination environment of the metal is likely to influence the catalytic activity of the metal centre.

Provided that the problem of parameter transferability can be overcome, and it would seem likely that this can be achieved, the CLFSE term as an additional energy term for modelling open-shell transition metals within Molecular Mechanics will prove to be a powerful and flexible tool for studying the chemistry of transition metal species in coordination chemistry, biochemistry and catalysis.

References

1. H.Fruhbeis, R.Klein and H.Wallmeier, *Agnew.Chem.Int.Ed.Engl.*, 1987, **26**, 403.
2. V.Burkert and N.L.Allinger, "Molecular Mechanics", ACS monograph 177, Washington, 1982.
3. N.L.Allinger, Y.H.Yuh and J.H.Lii, *J.Am.Chem.Soc.*, 1989, **111**, 8551.
4. R.Brooks, R.E.Bruccoleri, D.B.Olafsen, D.J.States, S.Swaininathan and M.Karplus, *J.Comput.Chem.*, 1983, **4**, 187.
5. P.K.Weiner and P.A.Kollman, *J.Comput.Chem.*, 1981, **2**, 287.
6. S.J.Weiner, P.A.Kollman, D.A.Case, V.C.Singh, C.Ghio, G.Alagona, S.Profeta and P.K.Weiner, *J.Am.Chem.Soc.*, 1984, **106**, 765.
7. S.L.Mayo, B.D.Olafson and W.A.Goddard, *J.Phys.Chem.*, 1990, **26**, 8897.
8. 1) MM1/MMP1 by N.L.Allinger er al., 2) MM2 by N.L.Allinger and Y.H.Yuh, 3) QCFF/PI by A.Warshel and M.Levitt, 4) MCA by E.Huler, R.Sharon and A.Warshel, 5) BIGSTRN by J.D.Andose, E.M.Engler, J.B.Collins, J.P.Hummel, K.Mislow and P.v.R.Schleyer and 6) BIGSTRN2 by D.J.Iverson and K.Mislow.
9. E.A.Mason and M.M.Kreevoy, *J.Am.Chem.Soc.*, 1955, **77**, 5808.
10. A.W.Burgess, L.L.Shipman, R.A.Nemenhoff and H.A.Scheraga, *J.Am.Chem.Soc.*, 1976, **98**, 23.
11. L.S.Bartell, *J.Am.Chem.Soc.*, 1977, **99**, 3279.
12. L.Radom, W.J.Hehre and J.A.Pople, *J.Am.Chem.Soc.*, 1972, **94**, 2371.
13. N.L.Allinger and S.Profeta Jr., *J.Comput.Chem.*, 1980, **1**, 181.
14. M.R.Snow, *J.Am.Chem.Soc.*, 1970, **92**, 3610.
15. R.D.Hancock, *Prog.Inorg.Chem.*, 1989, **37**, 187.
16. J.C.A.Boeyens, C.C.Fox and R.D.Hancock, *Inorg Chim Acta*, 1984, **87**, 1.
17. P.V.Bernhardt and P.Comba, *Helv. Chim Acta*, 1991, **74**, 1834; 1992, **75**, 645.
18. M.Yamaguchi, S.Yamamatsu, T.Furusawa, S.Yano, M.Saburi and S.Yoshikava, *Inorg.Chem.*, 1980, **19**, 2010.

19. R.D.Hancock, P.W.Nrwenya, A.Evers, P.W.Wade and J.C.A.Boeyens, *Inorg.Chem.*, 1990, **29**, 264.

20. T.W.Hambley, C.J.Hawkins, J.A.Palmer and M.R.Snow, *Aust.J.Chem.*, 1981, **34**, 45.

21. A.M.Bond, T.W.Hambley and M.R.Snow, *Inorg.Chem.*, 1985, **24**, 1920.

22. G.J.McDongall, R.D.Hancock and J.C.A.Boeyens, *J.Chem.Soc.Dalton Trans.*, 1978, 1438.

23. R.D.Hancock, S.M.Dobson, A.Evers, M.P.Nrwenya, P.Wade, J.C.A.Boeyens and K.P.Wainwright, *J.Am.Chem.Soc.*, 1988, **110**, 2788.

24. R.D.Hancock, S.M.Dobson and J.C.A.Boeyens, *Inorg.Chim Acta*, 1987, **133**, 221.

25. T.W.Hambley, *Inorg.Chem.*, 1988, **27**, 1073.

26. P.V.Bernhardt and P.Comba, *Inorg.Chem.*, 1992, **31**, 2638.

27. R.A.Jones, F.M.Real, G.Wilkinson, A.M.Galas, M.B.Hursthouse and K.M.A.Malik, *J.Chem.Soc.Dalton Trans.*, 1980, 511.

28. R.J.Gillespie, *J.Chem.Ed.*, 1970, **47**, 18.

29. D.L.Kepert, "Comprehensive Coordination Chemistry", Vol. 1, Pergamon Press, Oxford, 1987.

30. A.Vedani and D.W.Huhta, *J.Am.Chem.Soc.*, 1990, **112**, 4759.

31. V.S.Allured, C.M.Kelly and C.R.Landis, *J.Am.Chem.Soc.*, 1991, **113**, 1.

32. A.Vedani, D.W.Huhta and S.P.Jacober, *J.Am.Chem.Soc.*, 1989, **111**, 4075.

33. B.M.Pettitt and M.Karplus, *J.Am.Chem.Soc.*, 1985, **107**, 1166.

34. Z.Berkovitch-Yellin and L.Leiserowitz, *J.Am.Chem.Soc.*, 1980, **102**, 7677.

35. F.A.Cotton and G.Wilkinson, *Advanced Inorganic Chemistry*, 5th edn., Wiley-Interscience, USA, 1988.

36. R.J.Deeth, M.A.Hitchman, G.Lehmann and H.Sachs, *Inorg.Chem.*, 1984, **23**, 1310.

37. R.J.Deeth and M.A.Hitchman, *Inorg.Chem.*, 1986, **25**, 1225.

38. M.Gerloch, J.H.Harding and R.G.Woolley, *Struct.Bonding (Berlin)*, 1981, **46**, 1.

39. R.G.Woolley, *Mol.Phys.*, 1981, **42**, 703.

40. M.Gerloch and R.G.Woolley, *Prog.Inorg.Chem.*, 1983, **31**, 371.

41. M.Gerloch, *Magnetism and Ligand Field Analysis*, Cambridge University Press, New York, 1983.

42. C.E.Shaffer, *Pure Appl.Chem.*, 1970, **24**, 361.

43. C.E.Shaffer and C.K.Jorgenson, *Mol.Phys.*, 1965, **9**, 401.

44. R.J.Deeth and M.Gerloch, *Inorg.Chem.*, 1984, **23**, 3846.

45. R.J.Deeth and M.Gerloch, *Inorg.Chem.*, 1984, **23**, 3853.

46. R.J.Deeth and M.Gerloch, *Inorg.Chem.*, 1985, **24**, 1754.

47. R.J.Deeth, Ph.D. Thesis, University of Cambridge, 1985.

48. E.U.Condon and G.H.Shortly, *The Theory of Atomic Spectra*, Cambridge University Press, 1964.

49. G.Racah, *Phys.Rev.*, 1942, **62**, 438; ibid, 1943, **63**, 367.

50. P.Day, *Proc.Chem.Soc.*, 1964, 18.

51. R.J.Deeth and M.Gerloch, *Inorg.Chem.*, 1985, **24**, 4490.

52. J.E.Davies, M.Gerloch and D.J.Phillips, *J.Chem.Soc.Dalton Trans.*, 1979, 1836.

53. M.Gerloch and L.R.Hanton, *Inorg.Chem.*, 1981, **20**, 1046.

54. R.J.Deeth and M.Gerloch, *J.Chem.Soc.Dalton Trans.*, 1986, 1531.

55. R.J.Deeth and M.Gerloch, *Inorg.Chem.*, 1987, **26**, 2582.

56. A.Bencini, C.Benelli, D.Gatteschi and C.Zanchini, *Inorg.Chem.*, 1983, **22**, 2123.

57. D.W.Smith, *Struct.Bonding*, 1978, **35**, 87.

58. R.G.Woolley, *Chem.Phys.Lett.*, 1985, **118**, 207.

59. M.Gerloch, I.Morgenstern-Baderau and J.P.Audiere, *Inorg.Chem.*, 1979, **18**, 3220.

60. M.Gerloch and L.R.Hanton, *Inorg.Chem.*, 1980, **19**, 1692.

61. M.Gerloch and M.R.Manning, *Inorg.Chem.*, 1981, **20**, 1051.

62.M.Gerloch and L.R.Hanton, *Inorg.Chim.Acta*, 1981, **49**, 37.

63. R.J.Deeth, M.J.Duer and M.Gerloch, *Inorg.Chem.*, 1987, **26**, 2573.

64. N.D.Fenton and M.Gerloch, *Inorg.Chem.*, 1987, **28**, 3273.

65. C.A.Brown, M.J.Duer, M.Gerloch and R.F.McMeeking, *Mol.Phys.*, 1988, **64**, 793.

66. N.D.Fenton and M.Gerloch, *Inorg.Chem.*, 1989, **28**, 2767.

67. M.J.Duer and M.Gerloch, *J.Chem.Soc.Dalton Trans.*, 1989, 2109.

68. N.D.Fenton and M.Gerloch, *Inorg.Chem.*, 1990, **29**, 3726.

69. D.A.Cruse and M.Gerloch, *J.Chem.Soc.Dalton Trans.*, 1977, 152.

70. D.A.Cruse and M.Gerloch, *J.Chem.Soc.Dalton Trans.*, 1977, 1613.

71. M.Gerloch and I.Morgenstern-Baderau, *Inorg.Chem.*, 1979, **18**, 3225.

72. M.Gerloch, L.R.Hanton and M.R.Manning, *Inorg.Chim.Acta*, 1981, **48**, 205.

73. M.J.Duer and M.Gerloch, *Inorg.Chem.*, 1989, **28**, 4260.

74. R.J.Deeth, M.J.Duer and M.Gerloch, *Inorg.Chem.*, 1987, **26**, 2578.

75. L.Y.Martin, C.R.Sperati and D.H.Busch, *J.Am.Chem.Soc.*, 1977, **99**, 2968.

76. I.Bertini, D.Gatteschi and A.Scozzafava, *Inorg.Chem.*, 1976, **15**, 2014.

77. A.B.P.Lever, I.M.Walker, P.J.McCarthy, K.B.Mertes, A.Jircitano and R.Sheldon, *Inorg.Chem.*, 1983, **22**, 2252.

78. T.Ito, M.Kato and H.Ito, *Bull.Chem.Soc.Jpn.*, 1984, **57**, 2641.

79. M.A.Hitchman, *Transition Met.Chem.(New York)*, 1985, **9**, 1.

80. A.B.P.Lever, *Inorganic Electronic Spectroscopy*, 2nd edn., Elsevier, Amsterdam, 1984.

81. A.A.Rahman, M.P.Brown, M.M.Harding, C.E.Keggan and J.D.Nicholls, *Polyhedron*, 1988, **7**, 1147.

82. J.S.Griffith, *The theory of Transition-Metal Ions*, Cambridge University Press, 1961.

83. C.K.Jorgensen, *Struct.Bonding (Berlin)*, 1964, **1**, 3.

84. M.Bacci, *Chem.Phys.*, 1979, **40**, 237.

85. A.D.Liehr and C.J.Ballhausen, *Ann.Physics (Leipzig)*, 1958, **3**, 304.

86. H.Yamatera, *Acta Chem.Scand.,Ser.A*, 1979, **A33**, 107.

87. M.Gerloch, *Inorg.Chem.*, 1981, **20**, 638.

88. L.L.Lohr Jr. and W.N.Lipscomb, *Inorg.Chem.*, 1963, **2**, 911.

89. D.W.Smith, *Inorg.Chim.Acta*, 1977, **22**,107.

90. M.Bacci, *Chem.Phys.*, 1986, **104**, 191.

91. M.Bacci, *Chem.Phys.Lett.*, 1987, **134**, 143.

92. H.Jacobs, J.Bock and C.Stuve, *Jour.Less Comm.Met.*, 1987, **134**, 207.

93. P.Stoll, *Diss.ETH Zuerich*, 1926, **1**, 1.

94. T.Distler and P.A.Vaughan, *Inorg.Chem.*, 1967, **6**, 126.

95. T.Yamaguchi and O.Lindqvist, *Acta Chim.Scand.A*, 1981, **35**, 811.

96. P.George and D.S.McClure, *Prog.Inorg.Chem.*, **1**, 381.

97. Mazhar-Ul-Haque, C.N.Caughlan and K.Emerson, *Inorg.Chem.*, 1970, **9**, 2421.

98. D.L.Cullen and E.C.Lingafelter, *Inorg.Chem.*, 1970, **9**, 1858.

99. C.Muralikrishna, C.Mahadevan, S.Sastry, M.Seshasayee and S.Subramanian, *Acta Cryst.*, 1983, **C39**, 1630.

100. H.Mashiyama and N.Hoshiji, *Acta Cryst.*, 1989, **B45**, 467.

101. J.Lauher and J.Ibers, *Inorg.Chem.*, 1975, **14**, 348.

102. J.R.Wiesner, R.C.Srivastava, C.H.L.Kennard, M.Divaira and E.C.Lingafelter, *Acta Cryst.*, 1967, **23**, 565.

103. R.Clay, J.Murray-Rust and P.Murray-Rust, *Acta Cryst.*, 1975, **B31**, 289.

104. R.J.Deeth, *J.Chem.Soc.Dalton Trans.*, 1990, 355.

105. M.Di Vaira and P.L.Orioli, *Acta Cryst.*, 1968, **B24**, 1269.

106. M.Di Vaira and P.L.Orioli, *Inorg.Chem.*, 1967, **6**, 955.

107. M.Di Vaira and P.L.Orioli, *Acta Cryst.*, 1968, **B24**, 595.

108. R.G.Gillespie and R.S.Nyholm, *Q.Rev.,Chem.Soc.*, 1957, **7**, 339.

109. E.Clementi and D.L.Raimondi, *J.Chem.Phys.*, 1963, **38**, 2868.

110. For example, S.Mitra, *Prog.Inorg.Chem.*, 1973, **22**, 309; B.R.McGarvey, *Trans.Met.Chem.*, 1966, **3**, 89.

111. B.E.F.Fender, B.N.Figgis, J.B.Forsyth, P.A.Reynolds and E.Stevens, *Proc.Roy.Soc.London*, 1986, **A404**, 127; B.E.F.Fender, B.N.Figgis and J.B.Forsyth, *Aust.J.Chem.*, 1986, **39**, 1023.

112. M.N.Hughes, *The Inorganic Chemistry of Biological Processes*, Wiley-Interscience, UK, 1972.

113. P.M.Colman, H.C.Freeman, J.M.Guss, M.Murata, V.A.Norris, J.A.M.Ramshaw and M.P.Venkatappa, *Nature*, 1978, **272**, 319.

Appendix

The force field parameters listed below are those employed for all "organic" parameteriation in this work. These are parameters are not modified as part of the process of fitting the calculated structures to the experimentally observed structures unless explicitly detailed in the appropriate text.

A.1: Morse potential parameters

Bond	D_o, kcal	b_o, Å	α
n-h	93.00	1.026	2.280
n-c	72.00	1.460	2.290
c-h	105.78089	1.11495	1.81
c-c	88.00	1.526	1.915

A.2: Angle term parameters

Angle	k^a, kcal	θ_o	k^b, kcal	k'^c, kcal	k''^d, kcal
hn-n-hn*	36.0	107.5	0.0	0.0	0.0
c-c-n	50.0	109.5	25.0	35.0	35.0
hn-n-c*	35.0	122.0	2.0	23.3	2.0
hc-c-n*	51.5	109.49	2.0	2.0	40.0
hc-c-c*	44.4	110.0	2.0	2.0	38.38
hc-c-hc*	40.955204	109.64	2.0	2.0	2.0
c-n-c	111.0	111.00	25.3	30.7	30.7
c-c-c	46.6	110.5	28.5	60.2	60.2

* hn and hc represent hydrogen atoms bound to nitrogen and carbon atoms respectively.

[a] Force constant

[b] θ force constant for bond-bond cross term

[c] Force constant for first bond-angle cross term

[d] Force constant for second bond-angle cross term

A.3: Torsion term parameters

Torsion	k^a, kcal	periodicity	Sign for cos function	k^b, kcal
hn-n-c-hc	0.0	3.0	-1.0	0.0
hn-n-c-c	0.0	3.0	1.0	0.0
c-n-c-hc	0.0	3.0	1.0	0.0
c-n-c-c	0.0	3.0	1.0	0.0
n-c-c-hc	1.423	3.0	1.0	-10.5
hc-c-c-hc	1.423	3.0	1.0	-10.0
n-c-c-n	1.423	3.0	1.0	-11.0
c-c-c-n	0.474	3.0	1.0	-10.5
c-c-c-hc	0.474	3.0	1.0	-10.5

[a] Force constant

[b] Force constant for θ, θ, ϕ cross term.

A.4: Non-bonding parameters

atom	A	B	c
n	86900	2020	9
c	38900	1230	9
hn	445	15	9
hc	445	15	9
Cl	154684	3839.3	9
Br	154684	3839.3	9
M	25000	2020	9

For inclusion into equation A.1:-

$$E_{nb} = A'/r^{12} - B'/r^{c} \qquad \text{Eqn. A.1}$$

where A' and B' are the geometric mean of the A and B parameters of the two interacting atoms.